Machine Learning Methods in the Detection of Melanocytic Lesions

Interdepartmental Postgraduate Program of Studies in Medical Physics - Radiation Physics, University of Patras



Posonidis Athanasios

Supervisor: Prof. Sakellaropoulos George

Patras

January 2026

Members of the Examination Committee

Sakellaropoulos George, Professor, PhD

Kagadis George, Professor, PhD

Zampakis Petros, Associate Professor, MD, PhD

Ευχαριστίες

Θα ήθελα να ευχαριστήσω τον επιβλέποντα καθηγητή μου κ. Γεώργιο Σακελλαρόπουλο και τον κ. Βλαχόπουλο Γεώργιο, για την πολύτιμη καθοδήγησή τους και την συνεχή υποστήριξη καθ' όλη τη διάρκεια της εκπόνησης της παρούσας διπλωματικής εργασίας.

Επιπλέον θα ήθελα να ευχαριστήσω την οικογένεια μου, Ελευθέριο, Όλγα, Γεωργία και Ειρήνη για την συνεχή στήριξή τους.

Table of Contents

I. Abstract 7

1. **Dermatological Theoretical Background** **9**

1.1 Benign Nevi 9

1.1.1 Common Acquired Nevi 9

1.2 Types of Nevi 9

1.2.1 Ephelis 9

1.2.2 Junctional Nevus 9

1.2.3 Compound Melanocytic Nevus 9

1.2.4 Intradermal Nevus 10

1.3 Special Melanocytic Nevi 10

1.3.1 Blue Nevus 10

1.3.1.1 Common Blue Nevus 10

1.3.1.2 Cellular Blue Nevus 11

1.3.2 Sutton Nevus - Halo Nevus 11

1.3.3 Spitz Nevus 11

1.3.4 Pigmented Spitz Nevus – Reed Nevus 11

1.3.5 Nevi with Specific Names 12

1.4 Congenital Melanocytic Nevi (CMN) 12

1.5 Nevus Spillus 13

1.6 Atypical/Dysplastic Melanocytic Nevi 13

1.6.1 Dysplastic Melanocytic Nevi 13

1.6.2 Atypical Nevi Syndrome 14

1.7 Malignant Melanoma 14

1.8 Histologic Categorization of Malignant Melanoma 14

1.8.1 Superficial Spreading Melanoma 14

1.8.2 Nodular Melanoma 14

1.8.3 Lentigo Maligna Melanoma 15

1.8.4 Acral Lentiginous Melanoma 15

1.8.5 Rare Subtypes 15

1.9 Nevi/Melanoma Classification Rules 16

2. Dataset 16

3. Resampling Methods 17

3.1 Cross-Validation 17

3.1.1 k-fold Cross-Validation 18

4. Machine Learning 19

4.1 Types of Machine Learning Algorithms 19

4.1.1 Supervised Machine Learning Algorithms 19

4.1.2 Unsupervised Machine Learning Algorithms 20

4.1.3 Reinforcement Learning Algorithms 20

4.2 Naïve Bayes Classifier 20

4.3 Feature Selection 21

4.3.1 Minimal Redundancy – Maximal Relevance (mRMR) 21

4.3.1.1 Maximal Relevance 21

4.3.1.2 Minimal Redundancy 22

4.4 Random Forest Feature Importance 22

4.4.1 Random Forests 22

4.4.2 Permutation Importance 23

4.4.3 SHAP Importance 24

4.4.4 Mean Decrease in Impurity (MDI) 25

5. Performance Metrics 26

5.1 Accuracy 26

5.2 Confusion Matrix 26

5.3 True Positive Rate, False Positive Rate, AUC ROC and PR AUC 27

6. Methodology - Results 28

6.1 Naïve Bayes Classifier Results 28

6.2 Minimum Redundancy – Maximum Relevance Results 34

6.3 Random Forest Feature Importance Results 39

6.3.1 Model Evaluation 43

6.4 Comparison of Random Forest Feature Importance Results with mRMR and Naïve Bayes Classifier Results 44

7. Related Work 47

8. Discussion 52

8.1 Naïve Bayes Classifier 52

8.2 Minimum Redundancy – Maximum Relevance 53

8.3 Random Forest Feature Importance.....55

9. Limitations..... 56

10. Conclusion 57

11. Future Work..... 57

References 58

Appendix 61

i. Naïve Bayes Classifier Results 61
ii. Random Forest Feature Importance Results 78

I. Abstract

Melanoma is one of the deadliest cancers. Accurate and fast detection can influence drastically the outcome of the patient that is diagnosed.

The aim of this study is to provide a fast and accurate method based on classical machine learning methods, due to their explainability and lack of black box architecture. The dataset was created by Kalloniati Evaggelia during her PhD, implementing an SVM classifier, a Random Forest and Logistic Regression. In her study, the comparison of SVM, logistic regression and random forests showed that Random forests provided the best accuracy, followed by Logistic regression, with the worst accuracy showed by SVM.

In this study, a Naïve Bayes classifier was applied in the same dataset, which was split into subsets of Low Risk-Medium Risk, Low Risk-High Risk and Medium Risk-High Risk cases. Due to the small dataset size, 5-fold and 10-fold Cross-Validation was used. The results showed that differences in Cross-Validation were minimal, with the classifier exhibiting highest performance (AUC=1) for Low-High Risk classification with morphological features. For Low-Medium Risk classification, features relevant to texture heterogeneity, gray-level non-uniformity and directional intensity variations were able to perform better in the task of finer distinction. For Medium-High Risk classification, features that carry information about morphology and tissue irregularities and complexity were among the ones that could effectively differentiate the lesions.

Also, a Minimum Redundancy – Maximum Relevance algorithm was used for feature selection, which provided three features on each subset that had the highest relevance for class differentiation. These features performed well (AUC>0.81) on the Naïve Bayes Classifier. These features were combined and used with the Naïve Bayes Classifier with 5-fold Cross-Validation and provided a significant improvement, with an AUC>0.91 in all datasets.

For assessing feature importance, a Random Forest Feature Importance algorithm was used, measuring SHAP, MDI and Permutation importance. Features that were exhibited higher SHAP and MDI values were morphological, texture and intensity heterogeneity based. Differences were exhibited when features that performed well in the previous algorithms, had reduced importance in the Random Forest due to correlations. While SHAP and MDI could be interpreted, Permutation was unreliable in some datasets, due to the small dataset size.

These results demonstrate that classical machine learning can effectively classify skin lesions, even with small, imbalanced datasets, as shown by mRMR and RFFI algorithms assessment and can be used for future dermatological applications.

1. Dermatological Theoretical Background

It is important to shortly present the types of nevi so that is highlighted the importance of accurate and correct detection and classification of lesions.

Nevi or melanocytic lesions are clusters of cells responsible for the pigment of the skin, called melanocytes. They are categorized as benign or malignant. Common acquired nevus, congenital melanocytic nevus and atypical nevus are characterized as benign, and melanoma as malignant.

A further analysis of benign and malignant nevi and their characteristics follows, to set the basis for the study that follows.

1.1 Benign Nevi

1.1.1 Common Acquired Nevi

Common acquired nevi are the most common neoplasm in white populations. They are benign proliferations of nevocytic cells that develop in early life and increase in adolescence. Their number is an independent risk factor for melanoma. For patients with more than 50 nevi, the risk is four times to five times larger and for patients with more than 100 it is eight times to ten times larger.

1.2 Types of Nevi

1.2.1 Ephelis

This is the first stage of development of a melanocytic nevus and its' clinical features are a round or elliptical, brown-colored macule, with a diameter of a few millimeters. Histologically, it is described as a focal increase in melanin, with a mild increase of melanocytes in the basal layer of the epidermis.

1.2.2 Junctional Nevus

A junctional nevus clinically presents as elliptical or round macule, or a minimally raised papule with a mild to intense dark brown coloration. Histologically, in junctional melanocytic nevus, nests of melanocytes are observed at the dermoepidermal junction, predominantly located at the tips of the rete ridges and less frequently between them.

1.2.3 Compound Melanocytic Nevus

A compound melanocytic nevus is a round or elliptical maculopapular lesion, with light to dark brown coloration. Histologically, nests of melanocytes at the dermoepidermal junction are observed, as well as nests of melanocytes within the dermis. Cells within

the dermis are characterized by smaller nuclei, and at deeper layers they lose their capacity for pigment synthesis.

1.2.4 Intradermal Nevus

A intradermal nevus is clinically characterized as a flesh-colored nodule with smooth surface and well-defined borders. Histologically, in this type of lesions, melanocytes are present in the dermis exclusively, with aggregates of melanocytes forming nests in the upper dermis and cords in the deeper dermis, exhibiting a linear growth pattern.



Figure 1: Compound, Intradermal and Junctional Nevi

1.3 Special Melanocytic Nevi

In this category, there will be a brief description of the blue nevus, Sutton nevus, Spitz nevus and special site nevus.

1.3.1 Blue Nevus

Blue nevi are benign lesions that are caused by the proliferation of dendritic melanocytes inside the dermis. Their bluish coloration is caused by the Tyndall effect, which refers to the selective scattering of shorter wavelengths of light by melanin in the dermis. (A. Lallas, 2020)

1.3.1.1 Common Blue Nevus

A common blue nevus is clinically described as a solitary lesion, either papule or nodule, with elliptical or round shape with blue-gray or blue-black coloration. It is most commonly found on the head, neck, sacral region and the extremities. Histopathologically, the common blue nevus is composed of spindle-shaped melanocytes with elongated dermal projections, scattered throughout the mid and upper dermis.

1.3.1.2 Cellular Blue Nevus

The cellular blue nevus is the most common subtype of blue nevus, accounting for 15% of all cases. Histopathologically, the cellular blue nevus lacks stromal components and develops entirely within the dermis and subcutaneous tissue. It exhibits two distinct microscopic patterns: areas identical to those of the common blue nevus, and densely cellular nodular regions composed of spindle-shaped melanocytes.

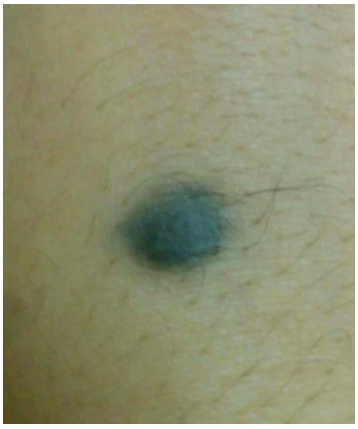


Figure 2: Blue Nevus

1.3.2 Sutton Nevus – Halo Nevus

Sutton nevus is a melanocytic nevus that is surrounded by a symmetrical halo of complete depigmentation. Histologically, they are compound or dermal nevi, characterized by a dense lymphocytic presence extending into the dermal components of the nevus. (A. Lallas, 2020)

1.3.3 Spitz Nevus

It typically presents as a symmetrical, hairless nodule with a reddish-pink or red hue. Common clinical features of Spitz nevi include small diameter (<5–6 mm), localization on the face and lower extremities, and a solitary lesion. However, multiple lesions may occasionally occur, either scattered or in clusters. Histopathologically, they are usually compound nevi, though they may also be junctional or dermal. Although eosinophilic hyaline granules or Kamino bodies were once considered pathognomonic for Spitz nevi, more recent reports have documented their presence in malignant melanoma as well.

1.3.4 Pigmented Spitz Nevus – Reed Nevus

The brown or black clinical variant of the Spitz nevus—also known as pigmented Spitz nevus or Reed nevus—exhibit the characteristic 'starburst pattern. Histologically, they

are well-circumscribed tumors composed of uniform spindle-shaped cells containing pigment. (A. Lallas, 2020)



Figure 3: Sutton/Halo Nevus, Spitz Nevus and Reed Nevus

1.3.5 Nevi with Specific Names

-The Meyerson nevus is a common melanocytic nevus surrounded by a peripheral eczematous halo. This halo typically resolves spontaneously or after topical corticosteroid application. (A. Lallas, 2020)

-The recurrent nevus appears following incomplete excision of a melanocytic nevus and is often clinically and/or histologically mistaken for malignant melanoma. Clinical features include flat pigmented lesions with asymmetric borders, arising within the scar of the previous excision, usually around six months postoperatively. (A. Lallas, 2020)

-The targetoid nevus is clinically characterized by a brown pigmented papule surrounded by a concentric brown ring, which in turn is encircled by a brownish halo.

-The eclipse nevus presents as a central light brown pigmented lesion surrounded by a thin, darker peripheral rim.

1.4 Congenital Melanocytic Nevi (CMN)

CMN are benign skin lesions present at birth. They are characterized by nests of melanocytes that may extend into the dermis and in some cases, deeper structures such as muscle or the central nervous system. They are categorized by size, small<1.5cm, medium<1.5-20cm and large or giant>20cm projected adult diameter. Larger lesions, particularly giant congenital melanocytic nevi, have a higher risk of malignant transformation into melanoma, although it is variable. These lesions may present with a wide range of clinical features and can be associated with extracutaneous conditions, particularly in cases of larger of giant nevi. (Marghoob, 2025)

1.5 Nevus Spillus

This type of nevus is characterized by a café au lait macule with the appearance of progressively increasing number of darker macules and papules in childhood.



Figure 4: Congenital Nevus and Nevus Spillus

1.6 Atypical/Dysplastic Melanocytic Nevi

1.6.1 Dysplastic Melanocytic Nevi

Clinical Characteristics

Dysplastic nevi are acquired melanocytic lesions that frequently exhibit common clinical characteristics with malignant melanoma. They can be diagnosed with the same ABCD rule depending on the presence of each criterion, and they can be differentiated accordingly.

Dysplastic nevi exhibit heterogeneity in their appearance. Most common subtypes are listed below.

- The ephelioid subtype, characterized by a flat surface and homogeneous dark brown to black hue
- The fried-egg subtype, characterized by a darker or lighter center compared to its' periphery, with the possibility of macular or papular elements present together
- The targetoid subtype, characterized by concentric zones with varying hue.
- The seborrheic keratosis-like subtype, characterized by a dark brown hue and a verrucous surface, resembling a cobblestone pattern
- The erythematous subtype, with a pink to red hue
- The melanoma mimic, that exhibits characteristics of the ABCD rule of malignant melanoma

They are usually located on the trunk and appear in puberty and are usually present in ages younger than 40 years.

1.6.2 Atypical Nevi Syndrome

There is a clinical differentiation between dysplastic nevi and atypical/dysplastic nevi syndrome, since the latter is associated with increased risk of malignant melanoma development. The classic definition states that patients with more than 100 melanocytic nevi, with at least one clinical atypical melanocytic nevus and one nevus with diameter larger than 8mm.

1.7 Malignant Melanoma

Malignant Melanoma is a malignant neoplasm that originates from melanocytes and is found mainly on the skin, and rarely in eyes, gastrointestinal tract, meninges and in oral and genital mucosa.

The contributing factors in the development of malignant melanoma are multiple, being both genetic and environmental.

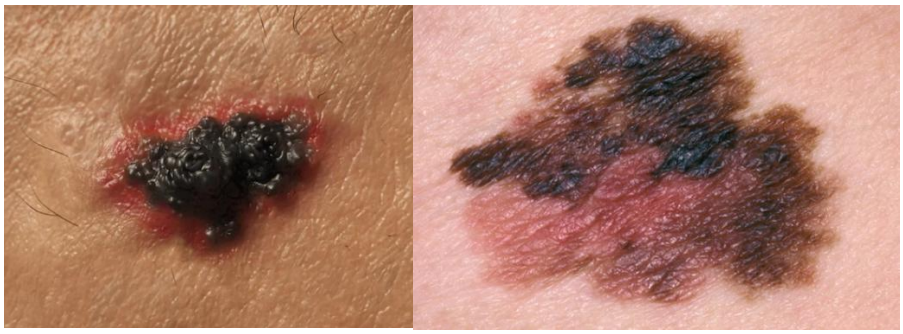


Figure 5: Different instances of Malignant Melanoma

1.8 Histologic Categorization of Malignant Melanoma

1.8.1 Superficial Spreading Melanoma

It is the most common type, and it accounts for the 70% of all malignant melanomas. It is associated with the intermittent exposure to sunlight. It appears as an asymmetric pigmented macule that follows the ABCD rule, and it develops into a plaque that may develop papules or small nodules.

1.8.2 Nodular Melanoma

It is the second most frequent subtype, accounting for 10-15% of malignant melanoma. It is the most aggressive subtype, with a clinical description of a dark-pigmented

nodule with relative symmetry and well-defined borders that ulcerates and bleeds. In a small percentage of cases, it appears with a reddish or pink hue.

1.8.3 Lentigo Maligna Melanoma

It is the third most frequent subtype, and it develops in areas that are exposed to sunlight. The determining factor for its' development is the chronic exposure to UV radiation. The clinical characteristics that define lentigo maligna melanoma is an asymmetric dark-pigmented macule or plaque with indistinct borders that can exhibit multiple colorations as it develops.

1.8.4 Acral Lentiginous Melanoma

This subtype refers to the melanoma of palmar surface of the hands, plantar surfaces of the feet and the nail unit. Clinically it appears as a dark pigmented macule or papule with indistinct borders and heterogeneous pigmentation. While it develops, it can have exophytic nodules or areas with blue-black hue. (A. Lallas, 2020)

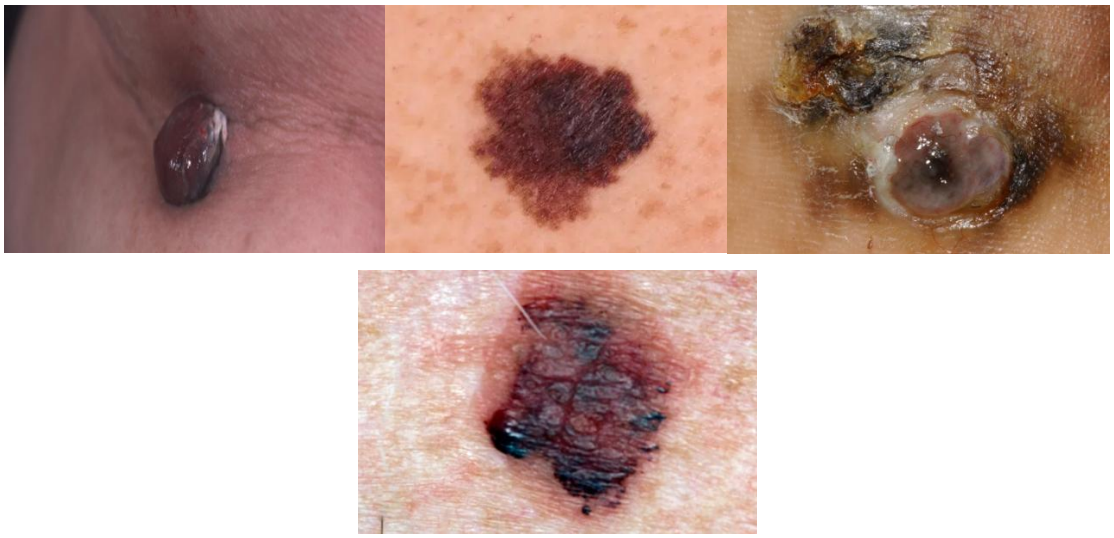


Figure 6: Nodular Melanoma, Superficial Spreading Melanoma, Acral Lentiginous Melanoma and Lentigo Maligna Melanoma

1.8.5 Rare Subtypes

- Amelanotic Melanoma
- Desmoplastic Melanoma
- Mucosal Melanoma
- Polypoid Melanoma
- Benign blue nevus

- Lentiginous Melanoma

1.9 Nevi/Melanoma Classification Rules

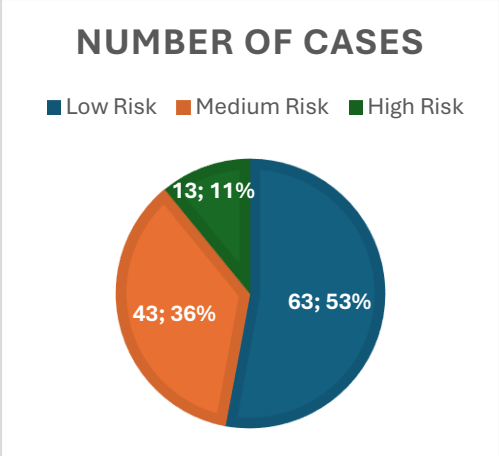
The ABCD(E) rule is a widely used technique, among others, to classify nevi. It was established by Kopf et al., and it uses 4 major characteristics of a nevus to recognize clinical malignant melanoma. These characteristics are A(asymmetry), B(border), C(color), D(diameter>6mm). Most melanomas have these characteristics, except for those that appear de novo. Also, some of the benign lesions mentioned before tend to have the same characteristics, leading to decreased diagnostic ability. To increase the sensitivity of this rule, E(evolution) was introduced, and it refers to the evolution that a nevus may exhibit, in instances of malignant melanoma. . (Ward W., 2017)

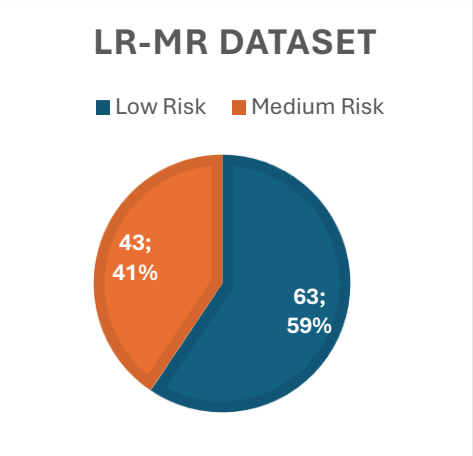
In addition to the previously mentioned rule, the Ugly Duckling sign is based on the observation that most benign nevi on an individual, share similar characteristics, so any lesion that appears clinically different from any other nevi might indicate malignancy, even if it doesn't meet any other standard criteria. (Ward W., 2017)

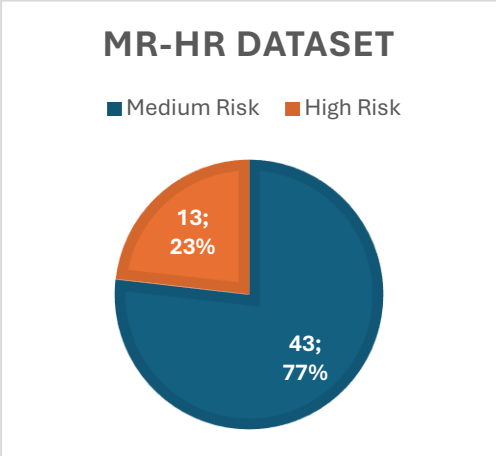
Another validated method is the 7-point checklist (Glasgow), which incorporates three major features and three minor features. Major features include change in size, irregular shape and irregular color and minor features include diameter>7mm, inflammation, oozing or bleeding and sensory changes. The presence of any major feature or multiple minor features increases the likelihood of melanoma and should lead to further diagnostic assessment. (Walter F., 2013)

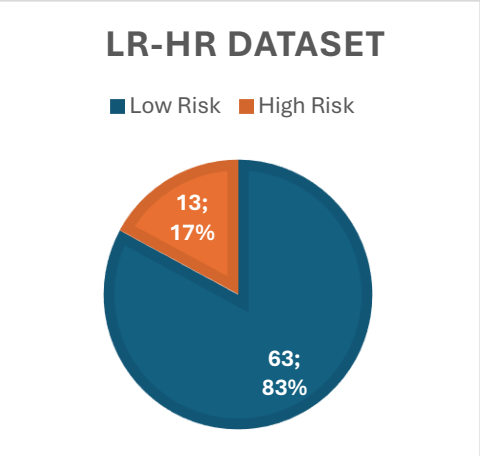
2. Dataset

This dataset is comprised of 127 features that were extracted from the dermoscopic images, after segmentation and image processing that was previously mentioned. The data class is decided after a histological examination that was performed after their removal. Benign lesions were classified as Low Risk(LR) and where 63 cases in total, atypical lesions were classified as Medium Risk (MR) and where 43 cases in total and malignant melanoma were classified as High Risk (HR) and where 13 cases in total. The dataset is imbalanced, and this was considered in cross-validation and metrics that were calculated to assess the model for classification, feature selection and feature importance. The graphs below show the class imbalance in the datasets that were used.









Segmentation of the dermoscopic images was done in MATLAB with morphological filtering. After that, 127 features were extracted. Morphological features were extracted from the binary image and texture characteristics were extracted from the monochromatic image. Texture characteristics of 1st order were extracted by the histogram of the monochromatic image, 2nd order from the greyscale co-occurrence matrix.

3. Resampling Methods

In these methods, samples are drawn repeatedly from a training set and a model is refitted on each sample, to gather additional information about the model. This allows to extract information that would be otherwise unavailable.

3.1 Cross-Validation

For a given dataset, a method for prediction is evaluated as acceptable, if it yields a low test error. Test error refers to the average error that results when a statistical learning

model is used for a certain prediction, which is not part of the model's training set. This error is usually not easily calculated, and is given by the expression:

Test error=1-Accuracy

It is clear that small test error means higher accuracy. Several approaches can be implemented to estimate test error, using the existing training data. Cross-Validation refers to a group of techniques that asses the test error by excluding a portion of the training data during model fitting and applying the statistical learning method to the excluded data. (Gareth James., 2013)

Different types of Cross-Validation exist, to name a few, Leave-One-Out Cross-Validation, k-Fold Cross-Validation, Time Series Cross-Validation. To increase the credibility of the prediction and for a larger training and testing set, 5-fold and 10-fold Cross-Validation was used.

3.1.1 k-fold Cross-Validation

This form of cross-validation requires the division of the dataset into k groups, named folds, of equal size approximately. One fold is used as the validation set or testing set, and the other k-1 sets are used as the training set of the model. The mean squared error, MSE_i is calculated on the fold used for validation. This repeats k times, until every fold is used as a validation set. Each time a new MSE is calculated, and the test error is estimated by averaging MSE_i, given by the expression $CV_{(k)} = \frac{1}{k}\sum_{i=1}^{k} MSE_i$. (Gareth James., 2013)

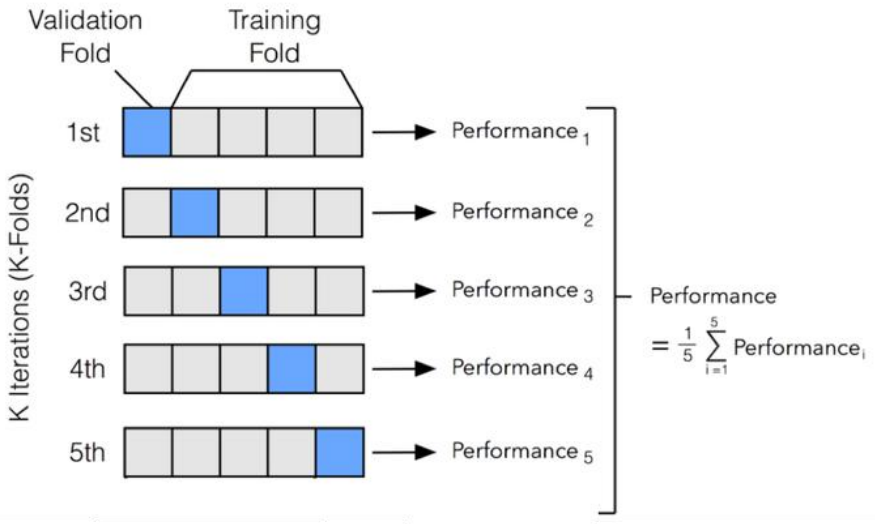


Figure 7: K-Fold Cross-Validation

Chosen folds for this study are 5 and 10, as it has been shown empirically to yield test error rate estimates that suffer neither from excessively high bias nor from very high variance. (Gareth James., 2013)

4. Machine Learning

Machine learning is a subfield of Artificial Intelligence (AI) refers to algorithms and models that enable computers to learn from data and improve with experience without explicit programming for every task. Specifically, it uses the theory of statistics in building mathematical models, making inference from a sample. To train the algorithm, an efficient algorithm is needed to solve the optimization problem, and store and process the amount of data available. After training, its' representation and algorithmic solution for inference needs to be efficient as well. An algorithm that satisfies these criteria can be used to solve classification problems, anomaly detection problems, regression problems, clustering problems and reinforcement problems, briefly explained below:

i. Classification problems refer to problems that require the prediction of a specific class for the given data, and either refers to binary or multiclass classification.
ii. Anomaly Detection problems refer to the analysis of a certain pattern. Changes (anomalies) from the pattern are detected by finding the outliers.
iii. Regression problems are used with continuous data and are used when a numeric output is needed.
iv. Clustering problems try to distinguish structures within the data and attempt to create clusters based on the similarity of this structure. Each class or cluster is then labeled.
v. Reinforcement problems are used when a decision must be made based on past experiences of learning. It learns by trial and error and changes its' behavior, based on rewards and penalties, in a continuously changing environment. (Alpaydin, 2014)

4.1 Types of Machine Learning Algorithms

Three general categories of machine learning algorithms are Supervised ML, Unsupervised ML and Reinforcement Learning.

4.1.1 Supervised Machine Learning Algorithms

In supervised learning the algorithm gets input-output pairs and learns a function that maps from input to output. The model then makes predictions on an unseen dataset

based on the previous training. It is mainly used for classification problems, where a certain class must be chosen for the new data, either between 2 classes or more (binary or multiclass classification), or regression problems, where the output is a continuous variable. (Stuart J. Russell, 2021) (Gareth James., 2013)

Usually, the dataset is split into training and testing data. While training the algorithm, the input data as well as the class is given to the algorithm. For validation, the testing data are used, and only input data are given, and prediction of the class is the required result. The next step is the evaluation of the model, with the proper metrics, such as confusion matrix, precision, recall, accuracy, F1 score, AUC ROC curve.

4.1.2 Unsupervised Machine Learning algorithms

The main difference between Unsupervised learning and Supervised learning is that there is no labeled data fed to the algorithm. The algorithm itself groups similar data points or recognizes structures in the dataset without human intervention. It is used for clustering problems, dimensionality reduction and anomaly detection.

4.1.3 Reinforcement learning Algorithms

Reinforcement learning refers to a machine learning algorithm that learns to make decisions through trial and error, receiving feedback from the environment based on their actions. The feedback refers to rewards and penalties, and the goal of the algorithm is to maximize the cumulative rewards.

This thesis is using a supervised machine learning model for the initial classification, specifically Naïve Bayes, for the binary classification across 3 datasets, with the following classes: LR-MR, LR-HR, MR-HR. A Random Forest classifier is implemented not for prediction of the classes mentioned above, but as a Feature importance classifier. (Stuart J. Russell, 2021)

4.2 Naïve Bayes Classifier

The Naïve Bayes Classifier is based on the Bayes Theorem. For determining the most probable hypothesis from a space H, given the observed data D is given by the Bayes Theorem. P(h) refers to the prior probability of h, that hypothesis h is true or correct, before the training data is observed. P(D) refers to the prior probability that training data D will be observed. P(D|h) refers to the probability of observing data D given that the hypothesis h is correct. The probability that is of interest in predicting a certain outcome is P(h|D), meaning that the hypothesis is true or correct given that data D are observed. The probability P(h|D) is called posterior probability of h. Bayes Theorem is summarized in this expression:

$$P(h|D) = \frac{P(D|h)P(h)}{P(D)}$$

If a set of candidate hypotheses H are considered, the algorithm aims to determine the most probable hypothesis h ∈ H given the observed data. A maximum a posteriori hypothesis is any maximally probable hypothesis. MAP can be calculated by calculating the posterior probability of each candidate hypothesis. h_{MAP} is a MAP hypothesis provided that $h_{MAP} \equiv \underset{h \in H}{argmax}\ P(h|D)$, or $h_{MAP} \equiv \underset{h \in H}{argmax}\ P(D|h)\,P(h)$. P(D) is independent of h and thus it is not part of the final expression.

Naïve Bayes is based on a strong assumption about the observed data D. It assumes that all observed data are conditionally independent given each candidate hypothesis. This is expressed as $P(h|D) = P(h)\prod_{i=1}^{n} P(d_i|h)$, where d_i is the i-th data. Even if correlation between data might exist, Naïve Bayes performs well even if correlations are ignored. (Mitchel, 1997), (Gareth James., 2013)

4.3 Feature selection

Large datasets can provide an equally large amount of features, some of which might be more informative about the task that needs to be performed such as classification etc. It is computationally and time efficient, specifically for larger datasets, to have the ability to distinguish features with these characteristics, making feature selection significant. It also provides easier interpretability, by including only the most relevant features. The removal of weak features leads to a more robust model, which is faster to train and has less likelihood for overfitting. Features that have zero variance and are highly correlated should be removed. A method of feature selection is the Minimal Redundancy – Maximal Relevance algorithm, which will be further discussed below. (Zhenyu Zhao, 2019)

4.3.1 Minimal Redundancy Maximal Relevance (mRMR)

4.3.1.1 Maximal Relevance

Maximal Relevance is based on the features that exhibit the strongest relevance to the target class. This relevance is commonly quantified using correlation or mutual information, of which the second is one of the most widely adopted measures to define dependency between variables.

For two random variables x and y, their mutual information is defined in terms of their probability density functions p(x), p(y) and p(x,y) as

$$MI(x;y) = \iint p(x,y) \log \frac{p(x,y)}{p(x)p(y)}\, dxdy.$$

Under the Maximal Relevance criterion, the selected features x_i are required to individually maximize the mutual information MI=(x_i;c) with the target class c, reflecting the largest dependency on the target class. In terms of sequential search, the m highest ranking features in the descending order of MI=(x_i;c) are not necessarily the best. That happens because features may have very similar information content, which is not considered and each feature is ranked in isolation with other features. This leads to the conclusion that individual features with good characteristics, as mentioned above, when combined, do not lead to good classification performance. The Maximal Relevance criterion is expressed as

$$\max D(S,c),\ D=\frac{1}{|S|}\sum_{x_i\in S} MI(x_i\,;c)\ .$$

With Dependency D=MI({x_i , i=1, …, m};c), S a feature set with m features {x_i}. Maximal Relevance approximates D(S,c) with the mean value of all mutual information values between individual feature x_i and class c. (Hanchuan Peng, 2005)

4.3.1.2 Minimal Redundancy

To select mutually exclusive features, the criterion of minimal Redundancy is expressed as

$$\min R(S),\ R=\frac{1}{|S|^2}\sum_{x_i,x_j\in S} MI(x_i\,,x_j).$$

The result after combining these two criteria, is the minimal-redundancy-maximal relevance, defined as

$$\max \Phi(D,R)\ ,\ \Phi=D-R.$$

4.4 Random Forest Feature Importance

4.4.1 Random Forests

Random forests are ensembles of hundreds of randomized decision trees, which cannot be immediately interpreted. To overcome this limitation, feature importance methods were employed by researchers, such as Mead Decrease in Impurity (MDI), permutation-based methods such as Mean Decrease in Accuracy (MDA) and Shapley Additive Explanations (SHAP). They are amongst the most popular supervised learning algorithms because they can adapt to non-linear relationships, handle high-dimensional data, perform well to low signal to noise ratio data and can be used effectively with minimal hyperparameter tuning. (Breiman, 2001), (Scott M. Lundberg, 2017), (Abhineet Agarwal, 2025), (Gilles Louppe, n.d.)

The advantage of random forests provides better accuracy than that of the single decision tree, which exhibits high variance. by using them as ensembles of randomized trees as mentioned above. It is based on the principle of introducing random perturbations in the learning procedure to produce several decision trees from the learning set. Also, an aggregation technique is used to combine the prediction of all these trees. (Gilles Louppe, n.d.)

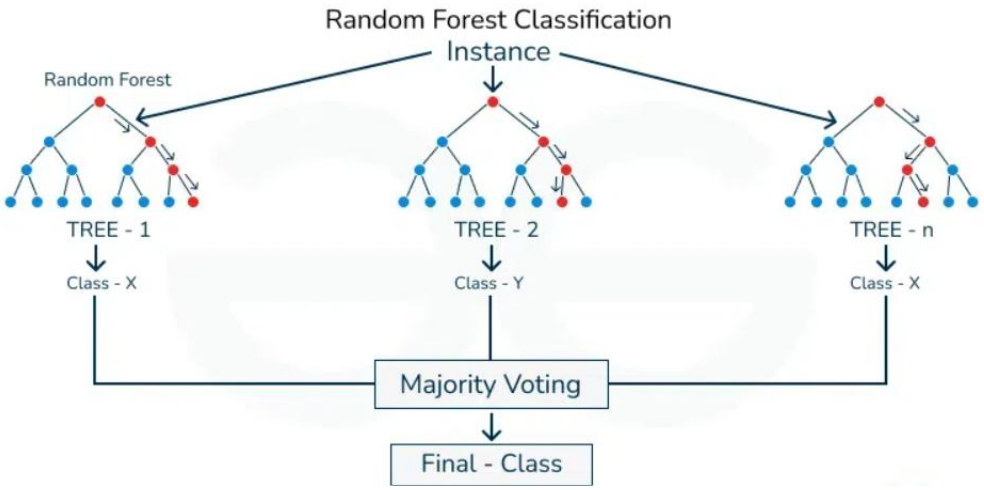


Figure 8: Random Forest Instance

4.4.2 Permutation Importance

Permutation Importance was first introduced by Breiman (2001) in the context of Random Forests. Later it was generalized to any supervised learning model, which allowed researchers to evaluate feature importance without model restriction. (Molnar, 2022)

It is a model inspection method to measure the contribution of each feature to a fitted model's statistical performance. This is specifically useful in non-linear estimators. The values of a single feature are randomly reordered and a new metric score for the new dataset is calculated. The importance of the feature that was reordered is proportional to how much the metric score degraded, compared to the initial one. This is repeated for all features, creating a ranked list that is based on the relative score degradation. Figure 9 below provides a visual representation of the procedure. (Ellis, 2024)

	feature_1	feature_2	feature_3	feature_4	feature_5	feature_6	feature_7	feature_8	feature_9	Target
0	0	0	9	0	0	0	0	0	0	0
1	1	1	5	1	1	1	1	1	1	1
2	2	2	2	2	2	2	2	2	2	2
3	3	3	0	3	3	3	3	3	3	3
4	4	4	3	4	4	4	4	4	4	4
5	5	5	6	5	5	5	5	5	5	5
6	6	6	4	6	6	6	6	6	6	6
7	7	7	7	7	7	7	7	7	7	7
8	8	8	8	8	8	8	8	8	8	8
9	9	9	1	9	9	9	9	9	9	9

Figure 9: Example of feature value shuffling

4.4.3 SHAP Importance

Shapley Additive Explanations (SHAP) is a model-agnostic framework used to interpret predictions of machine learning algorithms, based on Shapley values from cooperative game theory. It treats each feature as a player in a cooperative game, in which the pay-off is the output prediction of the model, based on a specific observation. Shapley value assigns each feature with a fair contribution to the prediction, by averaging its' marginal impact over all possible subsets of features. For a model f and an input observation $x \in \mathbb{R}^d$, the SHAP attribution value φ_i of feature i is expressed as:

$$\varphi_i = \sum_{S \subseteq F \setminus \{i\}} \frac{|S|!\,(|M| - |S| - 1)!}{|M|!} [f_x(S \cup \{i\}) - f_x(S)]$$

Where M is the number of input features, S is a subset of features and $f_x(S)=E[fx(x)|x_s]$ is the expected value of the function conditioned on S. The weighting term ensures that contributions are fairly averaged over all feature orderings. SHAP values satisfy important theoretical properties which are:

- Local accuracy: When approximating the original model f for a specific input x, local accuracy requires the explanation model to, at least match the output of f for the simplified input x', which corresponds to the original input x.
- Missingness: Missingness constrains features where $x_i'=0$ to have no attributed impact
- Consistency (Scott M. Lundberg, 2017), (Scott M. Lundberg, 2018)

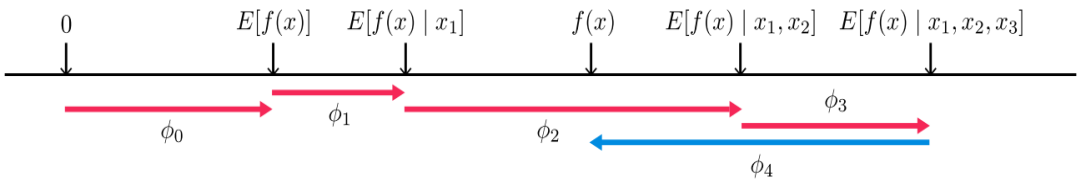


Figure 10: Feature Contribution for Prediction

The figure above shows that the SHAP values explain the output of a function f as a sum of the effects ϕ_i of each feature being introduced into a conditional expectation.

Overall, SHAP values are widely used due to their theoretically grounded framework helping to interpret individual model predictions, as they satisfy theoretical properties mentioned above.

4.4.4 Mean Decrease in Impurity (MDI)

In decision trees, forests and impurity-based variable importance, Mean Decrease in Impurity is a way to quantify the influence of input variables. Specifically in Random Forests, which achieve high predictive performance but are not easily interpretable, importance metrics such as MDI, also called Gini Importance, are widely used. A tree is built from a learning sample of size N drawn from $P(X_1,...,X_p,Y)$, where $(X_1,...,X_p)$ is a random input vector and Y a random output variable, using a repetitive procedure which identifies at each node t the split $s_t=s^*$ for which the partition of the N_t node samples into , t_L and t_R maximizes the decrease

$$\Delta i(s, t) = i(t) - p_L i(t_L) - p_R i(t_R)$$

where i(t) is a certain impurity measure of the parent node t. The construction of the tree stops, when nodes become pure in terms of Y or when all variables Xi are locally constant. (Gilles Louppe, n.d.)

When using ensembles of randomized trees, Breiman(2001,2002) proposed to evaluate the importance of a variable X_m for predicting Y by adding up the weighted impurity decreases $p(t)\Delta i(s_t,t)$ for all nodes t where X_m is used, averaged over all N_T trees, given by the expression

$$\text{Imp}(X_m) = \frac{1}{N_T} \sum_T \sum_{t \in T: v(s_t)=X_m} p(t) \Delta i(s_t, t)$$

and where p(t) is the proportion N_t/N of samples reaching t and $v(s_t)$ is the variable used in the split s_t. MDI is widely used, as it is computationally efficient but it can be biased when continuous variables are present. Despite this, it is a measure that can

be used to interpret the role of features in tree-based ensembles. (Carolin Strobl, 2007), (Breiman, 2001)

5. Performance Metrics

To correctly assess the results of a classifier, the use of the appropriate evaluation metrics should be calculated. In this study, accuracy, sensitivity, specificity, F1 Score and average AUC and plots of the ROC curve were used for the Naïve Bayes classifier. To assess the Random Forest Feature Importance results, AUC ROC, Precision Recall AUC (PR AUC) and F1 Score were used. (Hancock, 2023)

5.1 Accuracy

Accuracy is the most popular metric. It is the fraction of the correctly classified data, over the total number of data. This is a metric that is correctly used if the dataset is balanced. For imbalanced datasets, it provides overly optimistic results, the more imbalanced the datasets are. Another choice for accuracy, if needed to be reported, is balanced accuracy.

5.2 Confusion Matrix

A confusion matrix is a table used to compare predicted labels with true labels.

	Predicted Positive	**Predicted Negative**
Actual Positive	True Positive (TP)	False Negative (FN)
Actual Negative	False Positive (FP)	True Negative (TN)

Metrics that can be derived from the confusion matrix are presented below. Also a graph that shows the classes, the decision threshold and the misclassifications (FN and FP) is presented for clarification. (Ellis, 2024)

Accuracy	$\frac{TP + TN}{TP + TN + FP + FN}$
Precision	$\frac{TP}{TP + FP}$
Sensitivity (Recall) (TPR)	$\frac{TP}{TP + FN}$
Specificity (TNR)	$\frac{TN}{TN + FP}$
F1 Score	$2 * \frac{Precision * Recall}{Precision + Recall}$

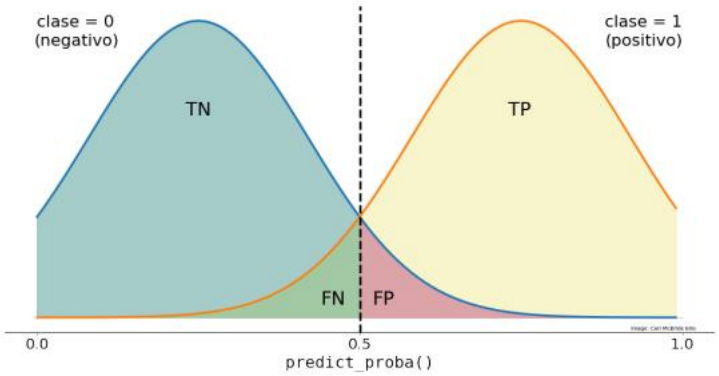


Figure 11: TN, TP, FN and FP

5.3 True Positive Rate, False Positive Rate, AUC ROC and PR AUC

True Positive Rate (TPR) was clarified in the previous section and measures the proportion of actual positive data that is correctly classified. True Negative Rate is a measure of actual negative data that is correctly classified.

The Receiver Operating Characteristic (ROC) curve shows the relationship between TPR and False Positive Rate (FPR) across all possible classification thresholds. By plotting a TPR – FPR curve for different thresholds, the ROC curve demonstrates how a classifier balances correctly identifying positives against incorrectly classifying negatives. The area under the ROC curve (ROC-AUC) provides a value that reflects the model's overall ability to distinguish between positive and negative cases. A ROC-AUC=1 represents the perfect classifier, while a value of 0.5 corresponds to random guessing. (Şeref Kerem Çorbacıoğlu, 2023)

Both Precision-Recall curves and ROC curves evaluate binary classifiers, but emphasis is given to different aspects. ROC curves measure how well a model separates positive and negative cases, while PR curves focus specifically on the model's ability to correctly identify positive cases. There is a theoretical mapping between ROC and PR curves, but a classifier that performs well according to ROC-AUC does not necessarily achieve a high PR-AUC, as these metrics respond differently to changes in prediction performance.

This differentiation becomes specifically important in the context of imbalanced datasets, when the positive class is relatively rare. ROC curves can be misleading in these scenarios, because the abundance of negative cases can suppress the impact of false positives, resulting in an inflated sense of classifier performance. PR curves, are directly influenced by false positives relative to true positives, thus providing a clearer picture of how well the model detects the minority class. That means that the area under the precision-recall curve (AUC-PR) is a more sensitive and informative metric

when evaluating classifiers on imbalanced data. ((Takaya Saito, 2015) , (Jesse Davis, 2006)

6. Methodology - Results

In this thesis the dataset analyzed before, was split into 3 excel files, Low Risk-Medium Risk, Low Risk-High Risk and Medium Risk-High Risk. Each one had 127 features and the two classes mentioned above. Python coding was chosen for its' time efficiency and easy implementation of libraries.

6.1 Naïve Bayes Classifier

Due to the nature of the data, a Gaussian Naïve Bayes Classifier was chosen. Each class was tested by Shapiro Wilks test for gaussian distribution. The result was that many features do not exhibit gaussian distribution. This has little influence on classifier that was chosen, because it has shown that it works well even without gaussian data distribution.

A stratified k-fold Cross-Validation was used, with k=5 and k=10. The goal was to maintain class proportions even if the dataset was imbalanced.

The algorithm was trained for classification with each one of 127 features. For each feature, metrics such as sensitivity, auc, f1 score, accuracy, tpr, fpr and specificity were calculated. After all folds where tested, the mean values for these metrics were calculated and the next feature was used to repeat the procedure. All ROC AUC Curves, accuracy, sensitivity, specificity and F1 Scores were saved and the list is presented below. For assessing the classifier performance with imbalanced data AUC and F1 Score perform better, but for comparison with the existing PhD that the dataset that was initially created, the other metrics were also calculated. The code shows the classifier and the metrics that are saved for each feature.

```
for feat in ft:
    f= dataset_arx[[feat]].values
    sens_list= []; spec_list = []; tpr_list = []; auc_list = []; f1_list = []; acc_list = []
    mean_fpr= np.linspace( start: 0,  stop: 1,  num: 100)

    for train_idx, test_idx in cv.split(f, newl):
        f_train, f_test = f[train_idx], f[test_idx]
        s_train, s_test = newl[train_idx], newl[test_idx]

        nb.fit(f_train, s_train)
        y_prob= nb.predict_proba(f_test)[:, 1]

        y_pred= nb.predict(f_test)
        fpr, tpr, _= roc_curve(s_test, y_prob)
        auc_val= auc(fpr, tpr)
        auc_list.append(auc_val)
```

The classifier provided the following results for each spreadsheet, for 5-fold and 10-fold Cross-Validation (LR-MR, MR-HR, LR-HR). Features presented in bold writing have AUC≥0.81:

Low Risk – High Risk 5-fold CV

Feature	Average AUC	Accuracy	F1-Score	Sensitivity	Specificity
Area'	**1**	0,935	0,95923	0,952564	0,833333
'Perimeter'	**0,994444**	0,934167	0,959333	0,952564	0,866667
'MajorAxisLength'	**0,994444**	0,921667	0,952541	0,969231	0,7
'MinorAxisLength'	**0,994444**	0,960833	0,975304	0,967949	0,933333
'ConvexArea'	**1**	0,960833	0,975304	0,967949	0,933333
'EquivDiameter'	**1**	0,935	0,95923	0,952564	0,833333
'Std'	**0,821368**	0,841667	0,908466	0,966667	0,233333
'Range'	**0,816667**	0,829167	0,906294	1	0
'Energy'	**0,983761**	0,935	0,959333	0,953846	0,866667
'CONT^a'	**0,867094**	0,83	0,893678	0,887179	0,566667
'CONT^r'	**0,877778**	0,83	0,891114	0,871795	0,633333
'SOQ^r'	**0,828632**	0,7625	0,832346	0,728205	0,933333
'SAV^r'	**0,983333**	0,921667	0,951259	0,952564	0,766667
'SVAR^r'	**0,895299**	0,855833	0,904278	0,870513	0,766667
'DVAR^a'	**0,867094**	0,83	0,893678	0,887179	0,566667
'DVAR^r'	**0,884615**	0,83	0,891114	0,871795	0,633333
'JAV^r'	**0,983333**	0,921667	0,951259	0,952564	0,766667
'LRE^r'	**0,922222**	0,816667	0,896215	0,969231	0,066667
'GLNU^a'	**0,944444**	0,908333	0,945157	0,969231	0,633333
'GLNU^r'	**0,972222**	0,908333	0,944541	0,953846	0,7
'RLNU^a'	**0,844872**	0,908333	0,945157	0,969231	0,633333
'RLNU'	**0,850427**	0,908333	0,945157	0,969231	0,633333
'LGRE^a'	**0,839744**	0,894167	0,9407	1	0,4
'LGRE^r'	**0,82906**	0,8425	0,913173	1	0,1
'LRLGE^a'	**0,816667**	0,83	0,903093	0,969231	0,166667
'LRLGE^r'	**0,866667**	0,816667	0,896215	0,969231	0,066667
'RLV^a'	**0,829915**	0,816667	0,896215	0,969231	0,066667
'RLV^r'	**0,927778**	0,816667	0,896215	0,969231	0,066667
'W MV^cH'	**0,891453**	0,7225	0,810617	0,760256	0,533333
'W STD^cH'	**0,858547**	0,843333	0,909931	0,969231	0,233333
'W STD^cD'	**0,869231**	0,869167	0,922986	0,953846	0,466667

Low Risk – Medium Risk 5-fold CV

Feature	Average AUC	Accuracy	F1-Score	Sensitivity	Specificity
'Std'	**0,825071**	0,800433	0,701056	0,605556	0,935897
'MeanAbsoluteDeviation'	**0,825214**	0,819481	0,7397	0,652778	0,935897
'COR^a'	**0,880698**	0,763636	0,647863	0,588889	0,891026
'SENTR^a'	**0,825285**	0,820346	0,760984	0,725	0,889744
'IMC1^r'	**0,814886**	0,783117	0,752435	0,813889	0,762821
'IMC2^a'	**0,818875**	0,782251	0,734827	0,769444	0,796154
'IMC2^r'	**0,831766**	0,792208	0,767737	0,861111	0,747436
'CLP^r'	**0,811467**	0,679221	0,422857	0,336111	0,920513
'SRE^a'	**0,82386**	0,698701	0,569744	0,538889	0,807692
'RLNU^a'	**0,811538**	0,755411	0,616061	0,511111	0,921795
'RLNU'	**0,821011**	0,736364	0,593035	0,488889	0,90641
'LGRE^a'	**0,847151**	0,794372	0,729598	0,744444	0,825641
'SRHGE^a'	**0,814316**	0,699134	0,55619	0,463889	0,860256
'SRHGE^r'	**0,821083**	0,717749	0,584048	0,491667	0,871795
'W MIN^cH'	**0,833191**	0,763636	0,704188	0,702778	0,814103
'W RNG^cH'	**0,830769**	0,716017	0,610299	0,555556	0,828205
'W MDAD^cV'	**0,88255**	0,831169	0,782745	0,75	0,889744
'W MAX^cD'	**0,834972**	0,688745	0,541709	0,502778	0,807692
'W RNG^cD'	**0,848575**	0,716883	0,627368	0,602778	0,79359

Medium Risk – High Risk 5-fold CV

Feature	Average AUC	Accuracy	F1-Score	Sensitivity	Specificity
'Area'	**0,865741**	0,839394	0,900585	0,955556	0,466667
'Perimeter'	**0,867593**	0,839394	0,899346	0,933333	0,533333
'MajorAxisLength'	**0,87037**	0,801515	0,871663	0,883333	0,533333
'MinorAxisLength'	**0,935185**	0,839394	0,901754	0,955556	0,5
'ConvexArea'	**0,878704**	0,839394	0,900585	0,955556	0,466667
'EquivDiameter'	**0,865741**	0,839394	0,900585	0,955556	0,466667
'Skewness'	**0,841667**	0,771212	0,860819	0,933333	0,233333
'Kurtosis'	**0,831481**	0,822727	0,892442	0,955556	0,4
'Maximum'	**0,943981**	0,912121	0,942251	0,952778	0,766667
'Range'	**0,952315**	0,892424	0,928849	0,927778	0,766667
'QCD'	**0,830556**	0,768182	0,868271	1	0
'CONT^a'	**0,948148**	0,857576	0,901667	0,863889	0,866667
'CONT^r'	**0,907407**	0,839394	0,878077	0,844444	0,866667
'COR^a'	**0,898148**	0,819697	0,874814	0,866667	0,7
'COR^r'	**0,87963**	0,730303	0,777857	0,683333	0,933333
'SOQ^a'	**0,936111**	0,856061	0,902415	0,888889	0,766667
'SAV^r'	**0,938889**	0,836364	0,893791	0,883333	0,666667
'SVAR^a'	**0,928704**	0,856061	0,902415	0,888889	0,766667

'SVAR^r'	**0,948148**	0,875758	0,914902	0,886111	0,866667
'SENTR^a'	**0,814815**	0,731818	0,841398	0,933333	0,1
'DVAR^a'	**0,974074**	0,859091	0,908095	0,886111	0,8
'DVAR^r'	**0,922222**	0,857576	0,897857	0,866667	0,866667
'JAV^r'	**0,938889**	0,836364	0,893791	0,883333	0,666667
'ACOR^a'	**0,87037**	0,75	0,841254	0,863889	0,433333
'CLS^a'	**0,82037**	0,783333	0,860836	0,880556	0,466667
'CLS^r'	**0,856481**	0,751515	0,834967	0,816667	0,566667
'CLP^a'	**0,962037**	0,856061	0,902415	0,888889	0,766667
'CLP^r'	**0,922222**	0,839394	0,88387	0,844444	0,866667
'LRE^r'	**0,917593**	0,768182	0,868271	1	0
'HGRE^a'	**0,844444**	0,786364	0,863846	0,886111	0,5
'LRLGE^r'	**0,826852**	0,768182	0,868271	1	0
'GLRV^a'	**0,972222**	0,856061	0,902251	0,888889	0,8
'RLV^r'	**0,864815**	0,768182	0,868271	1	0
'W STD^cH'	**0,886111**	0,875758	0,923791	0,977778	0,566667
'W MIN^cV'	**0,867593**	0,875758	0,923392	0,975	0,533333
'W STD^cV'	**0,847222**	0,804545	0,882101	0,952778	0,333333
'W STD^cD'	**0,896296**	0,948485	0,968235	0,977778	0,866667

Low Risk – High Risk 10-fold CV

Feature	Average AUC	Accuracy	F1-Score	Sensitivity	Specificity
Area'	**1**	0,948214	0,967459	0,966667	0,8
'Perimeter'	**1**	0,948214	0,966061	0,95	0,9
'MajorAxisLength'	**1**	0,948214	0,967459	0,966667	0,8
'MinorAxisLength'	**1**	0,9625	0,975152	0,966667	0,9
'ConvexArea'	**1**	0,9625	0,975152	0,966667	0,9
'EquivDiameter'	**1**	0,948214	0,967459	0,966667	0,8
'Maximum'	**0,832143**	0,830357	0,906374	1	0
'Range'	**0,821429**	0,830357	0,906374	1	0
'Energy'	**0,963095**	0,935714	0,958368	0,95	0,85
'CONT^a'	**0,891667**	0,833929	0,89653	0,904762	0,55
'CONT^r'	**0,902381**	0,832143	0,884802	0,869048	0,65
'SOQ^r'	**0,838095**	0,7625	0,825455	0,728571	0,95
'SAV^r'	**0,975**	0,935714	0,959883	0,966667	0,75
'SVAR^r'	**0,941667**	0,858929	0,903893	0,871429	0,8
'DVAR^a'	**0,891667**	0,833929	0,892334	0,888095	0,6
'DVAR^r'	**0,910714**	0,832143	0,883776	0,854762	0,7
'JAV^r'	**0,975**	0,935714	0,959883	0,966667	0,75
'LRE^a'	**0,835714**	0,817857	0,897582	0,983333	0
'LRE^r'	**0,966667**	0,830357	0,906374	1	0
'GLNU^a'	**0,960714**	0,910714	0,945524	0,966667	0,6
'GLNU^r'	**0,969048**	0,908929	0,9431	0,95	0,7
'RLNU^a'	**0,879762**	0,910714	0,945524	0,966667	0,6

'RLNU'	**0,888095**	0,910714	0,945524	0,966667	0,6
'LGRE^a'	**0,859524**	0,869643	0,926154	0,983333	0,25
'LGRE^r'	**0,87619**	0,844643	0,914066	1	0,1
'LRLGE^a'	**0,865476**	0,844643	0,909487	0,966667	0,2
'LRLGE^r'	**0,857143**	0,817857	0,897582	0,983333	0
'RLV^a'	**0,888095**	0,817857	0,897582	0,983333	0
'RLV^r'	**0,933333**	0,830357	0,906374	1	0
'W MV^cH'	**0,890476**	0,751786	0,827416	0,778571	0,65
'W STD^cH'	**0,852381**	0,869643	0,926227	0,983333	0,3
'W STD^cD'	**0,891667**	0,880357	0,93033	0,966667	0,45

Low Risk – Medium Risk 10-fold CV

Feature	Average AUC	Accuracy	F1-Score	Sensitivity	Specificity
'COR^a'	**0,862976**	0,765455	0,627381	0,59	0,883333
'SENTR^a'	**0,823452**	0,822727	0,758413	0,725	0,888095
'IMC1^r'	**0,812857**	0,774545	0,737399	0,81	0,745238
'IMC2^a'	**0,822024**	0,783636	0,731667	0,765	0,792857
'IMC2^r'	**0,827381**	0,792727	0,763658	0,855	0,745238
'SRE^a'	**0,833214**	0,69	0,579394	0,565	0,780952
'SRE^r'	**0,810357**	0,785455	0,740159	0,75	0,816667
'RLNU^a'	**0,812024**	0,753636	0,619841	0,515	0,921429
'RLNU'	**0,813452**	0,743636	0,604762	0,49	0,919048
'LGRE^a'	**0,867976**	0,801818	0,748687	0,775	0,82381
'SRHGE^a'	**0,82381**	0,715455	0,576905	0,52	0,852381
'SRHGE^r'	**0,825238**	0,708182	0,543254	0,49	0,857143
'GLRV^a'	**0,844048**	0,691818	0,613919	0,63	0,730952
'W MIN^cH'	**0,826071**	0,730909	0,6421	0,6	0,819048
'W RNG^cH'	**0,821429**	0,713636	0,604762	0,55	0,821429
'W MDAD^cV'	**0,869286**	0,832727	0,780794	0,75	0,888095
'W MAX^cD'	**0,84381**	0,694545	0,557222	0,51	0,828571
'W RNG^cD'	**0,853214**	0,734545	0,645476	0,605	0,82619

Medium Risk – High Risk 10-fold CV

Feature	Average AUC	Accuracy	F1-Score	Sensitivity	Specificity
'Area'	**0,88**	0,84	0,899242	0,955	0,45
'Perimeter'	**0,9125**	0,843333	0,899242	0,935	0,55
'MajorAxisLength'	**0,905**	0,82	0,882179	0,905	0,55
'MinorAxisLength'	**0,93**	0,84	0,901465	0,955	0,45
'ConvexArea'	**0,905**	0,84	0,899242	0,955	0,45
'EquivDiameter'	**0,88**	0,84	0,899242	0,955	0,45
'Skewness'	**0,8475**	0,796667	0,875354	0,94	0,35
'Kurtosis'	**0,8575**	0,863333	0,912374	0,95	0,55
'Maximum'	**0,9375**	0,913333	0,94329	0,955	0,8
'Range'	**0,9625**	0,893333	0,92583	0,925	0,8

'CONT^a'	**0,8875**	0,846667	0,891941	0,86	0,75
'CONT^r'	**0,835**	0,85	0,882222	0,84	0,8
'COR^a'	**0,925**	0,833333	0,882179	0,865	0,75
'COR^r'	**0,8625**	0,743333	0,763889	0,69	0,95
'SOQ^a'	**0,915**	0,883333	0,915512	0,91	0,8
'SAV^a'	**0,8275**	0,826667	0,897576	0,96	0,4
'SAV^r'	**0,9625**	0,86	0,901984	0,885	0,85
'SVAR^a'	**0,895**	0,883333	0,915512	0,91	0,8
'SVAR^r'	**0,9025**	0,88	0,909004	0,88	0,8
'DVAR^a'	**0,92**	0,88	0,911544	0,86	0,9
'DVAR^r'	**0,895**	0,866667	0,899278	0,88	0,75
'JAV^a'	**0,8275**	0,826667	0,897576	0,96	0,4
'JAV^r'	**0,9625**	0,86	0,901984	0,885	0,85
'ACOR^a'	**0,865**	0,756667	0,841782	0,865	0,4
'CLS^a'	**0,85**	0,8	0,872893	0,9	0,5
'CLS^r'	**0,825**	0,773333	0,839322	0,82	0,6
'CLP^a'	**0,975**	0,846667	0,887338	0,86	0,8
'CLP^r'	**0,9075**	0,88	0,910159	0,885	0,8
'LRE^r'	**0,8625**	0,77	0,868283	1	0
'NGLNU^a'	**0,8175**	0,713333	0,823608	0,91	0,1
'GLRV^a'	**0,975**	0,863333	0,899481	0,89	0,8
'RLV^r'	**0,8625**	0,77	0,868283	1	0
'W STD^cH'	**0,8425**	0,873333	0,923485	0,975	0,45
'W MIN^cV'	**0,8475**	0,873333	0,923088	0,975	0,5
'W STD^cD'	**0,82**	0,95	0,967532	0,975	0,8

In 5-fold Cross-Validation, there are 31 features in the LR-HR dataset, 19 features in the LR-MR dataset and 37 features in the MR-HR dataset that have Average AUC>0.81.

In 10-fold Cross-Validation, there are 32 features in the LR-HR dataset, 18 features in the LR-MR dataset and 35 features in the MR-HR dataset that have Average AUC>0.81.

Changing from 5-fold to 10-fold Cross-Validation provides minimal differences in the number of features that their Average AUC exceeds 0.81. The features in the MR-HR dataset performed best in the discrimination between classes, while the fewest features with Average AUC>0.81 for classification were found in the LR-MR dataset.

It is important to note that despite the similar results of 5-fold and 10-fold Cross-Validation, only two features were common in both LR-MR and MR-HR datasets. These were SENTR^a and GLRV^a with AUC 0.823 and 0.844 respectively and in the MR-HR dataset with a marginal AUC of 0.805 and 0.975 respectively. These

features can be further tested to assess whether they can be potential features that can facilitate the distinction between lesion classification.

6.2 Minimum Redundancy – Maximum Relevance Results

To calculate the Redundancy and Relevance of each dataset, mutual_info_classif and mutual_info_regression was used, from sklearn.feature_selection. For the features that were available and for dimensionality reduction, the top 10% was chosen to be reported, resulting in 13 features for each dataset.

Low Risk – Medium Risk

Feature	Relevance	Redundancy
'SENTR^a'	0,326153	0
'LGRE^a'	0,257712	0,017488
'W MIN^cH'	0,181143	0,048929
'ACOR^r'	0,116397	0,009673
'W MDAD^cV'	0,315752	0,198319
'MeanAbsoluteDeviation'	0,301738	0,194332
'W RNG^cD'	0,267222	0,176521
'COR^a'	0,244831	0,155204
'SRE^r'	0,184628	0,106776
'GLNU^a'	0,138009	0,087851
'SRHGE^r'	0,237565	0,185254
'IMC1^r'	0,146294	0,092211
'Maximum'	0,18521	0,138948

The selected features that have both high relevance and low redundancy are SENTR^a, which provided 0 redundancy. Features with high relevance and higher redundancy are W MDAD^cV and MeanAbsoluteDeviation.

Compared to the 5-fold Cross-Validation of the Naïve Bayes Classifier, SENTR^a had an average AUC 0.825, LGRE^a an AUC value of 0.847, W MDAD^cV an AUC of 0.882 and MeanAbsoluteDeviation an AUC of 0.825. There are features with relevance values lower than 0.3 that performed well, such as, COR^a with AUC of 0.880, SRHGE^r with AUC of 0.821, W RNG^nD with AUC of 0.849. The features with the highest relevance and lowest redundancy performed very well within the context of the 5-fold CV Bayesian classifier. Also features with high relevance and higher redundancy performed equally well.

With the 10-fold Cross-Validation, SENTR^a had an average AUC of 0.823, W MDAD^cV an AUC of 0.869, MeanAbsoluteDeviation is not on the features that had AUC>0.81, with features with lower relevance exhibiting better AUC values, such as LGRE^a with AUC of 0.867, COR^a with AUC of 0.863, SRHGE^r with AUC of 0.825 and W RNG^cD with AUC of 0.853.

The top 10% most relevant features selected by the mRMR algorithm, include the features that performed best in the Naïve Bayes Classifier in both 5-fold and 10-fold Cross-Validation. This shows that the mRMR algorithm effectively identified features with strong predictive potential for distinguishing low risk and medium risk cases, which reinforces the feature selection process.

Low Risk – High Risk

Feature	Relevance	Redundancy
'MinorAxisLength'	0,385604	0
'GLRV^r'	0,192776	0,0451
'W MV^cH'	0,151528	0,03474
'LRE^r'	0,197907	0,110119
'RLNU^a'	0,183834	0,126291
'W MIN^cD'	0,099867	0,043047
'SAV^r'	0,369664	0,299796
'W MED^cD'	0,075454	0,035615
'Std'	0,131474	0,087569
'Energy'	0,290678	0,230084
'W STD^cD'	0,248956	0,18655
'SRLGE^a'	0,114166	0,069622
'LGRE^r'	0,153647	0,126522

The feature with the maximum relevance is MinorAxisLength with also 0 redundancy, followed by SAV^r and Energy with a value slightly below 0.3. which had higher values of redundancy, suggesting overlap with other selected features.

In the 5-fold Cross-Validation with Naïve Bayes Classifier, MinorAxisLength provided an Average AUC of 0.994, SAV^r an AUC of 0.983, Energy an AUC of 0.984, W STD^cD an AUC of 0.0.869. Many features provided average AUC of 1 and were not predicted by the mRMR algorithm. The highest relevance-lowest redundancy feature provided by the mRMR algorithm was in the top 3 AUC values and also had the top F1-Score, along with ConvexArea, which had an AUC of 1.

In the 10-fold Cross-Validation, MinorAxisLength provided an Average AUC of 1, SAV^r an AUC of 0.975 and Energy and AUC of 0.963. MinorAxisLength had the highest AUC and F1-Score of 0.975. Features that also had the highest AUC and equally high F1-Score were not in the most relevant list of the mRMR algorithm.

The results of the mRMR algorithm show that MinorAxisLength is a feature which carries high relevance and can be used for the distinction between Low Risk and High-Risk cases, as it was exhibited by both 5-fold and 10-fold Cross-Validation NB classifier results. Also, features that perfomed very well in both versions of the classifier were predicted by the mRMR algorithm as features with high relevance, even if their redundancy was higher than the top feature.

Medium Risk – High Risk

Feature	Relevance	Redundancy
'SVAR^r'	0,377617	0
'Kurtosis'	0,190802	0,038385
'W STD^cD'	0,37315	0,200964
'LRLGE^r'	0,166846	0,10581
'ACOR^a'	0,289133	0,194185
'W MIN^cV'	0,21842	0,134612
'GLRV^a'	0,331609	0,255713
'W MV^cH'	0,114045	0,053267
'SENTR^r'	0,133414	0,068784
'CLP^r'	0,317625	0,252583
'SOQ^r'	0,194561	0,147599
'Maximum'	0,317597	0,275109
'GLRV^r'	0,239659	0,197494

In this matrix, SVAR^r exhibited the highest relevance and 0 redundancy, with features W STD^cD, GLRV^a and CLP^r contributing strongly but with higher redundancy.

In 5-fold Cross-Validation with Naïve Bayes Classifier, SVAR^r had an average AUC of 0.929, GLRV^a an AUC of 0.972, CLP^r an AUC of 0.922 and W STD^cD an AUC of 0.896. The feature with the highest AUC was not in the results of the mRMR algorithm, but the GLRV^a was the second best in terms of AUC value, even with higher redundancy value.

In 10-fold Cross-Validation, SVAR^r average AUC was 0.903, GLRV^a AUC was 0.975, CLP^r was 0.908 and W STD^cD an AUC of 0.820. In this version of the classifier, the feature with the highest AUC was GLRV^a along with CLP^a, with a higher F1-Score of 0.899 and 0.887 respectively. The most relevant feature did not

have the best performance, instead a feature with a higher redundancy value performed best.

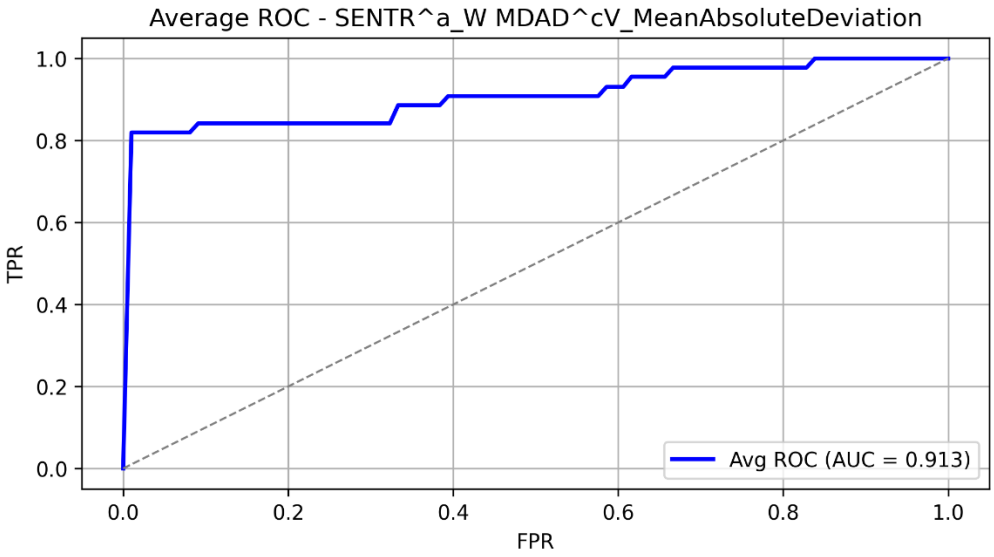
Again, in both Cross-Validation methods, the mRMR algorithm is able to provide features that have both high relevance and are significant for the class distinction between Medium Risk and High-Risk cases. Also, the specific classifier that was used in the previous section shows that the features that had high relevance were among the best performing features, with AUC above 0.81.

It is important to note that the features which were both included in the 10-fold Cross-Validation of the Naïve Bayes Classifier exhibit high relevance, strengthening their importance for classification.

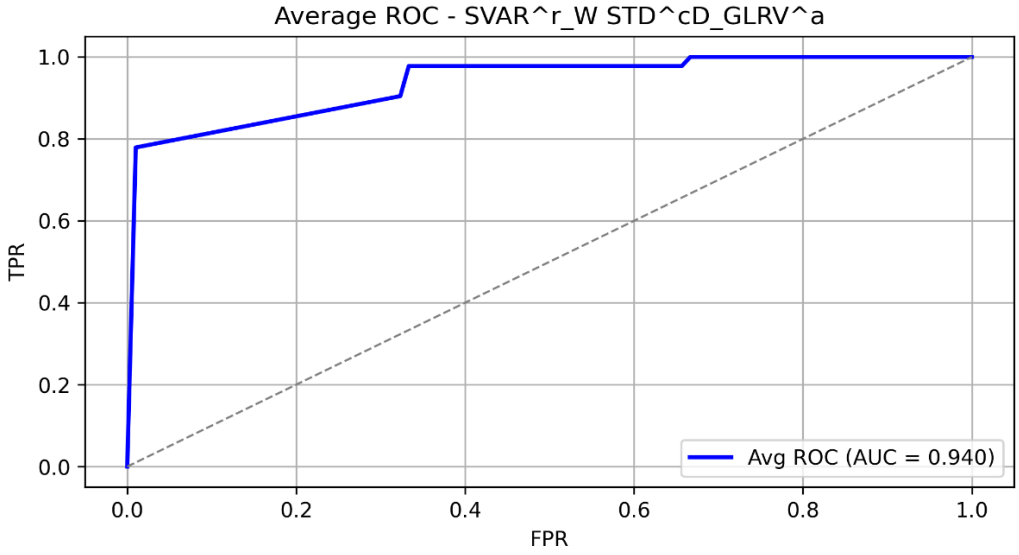
In total, the mRMR algorithm performed its' task for feature selection in each dataset, confirming that the features that were predicted each time were significant for proper classification.

Now the top 3 features of each dataset will be used together in the Naïve Bayes Classifier with 5-fold Cross-Validation.

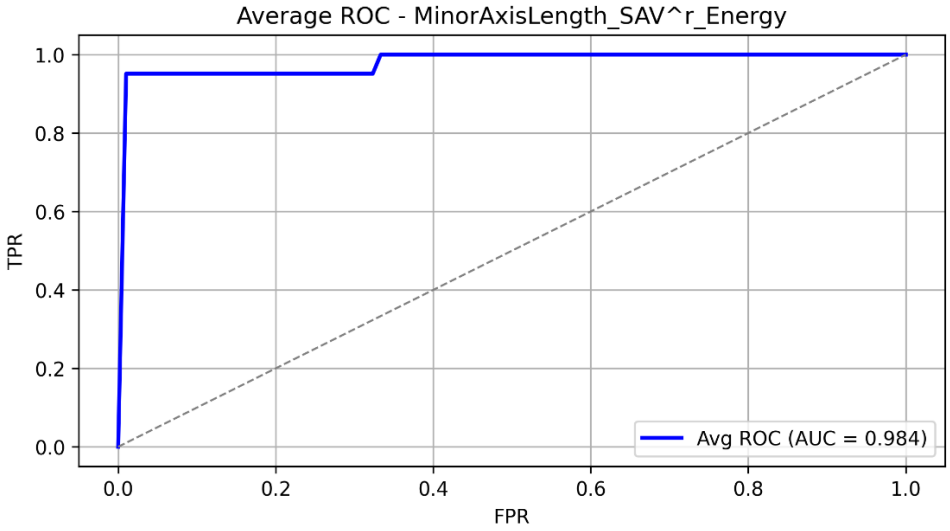
Low Risk Medium Risk Results					
Features	**Average_AUC**	**Accuracy**	**F1_Score**	**Sensitivity**	**Specificity**
SENTR^a_W MDAD^cV_MeanAbsolute Deviation	0,913105	0,877056	0,837484	0,794444	0,935897



Medium Risk High Risk Results					
Features	**Average_AUC**	**Accuracy**	**F1_Score**	**Sensitivity**	**Specificity**
SVAR^r_W STD^cD_GLRV^a	0,939815	0,893939	0,931471	0,933333	0,8



Low Risk High Risk Results					
Features	**Average_AUC**	**Accuracy**	**F1_Score**	**Sensitivity**	**Specificity**
MinorAxisLength_SAV^r_Energy	0,983761	0,935	0,959333	0,953846	0,866667



Results show that the combination of the features that have high relevance (0.3) in all datasets provide AUC values above 0.90. Specifically, the classifier provided for the

LR-MR dataset best performance, with AUC of 0.983, for the MR-HR dataset an AUC of 0.939 and for the LR-MR dataset an AUC of 0.913. Combining the features provides robustness to the model and high performance.

6.3 Random Forest Feature Importance Results

The algorithm implemented a 5-fold Cross-Validation with StratifiedKFold from sklearn.model_selection, permutation_importance, shap and for model evaluation, roc_auc_score, average_precision_score, f1_score. The results are presented in the following tables.

Low Risk – High Risk Results

MDI Ranking		SHAP Ranking	
Feature	**MDI**	**Feature**	**SHAP**
'MinorAxisLength'	0,085153	'MinorAxisLength'	0,042682
Area'	0,081722	'EquivDiameter'	0,039848
'JAV^r'	0,077816	'ConvexArea'	0,034516
'EquivDiameter'	0,072994	'SAV^r'	0,033691
'SAV^r'	0,06678	'JAV^r'	0,032354
'Perimeter'	0,064585	Area'	0,030741
'ConvexArea'	0,058698	'Perimeter'	0,028959
'MajorAxisLength'	0,05624	'MajorAxisLength'	0,023191
'GLNU^a'	0,040062	'CONT^r'	0,019422

We see that SHAP values are low, with MinorAxisLength being the feature with the highest value of 0.042682, followed by EquivDiameter=0.039848, ConvexArea=0.034516, JAV^r=0.035354, SAV^r=0.033691, Area=0.30741, Perimeter=0.028959, MajorAxisLength=0.023191, CONT^r=0.019422 and Energy=0.015141, This are the top 10 features based on SHAP values. These values are small in magnitude, indicating that individual features make modest contributions to predictions. Lower values are also something to be expected, as the dataset was small, with 13 high risk cases. The maximum tree depth was limited to 10, to avoid overfitting, with trees not exceeding average depth of 5.

Based on MDI ranking, the highest-ranking features were MinorAxisLength=0.085153, Area=0.081722, JAV^r=0.077816, EquivDiameter=0.072994, SAV^r=0.06678, Perimeter=0.064585, ConvexArea=0.058698, MajorAxisLength=0.05624, GLNU^a=0.040062 and Energy=0.036647. The features listed have contributed more to reducing impurity, specifically the top 3 listed, meaning they are more important in the model's decision making.

Permutation Importance has provided mostly 0 values, except Area, ConvexArea, MinorAxisLength, EquivDiameter and Energy with equal values to 0.005. For smaller datasets permutation is expected to provide these results.

Although permutation results were not informative, MinorAxisLength, EquivDiameter and Area had consistently higher values in both SHAP and MDI calculation. This shows that not only were these features that contributed to the classification result (SHAP), but they were frequently chosen for splits, contributed more to reducing impurity across the forest and the model relied on them to make predictions (MDI). Even for permutation, these features provided a low but non-zero result, but it cannot be correctly assessed.

Low Risk – Medium Risk Results

MDI Ranking		SHAP Ranking	
Feature	**MDI**	**Feature**	**SHAP**
'W MDAD^cV'	0,045858	'W RNG^cD'	0,020456
'SRE^a'	0,041003	'IMC2^r'	0,019811
'W MAX^cD'	0,037428	'W MDAD^cV'	0,019705
'IMC2^r'	0,035628	'COR^a'	0,017092
'MeanAbsoluteDeviation'	0,035455	'SENTR^a'	0,01667
'Std'	0,035318	'IMC1^r'	0,01636
'ENTR^a'	0,032449	'W MAX^cD'	0,015507
'SENTR^a'	0,02853	'W MIN^cH'	0,015446
'LGRE^a'	0,028157	'IMC2^a'	0,014271

Here the highest SHAP values are W RNG^cD=0.2046, IMC2^r=0.1981, W MDAD^cV=0.0197, COR^a=0.01709, SENTR^a=0.01667, IMC1^r=0.01636, W MAX^cD=0.01551, W MIN^cH=0.01545, IMC2^a=0.01427 and MeanAbsolutDeviation=0.01425.

Based on MDI ranking the top ten features are W MDAD^cV=0.04585, SRE^a=0.04100, W MAX^cD=0.03742, IMC2^r=0.03562, MeanAbsoluteDeviation=0.03545, Std=0.03531, ENTR^a=0.03245, SENTR^a=0.02853, LGRE^a=0.02815 and W RNG^cD=0.02643.

Permutation Importance yielded the following top ten results, W RNG^cH= 0,01632, MedianAbsoluteDeviation=0,00952, IQR=0,00952, CLS^a=0,00952,

MeanAbsoluteDeviation=0,00952, IMC2^r=0,00952, RLNU=0,00857, NGLNU^a=0,00762, COR^a=0,00762 and Area=0,00667.

Based on the results, W RNG^cD contributed the most to the classification result, but with lower MDI value, had less contribution in reducing impurity across the forest. Highest MDI was shown by W MDAD^cV, which had significant contribution to the classification result, along with IMC2^r and MAX^cD.

Medium Risk – High Risk Results

MDI Ranking		SHAP Ranking	
Feature	**MDI**	**Feature**	**SHAP**
'JAV^r'	0,066326	'JAV^r'	0,030158
'DVAR^r'	0,058353	'SAV^r'	0,023176
'SVAR^r'	0,048044	'CLP^r'	0,023068
'DVAR^a'	0,04642	'CLP^a'	0,021635
'GLRV^a'	0,045492	'SVAR^r'	0,020295
'CLP^a'	0,045	'Maximum'	0,019028
'Maximum'	0,042507	'DVAR^a'	0,018991
'SAV^r'	0,041554	'DVAR^r'	0,017986
'W STD^cD'	0,038803	'W STD^cD'	0,017691

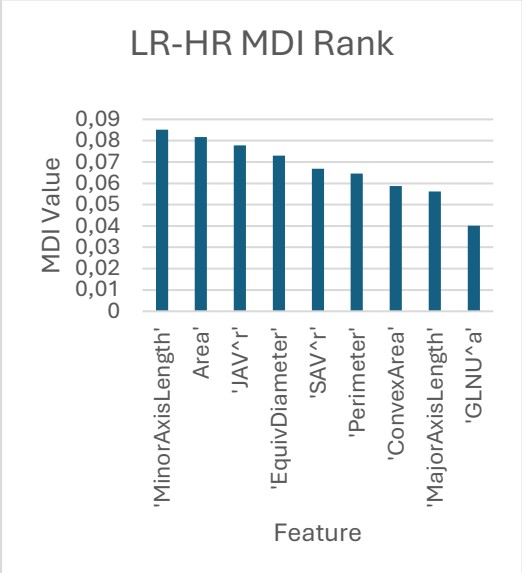
Based on SHAP values, highest contribution to the classification was exhibited by JAV^r=0,03016, followed by SAV^r=0,02318, CLP^r=0,02307, CLP^a=0,02164, SVAR^r=0,02029, Maximum=0,01902, DVAR^a=0,01899, DVAR^r=0,01799, W STD^cD=0,01769 and GLRV^a=0,01680.

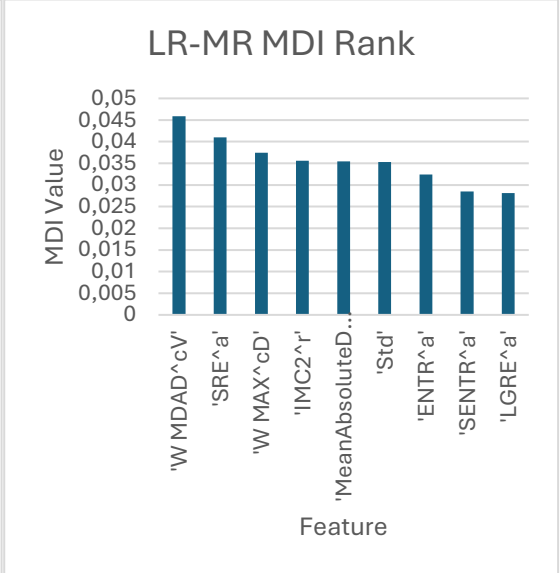
MDI Values provided the results JAV^r=0,06633, DVAR^r=0,05835, SVAR^r=0,04804, DVAR^a=0,04642, GLRV^a=0,04549, CLP^a=0,04499, Maximum=0,04251, SAV^r=0,04155, W STD^Cd=0,03880 and Range=0,03817.

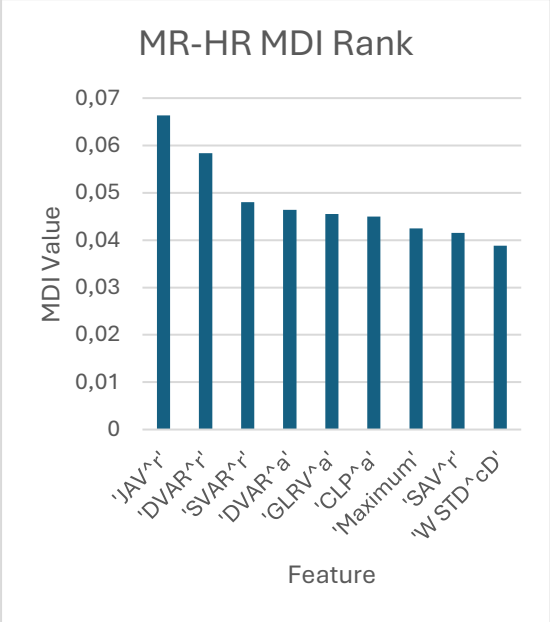
Permutation Importance provided Maximum and GLRV^a with 0.016818, W STD^cD, W RNG^cV, W STD^cH, CLS^r, W MIN^cV with 0.016667 and CLP^a, CLP^r and RANGE with 0.015.

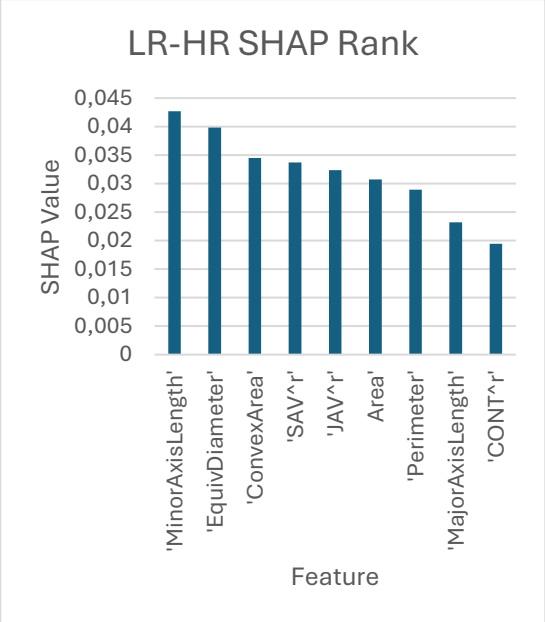
JAV^r, with highest values in both SHAP and MDI, indicating that the model relies on this feature for decision-making and that it contributes to the prediction.

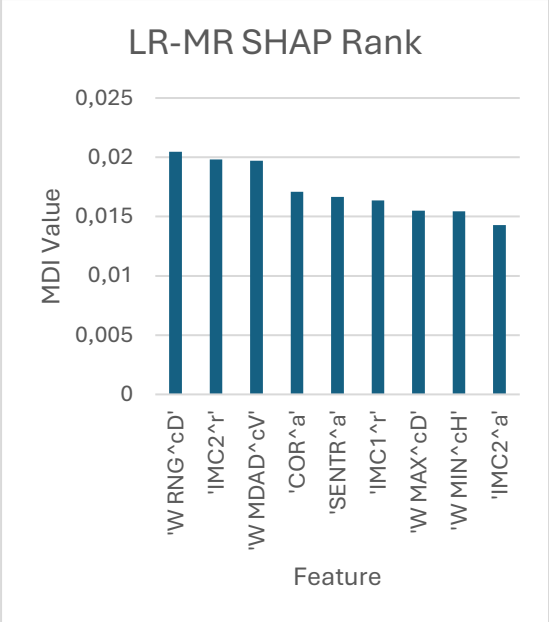
Below there are graphs according to each dataset, with the nine features with the highest MDI and SHAP rank.

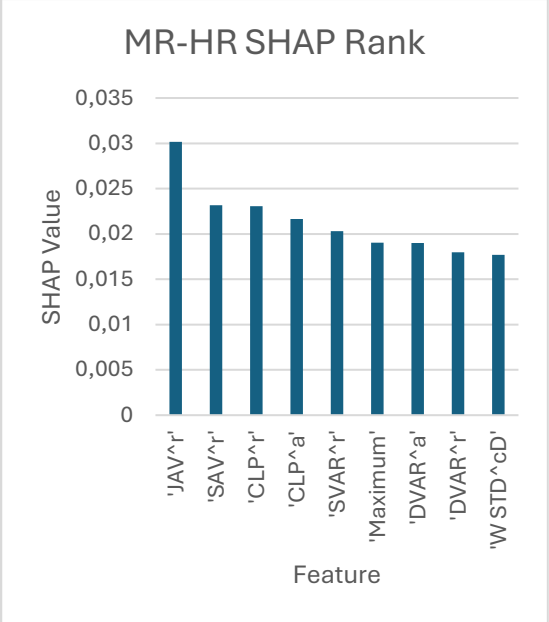












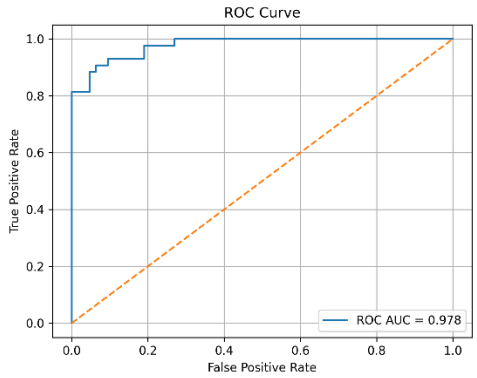
6.3.1 Model Evaluation

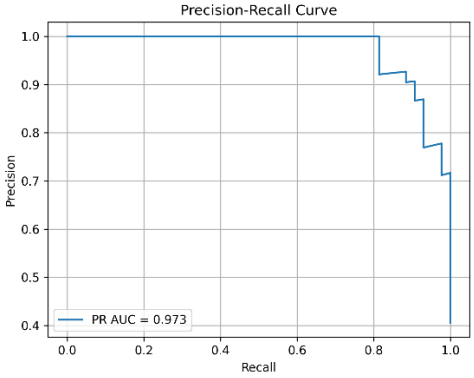
The model was evaluated using 5-fold Cross-Validation with AUC ROC, Precision-Recall AUC and F1-Score to ensure that the previously presented results were generated by an algorithm that is trustworthy. Precision-Recall AUC was chosen because it is a highly sensitive metric for imbalanced classes, emphasizing in correctly identifying the minority class.

As the table below shows, all the calculated metrics are overly optimistic. Overfitting is unlikely because shallow trees were used. Due to a small dataset, a few correctly classified cases can affect scores disproportionately. As for class imbalance, it also can amplify PR-AUC and F1-Score. Small test folds in 5-fold Cross-Validation can lead to inflated metrics.

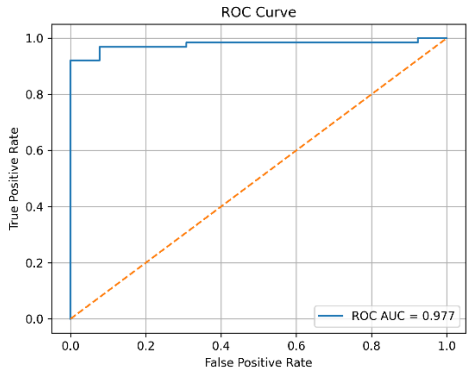
Low Risk – Medium Risk		Low Risk – High Risk		Medium Risk – High Risk	
Metric	Value	Metric	Value	Metric	Value
AUC ROC	**0.977852**	AUC ROC	**0.976801**	AUC ROC	**0.980322**
AUC PR	**0.972546**	AUC PR	**0.995718**	AUC PR	**0.994059**
F1 Score	**0.891566**	F1 Score	**0.976**	F1 Score	**0.965517**

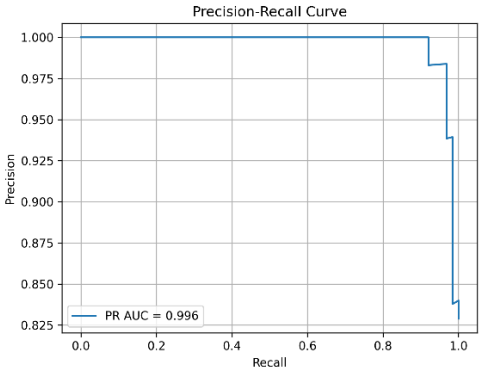
LR-MR RFFI Evaluation



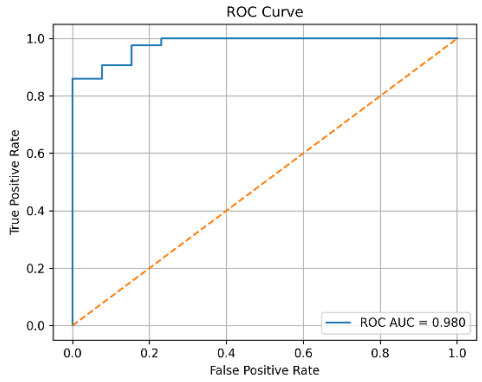


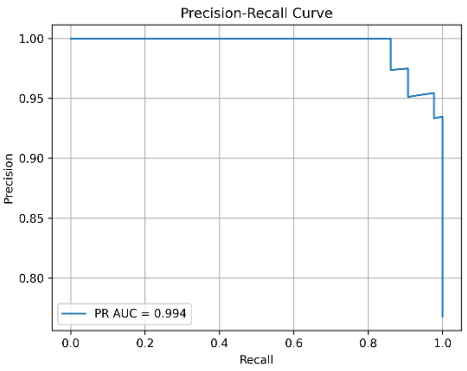
LR-HR RFFI Evaluation





MR-HR RFFI Evaluation





6.4 Comparison of Random Forest Feature Importance Results with mRMR and Naïve Bayes Classifier Results

Feature importance derived from the Random Forest provides information on what features are likely informative. These rankings are model-specific and should be used

as a starting point for feature selection in other classifiers, such as the Naïve Bayes that was tested before. The following comparison was done with the AUC values that were produced by the Naïve Bayes Classifier with 5-fold Cross-Validation, as minimal difference was present between 5-fold and 10-fold.

Low Risk Medium Risk Dataset										
Feature	**mRMR rank**	**SHAP**	**SHAP rank**	**Permutation**	**Perm. rank**	**MDI**	**MDI rank**	**Average AUC**	**Accuracy**	**F1-Score**
'W RNG^cD'	7	0,020456	1	0,005714	17	0,026432	10	0,848575	0,716883	0,627368
'W MDAD^cV'	5	0,019705	3	0,005714	15	0,045858	1	0,88255	0,831169	0,782745
'COR^a'	8	0,017092	4	0,007619	9	0,026155	11	0,880698	0,763636	0,647863
'SENTR^a'	1	0,01667	5	0,005714	14	0,02853	8	0,825285	0,820346	0,760984
'IMC1^r'	12	0,01636	6	-0,00654	127	0,024794	13	0,814886	0,783117	0,752435
'W MIN^cH'	3	0,015446	8	0,00381	21	0,017096	24	0,833191	0,763636	0,704188
'MeanAbsoluteDeviation'	6	0,014248	10	0,009524	2	0,035455	5	0,825214	0,819481	0,7397
'LGRE^a'	2	0,012865	15	0,003117	24	0,028157	9	0,847151	0,794372	0,729598
'SRHGE^r'	11	0,007251	26	0,005714	16	0,017817	22	0,821083	0,717749	0,584048

For the LR-MR dataset, SENTR^a has the highest relevance and zero redundancy as mentioned before, providing highly informative signal for predicting the target class, as supported by the performance of the Naïve Bayes classifier, with AUC=0.825. With SHAP values, the feature is ranked 5th and 8th in MDI showing that it contributes moderately to predictions and is used less frequently in tree splits. This shows that even if the feature is highly informative, the RF structure and splitting preferences affect how much it is used. W RNG^cD has the highest SHAP value, indicating it strongly influences predictions in the RF, it has a moderate to low MDI value. It is a feature which was not highly predictive of the target, as it was assessed by mRMR algorithm, but performed well in the Naïve Bayes classifier showing that it still contributes to the predictive performance, with AUC=0.849. W MDAD^cV is the feature that had the highest AUC in the NB classifier, it was frequently used in splits of the RFFI algorithm, it was highly contributing to predictions and was a feature with high relevance according to the mRMR algorithm. Its' performance in both RF and NB classifier demonstrates that it might be a feature candidate for generalization well across other models except those that were tested here.

Low Risk High Risk Dataset										
Feature	**mRMR rank**	**SHAP**	**SHAP rank**	**Permutation**	**Perm. rank**	**MDI**	**MDI rank**	**Average AUC**	**Accuracy**	**F1-Score**
'MinorAxisLength'	1	0,042682	1	0,005	1	0,085153	1	0,994444	0,960833	0,975304
'SAV^r'	7	0,033691	4	0	6	0,06678	5	0,983333	0,921667	0,951259
'Energy'	10	0,015141	10	0,005	1	0,036647	10	0,983761	0,935	0,959333
'W STD^cD'	11	0,014274	11	0	6	0,026813	12	0,869231	0,869167	0,922986
'RLNU^a'	5	0,006117	17	0	6	0,025094	13	0,844872	0,908333	0,945157
'Std'	9	0,004424	24	0	6	0,004555	32	0,821368	0,841667	0,908466
'LRE^r'	4	0,004148	25	0	6	0,010118	24	0,922222	0,816667	0,896215
'LGRE^r'	13	0,003415	29	0	6	0,007214	26	0,82906	0,8425	0,913173
'W MV^cH'	3	0,000921	47	0	6	0,002151	41	0,891453	0,7225	0,810617

The feature MinorAxisLength performed exceptionally well in NB classifier, with an AUC=0.994. It had the highest relevance and zero redundancy according to the mRMR algorithm and has the highest rank in the RF feature importance metrics. Apart from that, SAV^r and Energy also contribute to RF model predictions but not as significantly as the previous feature. Both features also perform well in the NB classifier, demonstrating good predictive performance across models.

The exceptional performance of a morphological feature as MinorAxisLength can be expected, as the dataset is comprised of Low Risk and High-Risk cases, which are more likely to have morphological differences that help the distinction of each case.

Medium Risk High Risk Dataset										
Feature	**mRMR rank**	**SHAP**	**SHAP rank**	**Permutation**	**Perm. rank**	**MDI**	**MDI rank**	**Average AUC**	**Accuracy**	**f1_score**
'CLP^r'	10	0,023068	3	0,015	8	0,019864	16	0,922222	0,839394	0,88387
'SVAR^r'	1	0,020295	5	-0,01091	125	0,048044	3	0,948148	0,875758	0,914902
'Maximum'	12	0,019028	6	0,016818	1	0,042507	7	0,943981	0,912121	0,942251
'W STD^cD'	3	0,017691	9	0,016667	3	0,038803	9	0,896296	0,948485	0,968235
'GLRV^a'	7	0,0168	10	0,016818	1	0,045492	5	0,972222	0,856061	0,902251
'W MIN^cV'	6	0,015432	11	0,016667	3	0,015596	18	0,867593	0,875758	0,923392
'ACOR^a'	5	0,010422	15	0	25	0,018016	17	0,87037	0,75	0,841254
'Kurtosis'	2	0,004964	27	-0,01091	125	0,01058	24	0,831481	0,822727	0,892442
'LRLGE^r'	4	0,0022	42	0	25	0,006669	38	0,826852	0,768182	0,868271

The feature SVAR^r was the feature with highest relevance and zero redundancy and has high MDI value. Its' negative permutation value suggests that shuffling the values

of the feature improves the performance of the RF model, meaning that this feature might be noisy or introduces instability. While the feature is informative on its' own, it is redundant or destabilizing within the RF algorithm, where other correlated features might already encode similar information, and given that the dataset is small, class imbalance is present, shallow trees were chosen to prevent overfitting and features have correlations.

The feature GLRV^a achieved exceptional performance in the NB classifier with AUC=0.9722 and had the second highest relevance according to the mRMR algorithm. It had both moderate contribution in splitting trees (MDI) and contributing to class prediction (SHAP).

7. Related work

The search for papers regarding melanoma classification with machine learning methods was done with keywords such as melanoma classification, Machine learning, svm, random forests, knn, k-nearest neighbor, decision trees, naïve Bayes, mRMR, random forest feature importance.

Murugan, Nair and Kumar 2019, used dermoscopic images, preprocessed with a median filter. Segmentation was done using a watershed algorithm, and feature extraction was also based on the ABCD rule, Gray Level co-occurrence Matrix features and shape features. Between the three classifiers, accuracy was highest in SVM for ABCD rule, shape feature and GLCM feature, with highest, the ABCD rule (89.43%). SVM outperforms the other algorithms, in which KNN performed the poorest in all features. (Murugan A., 2019)

Howal et al. 2025, used 25,000 dermoscopic pictures of skin lesions, such as melanoma, nevus and benign keratosis, found in the ISIC 2019 dataset. A CNN that consists of multiple Conv2D layers was used for feature extraction and three traditional machine learning algorithms were used for classification. CNN-SVM had the most accuracy (89.30%), Precision (91.10%), Recall (88.20%) and F1-Score (89.60%) and AUC 0.92. (Howal S., 2025)

Li et al., 2014, used images acquired from a spectroscopic system. Features were extracted based on statistical measurements and were fed to 3 different classifiers, an Artificial Neural Network, a Naive Bayes Classifier, and a k-Nearest Neighbor classifier. The best performance was achieved by the Naïve Bayes Classifier, with accuracy of 0.89. (Li L., 2014)

Putri et al. 2020, used the ISIC and HAM10000 datasets to apply a Naïve Bayes Classifier, with features extracted using Local Binary Pattern (LBP). The dataset had 9 different types of skin diseases. The classifier was applied to different dataset sizes, with the best accuracy of 94.44% appearing on the dataset with 90 cases, supporting that the classifier performs well with small datasets. (Putri H., 2020)

Akilandasowmya et al. 2024, used the Kaggle and ISIC datasets and extracted features with the SCSO-ResNet50 technique from pre-processed data. Feature optimization was done with EHS algorithm and ensemble classification was implemented with the Naïve Bayes Classifier, along with Random Forest, kNN, SVM and Linear Regression. The results were fed to the CNN classifier. For SCSO-ResNet50-EHS-CNN model has a maximum accuracy of 92.035% for the Kaggle skin cancer dataset with 20% test samples, and for the ISIC 2019 94.238%. (Akilandasowmya G., 2024)

Hoxha et al. 2025, used tissue index images from RGB imaging and hyperspectral imaging (HSI), fed into machine learning classifiers. For feature selection, a minimum Redundancy-maximum Relevance algorithm was used, resulting in the most important features to improve classification. Specifically, for tumor and peritumor classification, mRMR was used to provide features that were highly effective in the discrimination between the two classes. The final classification was split into 3 scenarios, with only RGB images, only tissue index images and their combination, providing accuracy of 0.8773 and 0.9175. (Hoxha D., 2025)

Khaleel and Lakizadeh, 2025, used the HAM10000 dataset and applied AlexNet, ResNet-50 and GoogleNet for feature extraction. A minimum redundancy maximum relevance algorithm was applied for the selection of the most relevant features, again enhancing the accuracy of classification. Classification was performed the bagging algorithm, yielding accuracy of 98.9% and F1-Score of 98.88% (Khaleel M., 2025).

Dalmolin et al. 2024, used ML models combined with explainable artificial intelligence to identify the most influential genes in the classification of five recurrent cancer types in women, breast cancer, lung adenocarcinoma, thyroid cancer, ovarian cancer and colon adenocarcinoma. Specifically, used Decision Trees, Random Forest and XGBoost, achieving accuracy of 98.69%, 99.82% and 99.37% respectively. For explainability reasons, SHAP was used to generate a list of features to understand which characteristics influenced the models' decision making. It identified genes that represented the 0.8% of the initial input features, increasing the confidence in the model and explainability. (Dalmolin M., 2024)

Pattnaik et al. 2025, used a dataset of 8000 dermoscopic images of 4 different classes. Classification was done with Random Forest and Gradient Boosted Decision Trees, after hyperparameter optimization by Bayesian search with 5-fold Cross-Validation. Gradient Boosted Decision Trees achieved accuracy of 89% and Random forest 86% and both achieved AUC>0.94. Shapley Additive Explanations was used to interpret feature contributions and was in agreement with established dermatological heuristics. (Pattnaik S., 2025)

Taraseviciene et al. 2024, used a small dataset and 662 extracted features, both for conventional image features and graph-based features from a superpixel graph using Delaunay triangulation. They were used for binary and 5-class classification of skin lesions, using MDI and SHAP value thresholds to identify the most important features for classification. The classification was performed for all features and for features that MDI and SHAP thresholds indicated as important. The best performance was achieved by the SHAP-based features, with performance metric F1-Score and weighted F1-Score as 0.9667 and 0.9248 for binary classification and 0.7213 and 0.7121 for 5-class classification, respectively. (Taraseviciene A., 2024)

Khater et al. 2023, applied multiple ML algorithms such as XGBoost, decision tree, random forest and kNN to the preprocessed images available of PH^2 dataset. The best results were provided by XGBoost, with accuracy of 94% and AUC= 0.9947, exhibiting excellent performance. Explainable artificial intelligence (XAI) provided some explanations with model-agnostic methods such as partial dependence plot, permutation importance and SHAP. Based on XAI, asymmetry and pigment network traits are among the most crucial characteristics in evaluating if a lesion is benign or malignant and are supported by pre-existing medical understanding. (Khater T., 2023)

Deep learning algorithms and neural networks are being steadily applied with increasing frequency in classification problems, such as melanoma classification. SVMs and other classical machine learning methods have proven their use in these tasks, and probabilistic classifiers such as Naïve Bayes are used in different fields or are not used in isolation.

Although mRMR has been widely used in medical applications such as radiomics and cancer classification, few studies explore its' potential for melanoma feature selection and the application of the selected features to a Naïve Bayes classifier.

While feature importance and explainability methods such as SHAP, MDI/Gini Importance and Permutation importance have been applied in AI-based cancer and skin lesion classification, there are fewer recent studies that emphasize the use of

Random Forest Feature Importance for the interpretation of skin lesion classifiers. Below there is a table of the papers mentioned above.

Table of Related Publications

Author	Title	Dataset	Method	Accuracy	F1-Score	AUC
Murugan A., Nair S., Kumar K. (2019)	Detection of Skin Cancer Using SVM, Random Forest and kNN Classifiers	ISIC 2017 1000 Dermatoscopic Images	KNN, Random Forest, SVM	SVM ABCD rule 89.43%, Shape feature 82.31% GLCM 85.72%	-	-
Howal S., Wagh S., Patil S., Yelure B. (2025)	A Hybric CNN-SVM Approach for Skin Lesion Classification Using the ISIC 2019 Dataset	ISIC 2019	CNN used for feature extraction, SVM, RF & DT classifiers	CNN-SVM 89.30%	89.60%	0.92
Li L., Zhang Q., Ding Y., Jiang H., Thiers B., Wang J. (2014)	Automatic diagnosis of melanoma using machine learning methods on a spectroscopic system	Spectroscopic Images	ANN, Naïve Bayes, kNN	Naïve Bayes 0.892	-	-
Putri H., Sari C., Setiadi D., Rachmawanto (2020)	Classification of Skin Diseases Types using Naïve Bayes Classifier based on Local Binary Pattern Features	ISIC, HAM10000	Naïve Bayes + LBP	94.44%	-	-
Akilandasowmya G., Nirmaladevi G., Suganthi SU., Aishwariya A. (2024)	Skin cancer diagnosis: Leveraging deep hidden features and ensemble classifiers for early detection and classification	Kaggle, ISIC 2019	SCSO-ResNet50 + EHS + ensemble classification (Naïve Bayes, RF, kNN, SVM, LR+CNN	92.04% (Kaggle) 94.24% (ISIC)	-	-
Hoxha D., Krt A., Stergar J., Tomanic T., Groselj A., Sersa G., Milanic M. (2025)	Skin Lesion Classification in Head and Neck Cancers Using Tissue Index Images Derived from Hyperspectral Imaging	RGB+HIS tissue images	mRMR+ ML classifiers	0.8773-0.9175	-	-
Khaleel M., Lakizadeh A. (2025)	Skin cancer diagnosis using hybrid deep pre-trained convolutional neural networks	HAM10000	mRMR+Bagging	98.9%	98.88%	-
Dalmolin M., Azevedo K., Souza L., Farias C., Lichtenfels M., Fernandes M. (2024)	Feature Selection in Cancer Classification: Utilizing Explainable Artificial Intelligence to Uncover Influential Genes in Machine Learning Models	The Cancer Genome Atlas (TCGA)	Decision Tree, Random Forest, XGBoost + SHAP	98.69% 99.82% 99.37%	-	-
Pattnaik S., Pattnaik S., Khalid M., Leo S., Sidhu G. (2025)	Skin Lesion Image Classification With Tree-Based Ensembles: Benchmarking Random Forest and Gradient Boosting	8000 dermoscopic images	Random Forest, Gradient Boosted Trees + SHAP	86% RF, 89% GBT	-	>0.94
Taraseviciene A., Sutiene K., Dimsa N., Valiukeviciene S. (2024)	Enhancing Multi-Class Prediction of Skin Lesions with Feature Importance Assessment	Small Dataset with 662 features	MDI, SHAP & no Threshold applied	0.9667 (binary), 0.7213 (5-class)	0.9248 (binary, weighted) 0.7121 (5-class, weighted)	-
Khater T., Ansari S., Mahmoud S., Hussain A., Tawfik H. (2023)	Skin cancer classification using explainable artificial intelligence on pre-extracted image features	PH^2 dataset	XGBoost, RF, kNN, Decision Tree +XAI	94% XGBoost	-	0.9947

8. Discussion

8.1 Naïve Bayes Classifier

The results of the classifier show that features that contain morphological information about the lesion perform exceptionally well in the Low Risk-High Risk dataset, regardless of the type of Cross-Validation. This can be expected due to the vast differences that can be observed in low-risk lesions in comparison to malignant lesions and is already demonstrated by the high use of the ABCD rule, which is based on morphological information. Features that are derived from Gray Level Run Length Matrix (GLRLM) analysis like GLNU^a, GLNU^r, RLNU^a and RLNU convey information about texture, heterogeneity and grey-level variability. In malignant lesions, these tend to have higher values, and thus, better ability to differentiate between classes.

For the Low Risk-Medium Risk dataset, features like SENTR^a, IMC2^r, RLNU^r, RLNU, LGRE^a, SRHGE^a, SRHGE^r and W MDAD^cV appear to perform very well in both 5 and 10-fold Cross-Validation. These features capture information about texture heterogeneity, gray-level non-uniformity and directional intensity variations. Differences are present between the two CV methods, with 5-fold CV having some first-order intensity statistics performing better, while 10-fold CV has higher order texture information features that perform better.

For the Medium Risk-High Risk dataset, in both CV methods, features with higher performance convey information about morphology, texture and heterogeneity. These include Area, Perimeter, MinorAxisLength, MajorAxisLength, ConvexArea and EquivDiameter. Texture features such as CONT, COR, SVAR, DVAR, CLP, HGRE and W STD describe heterogeneity and spatial intensity patterns within lesions. They encode tissue irregularity and complexity and perform well for risk differentiation.

Murugan, Nair and Kumar (2019) used kNN, Random Forest and SVM, extracted GLCM, shape and ABCD rule-based features. Accuracy was highest (89.43%) when SVM used ABCD rule-based features. This shows that even when a different classifier is implemented, morphological features provide enough information for the distinction between classes, something that is also shown in the MR-LR and LR-HR dataset of this study.

A study by Oukil et al. (2021), assesses the results of kNN, SVM and ANN, with features extracted in five different color spaces. It used the PH^2 dataset and achieved 99.51% accuracy with the SVM classifier. It solely uses color spaces for classification and a

widely used dataset, in contrast with the present study, which used a dataset with 119 cases in total and is highly imbalanced.

Also, Li (2023) extracted shape features, texture features using GLCM and color features. This is in line with the extracted features that this also study uses. Different SVM Linear Regression and Gaussian Naïve Bayes classifiers with 100-fold randomization method were applied with highest performance of the SVM rbf and SVM poly with AUC of 0.766 equally. Gaussian Naïve Bayes had the poorest performance, with AUC=0.691, with the ISIC and PH^2 dataset and after recursive feature elimination. This study evaluates the robustness of a Gaussian NB classifier for 3 different subsets of a small sized dataset, enabling a more fine-tuned analysis of feature behavior.

Kalloniati (2023), used the same dataset this study uses, to compare an SVM, a Linear Regression and a Random Forest algorithm, and reported that the LR algorithm performed best across all datasets. Specifically, for the MR-HR dataset SAV^r had AUC=0.953, for the LR-MR COR^a had AUC=0.858 and for the LR-HR dataset MinorAxisLength with AUC=0.991. The results from the Gaussian NB classifier that was used here, morphological features performed exceptionally in MR-HR and LR-HR datasets, with the highest AUC value equal to 1 for Area, ConvexArea and EquivDiameter in LR-MR dataset, and MinorAxisLength 0.935 in MR-HR dataset, and W MDAD^cV for LR-MR dataset with AUC 0.882 for 5-fold CV. For 10-fold CV the same features perform equally well.

8.2 Minimum Redundancy – Maximum Relevance

The algorithm was used only as a feature ranking method separately from the Gaussian NB classifier. The features from each dataset that provided relevance higher than 0.3 were then combined for classification in the classifier.

For the LR-MR dataset, the features with the highest relevance (>0.3) were SENTR^a, W MDAD^cV and MeanAbsoluteDeviation. SENTR^a is a GLCM texture feature that is based on entropy. It describes the degree of randomness and complexity in gray-level spatial distribution. W MDAD^cV is a measure of mean absolute deviation, which is a coefficient of variation. It provides information on how the intensity values vary across the lesion, relative to the overall intensity. MeanAbsoluteDeviation is a first-order statistical feature which measures the mean absolute deviation from the mean intensity and indicates overall variability in pixel values. Their higher relevance indicates that increased textural heterogeneity and higher variation in intensity are significant factors that can be implemented to differentiate LR and MR cases.

For the LR-HR dataset, MinorAxisLength and SAV^r had relevance higher than 0.3. Energy had marginally lower value. MinorAxisLength is a morphological feature that measures the shorter axis of the lesion. SAV^r (Short Area Variance) is a Gray Level Size Zone Matrix (GLSZM) texture feature that highlights small homogeneous zones in the lesion. Higher values indicate more heterogeneous fine-scaled texture. Lastly, having a marginally lower relevance than the threshold, Energy, is a first-order feature that provides information about overall intensity uniformity, with higher values indicating more uniform intensity distributions. Higher relevance shows that the lesion shape differences are important for LR HR differentiation, as was also mentioned before. Also, internal structural and intensity patterns have a significant role in LR-HR differentiation.

For the MR-HR dataset, SVAR^r, W STD^cD and GLRV^a had the highest relevance values. SVAR^r (Short-Run Variance) is a texture feature that measures the variability in lengths of short runs of pixels with similar intensity. W STD^cD provides information about intensity variability regions the lesion that have lower intensity. GLRV^a (Gray-Level Run Variance) is a GLRLM texture feature that measures the variance of consecutive pixel intensity runs and is a measure of texture heterogeneity along a direction. Higher relevance values show that irregular fine-texture patterns, heterogeneity in darker regions and texture irregularity have a significant role in MR-HR differentiation.

The combination of the top three features in each dataset was used for classification with the Naïve Bayes Classifier with 5-fold Cross Validation. The reduction of features provided results that showed performance improvement, further supporting that higher relevance features contribute meaningfully to the classification, indicating that these features could be prioritized for future projects.

Multiple studies that implement the Minimum Redundancy-Maximum Relevance feature selection method are available, with Hoxha et al. (2025) and Khaleel and Lakizadeh (2025), being some of the most relevant. In these studies, the use of mRMR provided in each instance, better results. Tian (2026) in his study with an RF model with deep learning-based radiomics features for melanoma diagnosis, reports as key predictive indicators entropy, a first-order statistic, long-run emphasis and wavelet contrast. (Z., 2026) To comment on the most relevant features of each dataset, morphological features have strong predictive potential for low and high risk cases. Texture features can be used for a finer assessment of medium and high risk as well as low and medium cases.

8.3 Random Forest Feature Importance

The results of the algorithm showed that for each dataset, there were features that had significantly higher contributions to the decision making of the RF, compared to each other.

Specifically, for the Low Risk-High Risk dataset, SHAP ranking highlighted that morphological features, such as MinorAxisLength, EquivDiameter, ConvexArea were the most influential for the model's prediction. This is in agreement with what was mentioned previously regarding morphological feature importance for Low-High Risk case classification. Following, features like SAV^r and JAV^r, which reflect variability among small and larger homogeneous regions respectively, had also high SHAP values, suggesting that internal textural heterogeneity was significantly influential in model predictions. Based on MDI ranking, the same categories of features were ranked the highest. Morphological and GLSZM features were used most frequently in tree splits. Permutation did not perform well as a importance metric in this dataset, so it cannot be properly assessed. What needs to be noted is that a non-zero value was recorded for features that had high MDI and SHAP values.

For the Low Risk-Medium Risk dataset, features capturing intensity variability and textural heterogeneity, were ranked higher in both SHAP and MDI importance. Specifically, features with higher SHAP values, such as W RNG^cD, IMC2^r and W MDAD^cV, were associated with variability in local intensities and internal structure influence model predictions, while MDI values highlighted features like SRE^a, W MAX^cD and IMC2^r, that measure both intensity extremes and textural patterns in different scales. These results suggest that both internal intensity and texture patterns are important characteristics that can distinguish between Low Risk-Medium Risk lesions. Permutation importance again did not provide adequate results, with highest value provided by the feature that had the highest SHAP rank.

For the Medium Risk-High Risk dataset, features like JAV^r and SAV^r that provide information about variability about large and small homogeneous regions, along with CLP^r and CLP^a reflecting cluster irregularity, had the highest influence in model predictions according to SHAP ranking. Based on MDI values, DVAR^r, GLRV^a and W STD^cD, features that capture multi-scale internal intensity and texture patterns, were more frequently used by the Random Forest to reduce impurity. These results, show again that internal intensity and texture organization are important for the distinction between Medium and High-Risk lesions. Permutation highlighted Maximum and GLRV^a as most important.

The overall model was assessed with F1-Score, AUC and PR-AUC, as it is more sensitive to class imbalance. The model assessment results indicate that the performance is overly optimistic. This means that the feature importance results should be considered as an indication of importance compared with the results of the previous sections of mRMR and the Naïve Bayes Classifier, as reported to the Results section, to support the importance of the features that performed well in the classification algorithm and also were selected in the feature extraction algorithm.

It is important to note that this comparison showed that features like MinorAxisLength, W MDAD^cV, SENTR^a and SAV^r, that performed well in the Naïve Bayes Classifier, when used in the Random Forest algorithm, were influenced by correlations with other features and the tree-building process, which limited their importance despite being highly informative.

9. Limitations

For the Naïve Bayes Classifier, a probability calibration was not applied. In addition, there are many features that do not follow Gaussian distribution. Although each feature was evaluated independently, the classifier might provide overconfident posterior probabilities. This is why the evaluation metrics reported are AUC and F1-Score, among others, so reported performance can have meaningful interpretation despite the lack of calibration.

For the Minimum Redundancy-Maximum Relevance algorithm, the smaller size of the datasets, Mutual Information that is used to calculate Relevance and Redundancy might be unstable. This might lead to the selection of weaker features and loss of features with higher importance. Also, the relevance and redundancy calculation was done with the whole dataset each time. This can produce noticeable data leakage for small datasets, which in turn can show overly optimistic results, when applied to a classifier.

In the Random Forest Feature Importance algorithm, permutation importance results were very unstable, not able to be assessed, which reflects the small dataset size. The model assessment results indicate that the performance is overly optimistic. This means that the feature importance results should be considered as an indication of importance compared with the results of the previous sections of mRMR and the Naïve Bayes Classifier, to compare the importance of the features that performed well in the classification algorithm and also were selected in the feature extraction algorithm.

10. Conclusion

This study demonstrates that both NB Classifier and mRMR algorithm provide results that are in agreement with current published studies and the empirical assessment that dermatologists use to classify lesions. This shows that, even with such a small and imbalanced dataset, a classical machine learning algorithm can be used effectively for lesion classification. The Minimum Redundancy Maximum Relevance algorithm highlighted as relevant for prediction, features that performed well in the previous classifier, while the Random Forest Feature Importance algorithm showed that the importance of features can be influenced significantly by the algorithm that uses them, as well as the dataset size. These findings provide both practical and methodological insights into future research in lesion classification.

While the dataset size makes it difficult to propose that certain features can be used for lesion classification, the findings show that assessment of these features should be done in larger datasets to examine their predictive ability.

11. Future Work

Future work could focus on overcoming the limitations of the current study, mainly by using a larger dataset. This could be done either by collecting more data from the hospital or applying data augmentation, if new data are not available. Application of Deep Learning algorithms could then be possible. Also, another method for feature extraction could be explored, to assess whether new predictive features can be obtained from the same dataset. Finally, features that were highly predictive of the target class in each dataset could be assessed further in larger datasets.

References

Abhineet Agarwal, A. K. Y. S. T. T. T., 2025. *Cornell University*. [Online]
Available at: https://arxiv.org/pdf/2307.01932
[Accessed December 2025].

Akilandasowmya G., N. G. S. S. A. A., 2024. Skin cancer diagnosis: Leveraging deep hidden features and ensemble classifiers for early detection and classification. *Biomedical Signal Processing and Control, Vol. 88, Part C.*.

Alpaydin, E., 2014. *Introduction to Machine Learning*. 3rd ed. ed. s.l.:The MIT Press.

Breiman, L., 2001. Random Forests. *Machine Learning*.

Carolin Strobl, A.-L. B. A. Z. T. H., 2007. Bias in random forest variable importance measures: Illustrations, sources and a solution. *BMC Bioinformatics*.

Dalmolin M., A. K. S. L. F. C. L. M. F. M., 2024. Feature Selection in Cancer Classification: Utilizing Explainable Artificial Intelligence to Uncover Influential Genes in Machine Learning Models. *AI*.

Ellis, C. M., 2024. *The Orange Book of Machine Learning: The essentials of making predictions using supervised regression and classification for tabular data*. [Online]
Available at: https://carl-mcbride-ellis.github.io/TOBoML/TOBoML.pd
[Accessed December 2025].

Gareth James., D. W. T. H. R. T., 2013. *An Introduction to Statistical Learning (7th ed.)*. s.l.:Springer.

Gilles Louppe, L. W. A. S. P. G., n.d. Understanding variable importances in forests of randomized trees.

Hanchuan Peng, F. L. C. D., 2005. Feature Selection Based on Mutual Information: Criteria of Max-Dependency, Max-Relevance and Min-Redundancy. *IEEE TRANSACTIONS ON PATTERN ANALYSIS AND MACHINE INTELLIGENCE*.

Hancock, J. K. T. &. J. J., 2023. Evaluating classifier performance with highly imbalanced Big Data. *Journal of Big Data 10, 42*, pp. https://link.springer.com/article/10.1186/s40537-023-00724-5.

Howal S., W. S. P. S. Y. B., 2025. A Hybrid CNN-SVM Approach for Skin Lesion Classification Using the ISIC 2019 Dataset.

Hoxha D., K. A. S. J. T. T. G. A. S. G. M. M., 2025. Skin Lesion Classification in Head and Neck Cancers Using Tissue Index Images Derived from Hyperspectral Imaging. *Cancers (Basel)*.

Jesse Davis, M. G., 2006. *University of Winsconsin Computer Sciences*. [Online]
Available at: https://pages.cs.wisc.edu/~shavlik/abstracts/davis.icml06.abstract.html
[Accessed December 2025].

Khaleel M., L. A., 2025. Skin cancer diagnosis using hybrid deep pre-trained convolutional neural networks. *International Journal of Artificial Intelligence* .

Khater T., A. S. M. S. H. A. T. H., 2023. Skin cancer classification using explainable artificial intelligence on pre-extracted image features. *Intelligent Systems with Applications*.

Li L., Z. Q. D. Y. J. H. T. B. W. J., 2014. Automatic diagnosis of melanoma using machine learning methods on a spectroscopic system. *BMC Medical Imaging*.

Li Z., J. Q. Y. X. Z. Y. Z. S., 2023. An Identification Method of Feature Interpretation for Melanoma Using Machine Learning. *Applied Sciences*.

Makandar A., S. A., 2025. Melanoma: A Computer-Aided Diagnosis using the ABCD Rule.

Marghoob, A. R. D. &. K., 2025. *Congenital melanocytic nevi*. [Online]
Available at: https://www.ncbi.nlm.nih.gov/books/NBK470214/
[Accessed 10 December 2025].

Mitchel, T., 1997. *Machine Learning*. s.l.:McGraw-Hill Science/Engineering/Math.

Molnar, C., 2022. *Interpretable Machine Learning*. s.l.:s.n.

Murugan A., N. S. K. K., 2019. Detection of Skin Cancer Using SVM, Random Forest, and kNN Classifiers.

Pattnaik S., P. S. K. M. L. S. S. G., 2025. Skin Lesion Image Classification With Tree-Based Ensembles: Benchmarking Random Forest and Gradient Boosting. *Cureus*.

Putri H., S. C. S. D. R., 2020. Classification of Skin Diseases Types using Naive Bayes Classifier based on Local Binary Pattern Features. *International Seminar on Application for Technology of Information and Communication (iSemantic)*.

Scott M. Lundberg, G. G. E. S.-I. L., 2018. Consisten Individualized Feature Attribution for Tree Ensembles.

Scott M. Lundberg, S.-I. L., 2017. A unified approach to interpreting model predictions.. *Advances in Neural Information Processing Systems.*.

Şeref Kerem Çorbacıoğlu, G. A., 2023. *National Library of Medicine*. [Online]
Available at: https://pmc.ncbi.nlm.nih.gov/articles/PMC10664195/
[Accessed December 2025].

Stuart J. Russell, P. N., 2021. *Artificial Intelligence: A Modern Approach*. 4th ed. ed. s.l.:Pearson Education .

Takaya Saito, M. R., 2015. *National Library of Medicine*. [Online]
Available at: https://pubmed.ncbi.nlm.nih.gov/25738806/
[Accessed December 2025].

Taraseviciene A., S. K. D. N. V. S., 2024. Enhancing Multi-Class Prediction of Skin Lesions with Feature Importance Assessement. *International Journal of Applied Mathematics and Computer Science*.

Tian, Z., 2026. A deep learning-based radiomics model for noninvasive diagnosis of melanoma. *Melanoma Research*, February.

Walter F., P. A. V. J. H. P. B. N. M. H. K. A. E. J., 2013. Using the 7-point checklist as a diagnostic aid for pigmented skin lesions in general practice: a diagnostic validation study. *British Journal of General Practice*.

Ward W., L. F. G. N. Y. J. F. J., 2017. Clinical Presentation and staging of Melanoma. In: *Cutaneous Melanoma: Etiology and Therapy*. s.l.:s.n., pp. p. 79-89.

Ward W., L. G., 2017. *Iowa Head and Neck Protocols*. [Online]
Available at: https://iowaprotocols.medicine.uiowa.edu/protocols/melanoma-evaluation-and-management-8th-edition-ajcc
[Accessed December 2025].

Z., T., 2026. A deep learning-based radiomics model for noninvasive diagnosis of melanoma. *Melanoma Research*, February.

Zhenyu Zhao, R. A. M. W., 2019. Maximum Relevance and Minimum Redundancy Feature Selection Methods for a Marketing Machine Learning Platform.

A. Lallas, Z. A. E. I. D. L., 2020. *DERMATOSCOPY A-Z*. s.l.:s.n.

Καλλονιάτη, Ε., 2023. *ΚΛΙΝΙΚΑ ΚΑΙ ΔΕΡΜΑΤΟΣΚΟΠΙΚΑ ΧΑΡΑΚΤΗΡΙΣΤΙΚΑ ΜΕΛΑΝΟΚΥΤΤΑΡΙΚΩΝ ΑΛΛΟΙΩΣΕΩΝ ΤΟΥ ΔΕΡΜΑΤΟΣ: ΣΥΣΧΕΤΙΣΗ ΜΕ ΤΑ ΙΣΤΟΠΑΘΟΛΟΓΙΚΑΕΥΡΗΜΑΤΑ ΚΑΙ ΑΝΑΛΥΣΗ ΕΙΚΟΝΑΣ*. Πατρα: s.n.

Appendix

i. Naïve Bayes Results

Low Risk – High Risk 5-fold CV

Feature	Average AUC	Accuracy	F1-Score	Sensitivity	Specificity
Area'	**1**	0,935	0,95923	0,952564	0,833333
'Perimeter'	**0,994444**	0,934167	0,959333	0,952564	0,866667
'Eccentricity'	0,351709	0,829167	0,906294	1	0
'MajorAxisLength'	**0,994444**	0,921667	0,952541	0,969231	0,7
'MinorAxisLength'	**0,994444**	0,960833	0,975304	0,967949	0,933333
'ConvexArea'	**1**	0,960833	0,975304	0,967949	0,933333
'EquivDiameter'	**1**	0,935	0,95923	0,952564	0,833333
'Solidity'	0,617949	0,829167	0,904097	0,969231	0,2
'Extent'	0,537179	0,8425	0,912074	0,984615	0,2
'Compactness'	0,750855	0,8425	0,910934	0,969231	0,266667
'Mean'	0,587179	0,829167	0,906294	1	0
'Std'	**0,821368**	0,841667	0,908466	0,966667	0,233333
'Skewness'	0,583761	0,815833	0,898358	0,984615	0
'Kurtosis'	0,586752	0,816667	0,895536	0,952564	0,133333
'Median'	0,604487	0,829167	0,906294	1	0
'Minimum'	0,71688	0,829167	0,906294	1	0
'P10th'	0,556624	0,829167	0,906294	1	0
'P90th'	0,723077	0,828333	0,904762	0,984615	0,066667
'Maximum'	0,792521	0,829167	0,906294	1	0
'IQR'	0,675641	0,815833	0,89658	0,967949	0,066667
'Range'	**0,816667**	0,829167	0,906294	1	0
'MeanAbsoluteDeviation'	0,755128	0,828333	0,900488	0,951282	0,233333
'MedianAbsoluteDeviation'	0,703846	0,8025	0,887247	0,951282	0,066667
'CV'	0,590598	0,829167	0,906294	1	0
'QCD'	0,510684	0,829167	0,906294	1	0
'Energy'	**0,983761**	0,935	0,959333	0,953846	0,866667
'Entropy'	0,52735	0,815833	0,897747	0,983333	0
'ASM^a'	0,598291	0,830833	0,903663	0,969231	0,166667
'ASM^r'	0,625641	0,829167	0,906294	1	0
'CONT^a'	**0,867094**	0,83	0,893678	0,887179	0,566667
'CONT^r'	**0,877778**	0,83	0,891114	0,871795	0,633333
'COR^a'	0,579915	0,829167	0,906294	1	0
'COR^r'	0,641453	0,711667	0,824491	0,828205	0,2
'SOQ^a'	0,589316	0,829167	0,906294	1	0
'SOQ^r'	**0,828632**	0,7625	0,832346	0,728205	0,933333

'IDM^a'	0,453846	0,829167	0,906294	1	0
'IDM^r'	0,55812	0,829167	0,906294	1	0
'SAV^a'	0,621368	0,829167	0,906294	1	0
'SAV^r'	**0,983333**	0,921667	0,951259	0,952564	0,766667
'SVAR^a'	0,589316	0,829167	0,906294	1	0
'SVAR^r'	**0,895299**	0,855833	0,904278	0,870513	0,766667
'SENTR^a'	0,570513	0,829167	0,906294	1	0
'SENTR^r'	0,59359	0,841667	0,912698	1	0,066667
'ENTR^a'	0,483333	0,829167	0,906294	1	0
'ENTR^r'	0,554274	0,815833	0,897747	0,983333	0
'DVAR^a'	**0,867094**	0,83	0,893678	0,887179	0,566667
'DVAR^r'	**0,884615**	0,83	0,891114	0,871795	0,633333
'DENTR^a'	0,431624	0,815833	0,898358	0,984615	0
'DENTR^r'	0,605128	0,829167	0,906294	1	0
'IMC1^a'	0,44359	0,829167	0,906294	1	0
'IMC1^r'	0,562821	0,829167	0,906294	1	0
'IMC2^a'	0,575641	0,829167	0,906294	1	0
'IMC2^r'	0,523932	0,829167	0,906294	1	0
'MCCF^a'	0,631197	0,829167	0,906294	1	0
'MCCF^r'	0,580342	0,829167	0,906294	1	0
'JMX^a'	0,573504	0,830833	0,903663	0,969231	0,166667
'JMX^r'	0,776068	0,829167	0,906294	1	0
'JAV^a'	0,621368	0,829167	0,906294	1	0
'JAV^r'	**0,983333**	0,921667	0,951259	0,952564	0,766667
'DAV^a'	0,711966	0,829167	0,906294	1	0
'DAV^r'	0,732479	0,829167	0,906294	1	0
'IDF^a'	0,405128	0,829167	0,906294	1	0
'IDF^r'	0,497436	0,829167	0,906294	1	0
'NIDF^a'	0,635897	0,829167	0,906294	1	0
'NIDF^r'	0,688034	0,829167	0,906294	1	0
'ACOR^a'	0,594017	0,829167	0,906294	1	0
'ACOR^r'	0,586752	0,829167	0,906294	1	0
'CLS^a'	0,639316	0,829167	0,906294	1	0
'CLS^r'	0,670085	0,841667	0,9116	0,984615	0,133333
'CLP^a'	0,636325	0,8025	0,889811	0,969231	0
'CLP^r'	0,744017	0,801667	0,883506	0,938462	0,166667
'SRE^a'	0,567094	0,828333	0,904762	0,984615	0,066667
'SRE^r'	0,763248	0,815833	0,89597	0,966667	0,066667
'LRE^a'	0,765812	0,816667	0,896215	0,969231	0,066667
'LRE^r'	**0,922222**	0,816667	0,896215	0,969231	0,066667
'GLNU^a'	**0,944444**	0,908333	0,945157	0,969231	0,633333
'GLNU^r'	**0,972222**	0,908333	0,944541	0,953846	0,7
'RLNU^a'	**0,844872**	0,908333	0,945157	0,969231	0,633333
'RLNU'	**0,850427**	0,908333	0,945157	0,969231	0,633333
'RP^a'	0,378632	0,829167	0,906294	1	0
'RP^r'	0,382906	0,829167	0,906294	1	0

'LGRE^a'	**0,839744**	0,894167	0,9407	1	0,4
'LGRE^r'	**0,82906**	0,8425	0,913173	1	0,1
'HGRE^a'	0,649573	0,829167	0,906294	1	0
'HGRE^r'	0,697436	0,829167	0,906294	1	0
'SRLGE^a'	0,497863	0,829167	0,906294	1	0
'SRLGE^r'	0,617521	0,656667	0,774661	0,764103	0,166667
'SRHGE^a'	0,476496	0,829167	0,906294	1	0
'SRHGE^r'	0,673932	0,8025	0,888517	0,966667	0
'LRLGE^a'	**0,816667**	0,83	0,903093	0,969231	0,166667
'LRLGE^r'	**0,866667**	0,816667	0,896215	0,969231	0,066667
'LRHGE^a'	0,547863	0,829167	0,906294	1	0
'LRHGE^r'	0,477778	0,829167	0,906294	1	0
'NGLNU^a'	0,509402	0,829167	0,906294	1	0
'NGLNU^r'	0,595726	0,829167	0,906294	1	0
'NRLNU^a'	0,652991	0,828333	0,904151	0,983333	0,066667
'NRLNU^r'	0,690171	0,789167	0,877617	0,933333	0,1
'GLRV^a'	0,682906	0,749167	0,845367	0,885897	0,066667
'GLRV^r'	0,779487	0,789167	0,876136	0,920513	0,166667
'RLV^a'	**0,829915**	0,816667	0,896215	0,969231	0,066667
'RLV^r'	**0,927778**	0,816667	0,896215	0,969231	0,066667
'RE^a'	0,649573	0,815	0,896825	0,969231	0,066667
'RE^r'	0,618376	0,815833	0,898358	0,984615	0
'W MV^cH'	**0,891453**	0,7225	0,810617	0,760256	0,533333
'W MED^cH'	0,451282	0,829167	0,906294	1	0
'W MAX^cH'	0,70812	0,815833	0,896649	0,967949	0,066667
'W MIN^cH'	0,317521	0,816667	0,898413	0,984615	0
'W RNG^cH'	0,663248	0,829167	0,906294	1	0
'W STD^cH'	**0,858547**	0,843333	0,909931	0,969231	0,233333
'W MDAD^cH'	0,613248	0,815	0,894921	0,966667	0,066667
'W MNAD^cH'	0,633333	0,815833	0,898358	0,984615	0
'W MV^cV'	0,749573	0,829167	0,906294	1	0
'W MED^cV'	0,597436	0,841667	0,91103	0,983333	0,166667
'W MAX^cV'	0,635043	0,815833	0,895048	0,953846	0,166667
'W MIN^cV'	0,52094	0,829167	0,906294	1	0
'W RNG^cV'	0,471368	0,829167	0,906294	1	0
'W STD^cV'	0,736325	0,815833	0,898358	0,984615	0
'W MDAD^cV'	0,654274	0,841667	0,91164	0,984615	0,166667
'W MNAD^cV'	0,479915	0,829167	0,906294	1	0
'W MV^cD'	0,629487	0,775833	0,86997	0,933333	0
'W MED^cD'	0,515385	0,7625	0,853914	0,907692	0,1
'W MAX^cD'	0,725214	0,8025	0,888644	0,953846	0,1
'W MIN^cD'	0,685897	0,840833	0,909361	0,966667	0,233333
'W RNG^cD'	0,755556	0,854167	0,917908	0,983333	0,233333
'W STD^cD'	**0,869231**	0,869167	0,922986	0,953846	0,466667
'W MDAD^cD'	0,47906	0,841667	0,91164	0,984615	0,166667
'W MNAD^cD'	0,748291	0,815833	0,896825	0,969231	0,066667

Low Risk – Medium Risk 5-fold CV

Feature	Average AUC	Accuracy	F1-Score	Sensitivity	Specificity
Area'	0,776068	0,736364	0,548442	0,436111	0,937179
'Perimeter'	0,749573	0,708225	0,525714	0,436111	0,888462
'Eccentricity'	0,54886	0,556277	0,069697	0,047222	0,905128
'MajorAxisLength'	0,736966	0,717316	0,531775	0,436111	0,903846
'MinorAxisLength'	0,767094	0,74632	0,605714	0,55	0,873077
'ConvexArea'	0,743234	0,72684	0,539618	0,436111	0,920513
'EquivDiameter'	0,763462	0,745887	0,579655	0,505556	0,903846
'Solidity'	0,478063	0,585281	0	0	0,984615
'Extent'	0,468305	0,566234	0	0	0,953846
'Compactness'	0,505556	0,585281	0,036364	0,022222	0,967949
'Mean'	0,519516	0,594372	0,315326	0,233333	0,846154
'Std'	**0,825071**	0,800433	0,701056	0,605556	0,935897
'Skewness'	0,719088	0,669697	0,535482	0,463889	0,812821
'Kurtosis'	0,785114	0,660173	0,677758	0,863889	0,529487
'Median'	0,492806	0,594372	0,315326	0,233333	0,846154
'Minimum'	0,6125	0,546753	0,092308	0,072222	0,870513
'P10th'	0,65057	0,641991	0,367599	0,258333	0,90641
'P90th'	0,791809	0,697403	0,590038	0,533333	0,812821
'Maximum'	0,739423	0,707359	0,64924	0,705556	0,714103
'IQR'	0,789459	0,782251	0,675219	0,586111	0,920513
'Range'	0,745726	0,668831	0,577112	0,555556	0,748718
'MeanAbsoluteDeviation'	**0,825214**	0,819481	0,7397	0,652778	0,935897
'MedianAbsoluteDeviation'	0,764138	0,792208	0,7	0,608333	0,920513
'CV'	0,71916	0,716017	0,52629	0,422222	0,920513
'QCD'	0,735826	0,724675	0,543671	0,444444	0,920513
'Energy'	0,639174	0,689177	0,463492	0,366667	0,905128
'Entropy'	0,451353	0,585281	0	0	0,984615
'ASM^a'	0,792165	0,763636	0,678875	0,630556	0,857692
'ASM^r'	0,771581	0,764069	0,7384	0,813889	0,729487
'CONT^a'	0,545157	0,547186	0,143922	0,119444	0,84359
'CONT^r'	0,497151	0,594372	0	0	1
'COR^a'	**0,880698**	0,763636	0,647863	0,588889	0,891026
'COR^r'	0,711752	0,716017	0,503726	0,394444	0,937179
'SOQ^a'	0,795085	0,708658	0,662334	0,702778	0,717949
'SOQ^r'	0,420869	0,490043	0,362089	0,475	0,508974
'IDM^a'	0,488319	0,548052	0,044444	0,025	0,903846
'IDM^r'	0,561752	0,575758	0,158681	0,119444	0,892308
'SAV^a'	0,664744	0,595671	0,380403	0,305556	0,797436

'SAV^r'	0,577991	0,517749	0,562125	0,761111	0,34359
'SVAR^a'	0,79302	0,708658	0,662334	0,702778	0,717949
'SVAR^r'	0,500285	0,48961	0,164603	0,172222	0,717949
'SENTR^a'	**0,825285**	0,820346	0,760984	0,725	0,889744
'SENTR^r'	0,538746	0,566234	0,269286	0,266667	0,784615
'ENTR^a'	0,79594	0,810823	0,740387	0,702778	0,891026
'ENTR^r'	0,627707	0,604329	0,455427	0,416667	0,732051
'DVAR^a'	0,556339	0,509524	0,133333	0,144444	0,765385
'DVAR^r'	0,51047	0,584848	0	0	0,983333
'DENTR^a'	0,459758	0,557576	0,044444	0,025	0,920513
'DENTR^r'	0,681125	0,622511	0,53808	0,552778	0,667949
'IMC1^a'	0,537179	0,537662	0,130769	0,091667	0,839744
'IMC1^r'	**0,814886**	0,783117	0,752435	0,813889	0,762821
'IMC2^a'	**0,818875**	0,782251	0,734827	0,769444	0,796154
'IMC2^r'	**0,831766**	0,792208	0,767737	0,861111	0,747436
'MCCF^a'	0,58255	0,60303	0,334427	0,255556	0,838462
'MCCF^r'	0,438462	0,594372	0	0	1
'JMX^a'	0,613746	0,641126	0,387179	0,280556	0,889744
'JMX^r'	0,708618	0,621645	0,577765	0,647222	0,602564
'JAV^a'	0,664744	0,595671	0,380403	0,305556	0,797436
'JAV^r'	0,577991	0,517749	0,562125	0,761111	0,34359
'DAV^a'	0,492735	0,575758	0,04	0,025	0,952564
'DAV^r'	0,573718	0,594372	0,117172	0,072222	0,953846
'IDF^a'	0,549074	0,557576	0,044444	0,025	0,920513
'IDF^r'	0,535399	0,575758	0,033333	0,022222	0,953846
'NIDF^a'	0,475641	0,557576	0,084444	0,05	0,905128
'NIDF^r'	0,589387	0,585281	0,225348	0,163889	0,875641
'ACOR^a'	0,706054	0,614719	0,425238	0,352778	0,797436
'ACOR^r'	0,593447	0,5671	0,146667	0,133333	0,857692
'CLS^a'	0,686396	0,649784	0,316934	0,258333	0,921795
'CLS^r'	0,556909	0,548052	0,281324	0,263889	0,748718
'CLP^a'	0,798291	0,717316	0,63951	0,625	0,780769
'CLP^r'	**0,811467**	0,679221	0,422857	0,336111	0,920513
'SRE^a'	**0,82386**	0,698701	0,569744	0,538889	0,807692
'SRE^r'	0,803917	0,782684	0,738585	0,75	0,805128
'LRE^a'	0,509687	0,632035	0,24987	0,161111	0,95
'LRE^r'	0,430912	0,593939	0,110769	0,066667	0,95
'GLNU^a'	0,712393	0,698268	0,501047	0,411111	0,888462
'GLNU^r'	0,655627	0,651082	0,389188	0,3	0,889744
'RLNU^a'	**0,811538**	0,755411	0,616061	0,511111	0,921795
'RLNU'	**0,821011**	0,736364	0,593035	0,488889	0,90641
'RP^a'	0,572507	0,5671	0,128889	0,072222	0,903846
'RP^r'	0,487821	0,575758	0,147475	0,094444	0,905128
'LGRE^a'	**0,847151**	0,794372	0,729598	0,744444	0,825641
'LGRE^r'	0,725712	0,669697	0,612647	0,630556	0,696154
'HGRE^a'	0,726425	0,642857	0,525387	0,488889	0,748718

'HGRE^r'	0,48547	0,48961	0,518334	0,711111	0,332051
'SRLGE^a'	0,455556	0,584848	0,136752	0,091667	0,919231
'SRLGE^r'	0,401282	0,471861	0,4415	0,658333	0,357692
'SRHGE^a'	**0,814316**	0,699134	0,55619	0,463889	0,860256
'SRHGE^r'	**0,821083**	0,717749	0,584048	0,491667	0,871795
'LRLGE^a'	0,550997	0,622944	0,20987	0,138889	0,95
'LRLGE^r'	0,40292	0,575325	0,030769	0,022222	0,95
'LRHGE^a'	0,514174	0,604329	0,231409	0,161111	0,905128
'LRHGE^r'	0,569516	0,585714	0,17683	0,116667	0,905128
'NGLNU^a'	0,763177	0,772727	0,68493	0,633333	0,873077
'NGLNU^r'	0,513105	0,575758	0	0	0,969231
'NRLNU^a'	0,787821	0,661905	0,49641	0,494444	0,775641
'NRLNU^r'	0,788034	0,697835	0,580826	0,544444	0,805128
'GLRV^a'	0,802279	0,707792	0,635212	0,658333	0,748718
'GLRV^r'	0,522365	0,55671	0,033333	0,022222	0,923077
'RLV^a'	0,528846	0,632035	0,24987	0,161111	0,95
'RLV^r'	0,444444	0,593939	0,110769	0,066667	0,95
'RE^a'	0,307977	0,55671	0,036364	0,025	0,921795
'RE^r'	0,690812	0,642424	0,619007	0,7	0,607692
'W MV^cH'	0,605128	0,585714	0,468364	0,575	0,580769
'W MED^cH'	0,741809	0,698268	0,593778	0,563889	0,792308
'W MAX^cH'	0,799715	0,669697	0,542129	0,486111	0,796154
'W MIN^cH'	**0,833191**	0,763636	0,704188	0,702778	0,814103
'W RNG^cH'	**0,830769**	0,716017	0,610299	0,555556	0,828205
'W STD^cH'	0,565456	0,594372	0	0	1
'W MDAD^cH'	0,763675	0,699134	0,569706	0,519444	0,825641
'W MNAD^cH'	0,558547	0,603896	0,1	0,088889	0,95
'W MV^cV'	0,50933	0,55671	0,127731	0,119444	0,861538
'W MED^cV'	0,702137	0,707792	0,532234	0,416667	0,905128
'W MAX^cV'	0,740242	0,650216	0,424935	0,361111	0,838462
'W MIN^cV'	0,781553	0,679221	0,607268	0,608333	0,735897
'W RNG^cV'	0,780199	0,668831	0,530226	0,483333	0,79359
'W STD^cV'	0,500071	0,594372	0	0	1
'W MDAD^cV'	**0,88255**	0,831169	0,782745	0,75	0,889744
'W MNAD^cV'	0,502635	0,565801	0,069697	0,044444	0,920513
'W MV^cD'	0,486254	0,414286	0,469849	0,666667	0,234615
'W MED^cD'	0,557265	0,585281	0	0	0,984615
'W MAX^cD'	**0,834972**	0,688745	0,541709	0,502778	0,807692
'W MIN^cD'	0,798291	0,726407	0,628796	0,583333	0,828205
'W RNG^cD'	**0,848575**	0,716883	0,627368	0,602778	0,79359
'W STD^cD'	0,609117	0,585281	0,545599	0,622222	0,555128
'W MDAD^cD'	0,663105	0,604762	0,326061	0,258333	0,842308
'W MNAD^cD'	0,54651	0,594372	0,133333	0,113889	0,916667

Medium Risk – High Risk 5-fold CV

Feature	Average AUC	Accuracy	F1-Score	Sensitivity	Specificity
'Area'	**0,865741**	0,839394	0,900585	0,955556	0,466667
'Perimeter'	**0,867593**	0,839394	0,899346	0,933333	0,533333
'Eccentricity'	0,437037	0,768182	0,868271	1	0
'MajorAxisLength'	**0,87037**	0,801515	0,871663	0,883333	0,533333
'MinorAxisLength'	**0,935185**	0,839394	0,901754	0,955556	0,5
'ConvexArea'	**0,878704**	0,839394	0,900585	0,955556	0,466667
'EquivDiameter'	**0,865741**	0,839394	0,900585	0,955556	0,466667
'Solidity'	0,325926	0,731818	0,845113	0,955556	0
'Extent'	0,498148	0,713636	0,832247	0,933333	0
'Compactness'	0,50463	0,731818	0,845113	0,955556	0
'Mean'	0,468519	0,768182	0,868271	1	0
'Std'	0,65463	0,768182	0,868271	1	0
'Skewness'	**0,841667**	0,771212	0,860819	0,933333	0,233333
'Kurtosis'	**0,831481**	0,822727	0,892442	0,955556	0,4
'Median'	0,49213	0,768182	0,868271	1	0
'Minimum'	0,516204	0,768182	0,868271	1	0
'P10th'	0,678704	0,768182	0,868271	1	0
'P90th'	0,62963	0,768182	0,868271	1	0
'Maximum'	**0,943981**	0,912121	0,942251	0,952778	0,766667
'IQR'	0,770833	0,768182	0,868271	1	0
'Range'	**0,952315**	0,892424	0,928849	0,927778	0,766667
'MeanAbsoluteDeviation'	0,683333	0,768182	0,868271	1	0
'MedianAbsoluteDeviation'	0,69213	0,768182	0,868271	1	0
'CV'	0,800926	0,768182	0,868271	1	0
'QCD'	**0,830556**	0,768182	0,868271	1	0
'Energy'	0,634259	0,768182	0,863041	0,955556	0,166667
'Entropy'	0,466667	0,768182	0,868271	1	0
'ASM^a'	0,781481	0,768182	0,861212	0,933333	0,233333
'ASM^r'	0,591667	0,748485	0,849969	0,930556	0,133333
'CONT^a'	**0,948148**	0,857576	0,901667	0,863889	0,866667
'CONT^r'	**0,907407**	0,839394	0,878077	0,844444	0,866667
'COR^a'	**0,898148**	0,819697	0,874814	0,866667	0,7
'COR^r'	**0,87963**	0,730303	0,777857	0,683333	0,933333
'SOQ^a'	**0,936111**	0,856061	0,902415	0,888889	0,766667
'SOQ^r'	0,69537	0,642424	0,72337	0,605556	0,766667
'IDM^a'	0,655556	0,713636	0,829447	0,933333	0
'IDM^r'	0,268519	0,75	0,856692	0,977778	0
'SAV^a'	0,801852	0,786364	0,870175	0,933333	0,333333
'SAV^r'	**0,938889**	0,836364	0,893791	0,883333	0,666667
'SVAR^a'	**0,928704**	0,856061	0,902415	0,888889	0,766667
'SVAR^r'	**0,948148**	0,875758	0,914902	0,886111	0,866667
'SENTR^a'	**0,814815**	0,731818	0,841398	0,933333	0,1
'SENTR^r'	0,733333	0,801515	0,882601	0,975	0,2
'ENTR^a'	0,80463	0,731818	0,841398	0,933333	0,1

'ENTR^r'	0,512037	0,768182	0,868271	1	0
'DVAR^a'	**0,974074**	0,859091	0,908095	0,886111	0,8
'DVAR^r'	**0,922222**	0,857576	0,897857	0,866667	0,866667
'DENTR^a'	0,639815	0,713636	0,829447	0,933333	0
'DENTR^r'	0,571296	0,768182	0,868271	1	0
'IMC1^a'	0,473148	0,731818	0,843826	0,955556	0
'IMC1^r'	0,699074	0,80303	0,880378	0,952778	0,333333
'IMC2^a'	0,722222	0,748485	0,841548	0,883333	0,3
'IMC2^r'	0,768519	0,748485	0,845263	0,905556	0,2
'MCCF^a'	0,777778	0,768182	0,868271	1	0
'MCCF^r'	0,481481	0,768182	0,868271	1	0
'JMX^a'	0,659259	0,713636	0,819382	0,888889	0,166667
'JMX^r'	0,789815	0,80303	0,87914	0,930556	0,433333
'JAV^a'	0,801852	0,786364	0,870175	0,933333	0,333333
'JAV^r'	**0,938889**	0,836364	0,893791	0,883333	0,666667
'DAV^a'	0,742593	0,731818	0,840819	0,933333	0,066667
'DAV^r'	0,628704	0,768182	0,868271	1	0
'IDF^a'	0,659259	0,713636	0,829447	0,933333	0
'IDF^r'	0,29537	0,75	0,856692	0,977778	0
'NIDF^a'	0,656481	0,731818	0,843826	0,955556	0
'NIDF^r'	0,562037	0,768182	0,868271	1	0
'ACOR^a'	**0,87037**	0,75	0,841254	0,863889	0,433333
'ACOR^r'	0,723148	0,768182	0,865263	0,977778	0,066667
'CLS^a'	**0,82037**	0,783333	0,860836	0,880556	0,466667
'CLS^r'	**0,856481**	0,751515	0,834967	0,816667	0,566667
'CLP^a'	**0,962037**	0,856061	0,902415	0,888889	0,766667
'CLP^r'	**0,922222**	0,839394	0,88387	0,844444	0,866667
'SRE^a'	0,549074	0,731818	0,840111	0,930556	0,1
'SRE^r'	0,440741	0,731818	0,843826	0,952778	0
'LRE^a'	0,746296	0,768182	0,868271	1	0
'LRE^r'	**0,917593**	0,768182	0,868271	1	0
'GLNU^a'	0,759259	0,856061	0,913381	0,977778	0,466667
'GLNU^r'	0,792593	0,874242	0,922738	0,977778	0,533333
'RLNU^a'	0,666667	0,837879	0,902924	0,977778	0,4
'RLNU'	0,730556	0,856061	0,911842	0,975	0,466667
'RP^a'	0,617593	0,731818	0,843826	0,955556	0
'RP^r'	0,372222	0,768182	0,868271	1	0
'LGRE^a'	0,646296	0,769697	0,866316	0,977778	0,1
'LGRE^r'	0,659259	0,768182	0,868271	1	0
'HGRE^a'	**0,844444**	0,786364	0,863846	0,886111	0,5
'HGRE^r'	0,618519	0,768182	0,868271	1	0
'SRLGE^a'	0,600926	0,768182	0,868271	1	0
'SRLGE^r'	0,62037	0,786364	0,877627	1	0,066667
'SRHGE^a'	0,722222	0,75	0,852977	0,955556	0,1
'SRHGE^r'	0,70463	0,75	0,856692	0,977778	0
'LRLGE^a'	0,576852	0,75	0,856692	0,977778	0

'LRLGE^r'	**0,826852**	0,768182	0,868271	1	0
'LRHGE^a'	0,669444	0,768182	0,868271	1	0
'LRHGE^r'	0,675	0,768182	0,868271	1	0
'NGLNU^a'	0,775	0,677273	0,805003	0,888889	0
'NGLNU^r'	0,525	0,768182	0,868271	1	0
'NRLNU^a'	0,594444	0,731818	0,834556	0,908333	0,166667
'NRLNU^r'	0,481481	0,731818	0,843826	0,952778	0
'GLRV^a'	**0,972222**	0,856061	0,902251	0,888889	0,8
'GLRV^r'	0,784259	0,769697	0,836984	0,769444	0,8
'RLV^a'	0,751852	0,768182	0,868271	1	0
'RLV^r'	**0,864815**	0,768182	0,868271	1	0
'RE^a'	0,552778	0,695455	0,816582	0,908333	0
'RE^r'	0,694444	0,804545	0,878156	0,930556	0,4
'W MV^cH'	0,77037	0,692424	0,764474	0,713889	0,633333
'W MED^cH'	0,562963	0,751515	0,850175	0,933333	0,166667
'W MAX^cH'	0,575	0,75	0,856692	0,977778	0
'W MIN^cH'	0,725926	0,859091	0,917559	0,977778	0,5
'W RNG^cH'	0,650926	0,804545	0,884879	0,977778	0,266667
'W STD^cH'	**0,886111**	0,875758	0,923791	0,977778	0,566667
'W MDAD^cH'	0,666667	0,713636	0,821604	0,911111	0,1
'W MNAD^cH'	0,712037	0,75	0,85447	0,955556	0,1
'W MV^cV'	0,731481	0,677273	0,79146	0,816667	0,233333
'W MED^cV'	0,284259	0,713636	0,832247	0,930556	0
'W MAX^cV'	0,667593	0,768182	0,868271	1	0
'W MIN^cV'	**0,867593**	0,875758	0,923392	0,975	0,533333
'W RNG^cV'	0,791667	0,839394	0,90613	1	0,3
'W STD^cV'	**0,847222**	0,804545	0,882101	0,952778	0,333333
'W MDAD^cV'	0,630556	0,713636	0,825405	0,908333	0,1
'W MNAD^cV'	0,589815	0,731818	0,843826	0,955556	0
'W MV^cD'	0,607407	0,768182	0,868271	1	0
'W MED^cD'	0,428704	0,7	0,810263	0,888889	0,066667
'W MAX^cD'	0,585185	0,768182	0,868271	1	0
'W MIN^cD'	0,598148	0,768182	0,868271	1	0
'W RNG^cD'	0,538889	0,768182	0,868271	1	0
'W STD^cD'	**0,896296**	0,948485	0,968235	0,977778	0,866667
'W MDAD^cD'	0,582407	0,713636	0,821604	0,911111	0,1
'W MNAD^cD'	0,752778	0,768182	0,862333	0,955556	0,166667

Low Risk – High Risk 10-fold CV

Feature	Average AUC	Accuracy	F1-Score	Sensitivity	Specificity
Area'	**1**	0,948214	0,967459	0,966667	0,8
'Perimeter'	**1**	0,948214	0,966061	0,95	0,9
'Eccentricity'	0,358333	0,830357	0,906374	1	0
'MajorAxisLength'	**1**	0,948214	0,967459	0,966667	0,8

'MinorAxisLength'	**1**	0,9625	0,975152	0,966667	0,9
'ConvexArea'	**1**	0,9625	0,975152	0,966667	0,9
'EquivDiameter'	**1**	0,948214	0,967459	0,966667	0,8
'Solidity'	0,582143	0,803571	0,888382	0,952381	0,1
'Extent'	0,555952	0,830357	0,905092	0,983333	0,1
'Compactness'	0,72619	0,816071	0,896001	0,966667	0,1
'Mean'	0,488095	0,830357	0,906374	1	0
'Std'	0,785714	0,830357	0,901868	0,952381	0,2
'Skewness'	0,546429	0,816071	0,897399	0,983333	0
'Kurtosis'	0,609524	0,803571	0,886227	0,95	0,05
'Median'	0,507143	0,830357	0,906374	1	0
'Minimum'	0,753571	0,830357	0,906374	1	0
'P10th'	0,582143	0,830357	0,906374	1	0
'P90th'	0,689881	0,816071	0,897399	0,983333	0
'Maximum'	**0,832143**	0,830357	0,906374	1	0
'IQR'	0,6625	0,803571	0,888608	0,966667	0
'Range'	**0,821429**	0,830357	0,906374	1	0
'MeanAbsoluteDeviation'	0,752381	0,816071	0,894176	0,952381	0,1
'MedianAbsoluteDeviation'	0,714286	0,791071	0,880989	0,952381	0
'CV'	0,607143	0,830357	0,906374	1	0
'QCD'	0,530952	0,830357	0,906374	1	0
'Energy'	**0,963095**	0,935714	0,958368	0,95	0,85
'Entropy'	0,536905	0,830357	0,906374	1	0
'ASM^a'	0,57381	0,832143	0,901685	0,966667	0,2
'ASM^r'	0,575	0,830357	0,906374	1	0
'CONT^a'	**0,891667**	0,833929	0,89653	0,904762	0,55
'CONT^r'	**0,902381**	0,832143	0,884802	0,869048	0,65
'COR^a'	0,575	0,830357	0,906374	1	0
'COR^r'	0,663095	0,676786	0,789191	0,769048	0,25
'SOQ^a'	0,575	0,830357	0,906374	1	0
'SOQ^r'	**0,838095**	0,7625	0,825455	0,728571	0,95
'IDM^a'	0,558333	0,830357	0,906374	1	0
'IDM^r'	0,567857	0,830357	0,906374	1	0
'SAV^a'	0,628571	0,830357	0,906374	1	0
'SAV^r'	**0,975**	0,935714	0,959883	0,966667	0,75
'SVAR^a'	0,589286	0,830357	0,906374	1	0
'SVAR^r'	**0,941667**	0,858929	0,903893	0,871429	0,8
'SENTR^a'	0,559524	0,830357	0,906374	1	0
'SENTR^r'	0,707143	0,830357	0,906374	1	0
'ENTR^a'	0,511905	0,830357	0,906374	1	0
'ENTR^r'	0,552381	0,830357	0,906374	1	0
'DVAR^a'	**0,891667**	0,833929	0,892334	0,888095	0,6
'DVAR^r'	**0,910714**	0,832143	0,883776	0,854762	0,7
'DENTR^a'	0,528571	0,816071	0,897399	0,983333	0
'DENTR^r'	0,52619	0,830357	0,906374	1	0
'IMC1^a'	0,477381	0,816071	0,897399	0,983333	0

'IMC1^r'	0,516667	0,830357	0,906374	1	0
'IMC2^a'	0,507143	0,830357	0,906374	1	0
'IMC2^r'	0,469048	0,830357	0,906374	1	0
'MCCF^a'	0,654762	0,830357	0,906374	1	0
'MCCF^r'	0,57619	0,830357	0,906374	1	0
'JMX^a'	0,52619	0,830357	0,899304	0,95	0,25
'JMX^r'	0,702381	0,844643	0,914066	1	0,1
'JAV^a'	0,628571	0,830357	0,906374	1	0
'JAV^r'	**0,975**	0,935714	0,959883	0,966667	0,75
'DAV^a'	0,783333	0,830357	0,906374	1	0
'DAV^r'	0,744048	0,830357	0,906374	1	0
'IDF^a'	0,544048	0,830357	0,906374	1	0
'IDF^r'	0,545238	0,817857	0,898755	0,985714	0
'NIDF^a'	0,708333	0,830357	0,906374	1	0
'NIDF^r'	0,710714	0,830357	0,906374	1	0
'ACOR^a'	0,608333	0,830357	0,906374	1	0
'ACOR^r'	0,655952	0,830357	0,906374	1	0
'CLS^a'	0,655952	0,830357	0,906374	1	0
'CLS^r'	0,677381	0,842857	0,912967	1	0,05
'CLP^a'	0,614286	0,830357	0,906374	1	0
'CLP^r'	0,75	0,828571	0,903993	0,983333	0,05
'SRE^a'	0,589286	0,816071	0,895201	0,966667	0,05
'SRE^r'	0,764286	0,817857	0,89663	0,969048	0,1
'LRE^a'	**0,835714**	0,817857	0,897582	0,983333	0
'LRE^r'	**0,966667**	0,830357	0,906374	1	0
'GLNU^a'	**0,960714**	0,910714	0,945524	0,966667	0,6
'GLNU^r'	**0,969048**	0,908929	0,9431	0,95	0,7
'RLNU^a'	**0,879762**	0,910714	0,945524	0,966667	0,6
'RLNU'	**0,888095**	0,910714	0,945524	0,966667	0,6
'RP^a'	0,416667	0,830357	0,906374	1	0
'RP^r'	0,372619	0,830357	0,906374	1	0
'LGRE^a'	**0,859524**	0,869643	0,926154	0,983333	0,25
'LGRE^r'	**0,87619**	0,844643	0,914066	1	0,1
'HGRE^a'	0,630952	0,830357	0,906374	1	0
'HGRE^r'	0,69881	0,830357	0,906374	1	0
'SRLGE^a'	0,459524	0,830357	0,906374	1	0
'SRLGE^r'	0,647619	0,655357	0,772338	0,742857	0,2
'SRHGE^a'	0,519048	0,830357	0,906374	1	0
'SRHGE^r'	0,708333	0,817857	0,896374	0,971429	0,1
'LRLGE^a'	**0,865476**	0,844643	0,909487	0,966667	0,2
'LRLGE^r'	**0,857143**	0,817857	0,897582	0,983333	0
'LRHGE^a'	0,525	0,830357	0,906374	1	0
'LRHGE^r'	0,55119	0,830357	0,906374	1	0
'NGLNU^a'	0,619048	0,830357	0,906374	1	0
'NGLNU^r'	0,680952	0,830357	0,906374	1	0
'NRLNU^a'	0,692857	0,832143	0,904249	0,969048	0,15

'NRLNU^r'	0,727381	0,832143	0,905421	0,971429	0,15
'GLRV^a'	0,70119	0,805357	0,887326	0,966667	0
'GLRV^r'	0,72619	0,791071	0,878352	0,95	0
'RLV^a'	**0,888095**	0,817857	0,897582	0,983333	0
'RLV^r'	**0,933333**	0,830357	0,906374	1	0
'RE^a'	0,589286	0,801786	0,888425	0,966667	0
'RE^r'	0,45119	0,816071	0,897399	0,983333	0
'W MV^cH'	**0,890476**	0,751786	0,827416	0,778571	0,65
'W MED^cH'	0,380952	0,817857	0,897582	0,983333	0
'W MAX^cH'	0,640476	0,816071	0,892894	0,95	0,15
'W MIN^cH'	0,467857	0,830357	0,906374	1	0
'W RNG^cH'	0,636905	0,817857	0,897582	0,983333	0
'W STD^cH'	**0,852381**	0,869643	0,926227	0,983333	0,3
'W MDAD^cH'	0,572619	0,830357	0,904176	0,983333	0,05
'W MNAD^cH'	0,679762	0,816071	0,897399	0,983333	0
'W MV^cV'	0,769048	0,830357	0,906374	1	0
'W MED^cV'	0,620238	0,844643	0,911868	0,983333	0,15
'W MAX^cV'	0,555952	0,816071	0,893803	0,95	0,15
'W MIN^cV'	0,534524	0,830357	0,906374	1	0
'W RNG^cV'	0,503571	0,830357	0,906374	1	0
'W STD^cV'	0,757143	0,830357	0,904176	0,983333	0,05
'W MDAD^cV'	0,65119	0,842857	0,911685	0,983333	0,15
'W MNAD^cV'	0,540476	0,830357	0,906374	1	0
'W MV^cD'	0,564286	0,792857	0,879707	0,952381	0
'W MED^cD'	0,578571	0,801786	0,886793	0,966667	0
'W MAX^cD'	0,735714	0,816071	0,89346	0,952381	0,15
'W MIN^cD'	0,679762	0,844643	0,911941	0,969048	0,2
'W RNG^cD'	0,771429	0,857143	0,91956	0,983333	0,2
'W STD^cD'	**0,891667**	0,880357	0,93033	0,966667	0,45
'W MDAD^cD'	0,488095	0,842857	0,911685	0,983333	0,15
'W MNAD^cD'	0,758333	0,816071	0,897399	0,983333	0

Low Risk – Medium Risk 10-fold CV

Feature	Average AUC	Accuracy	F1-Score	Sensitivity	Specificity
Area'	0,780952	0,732727	0,555	0,445	0,935714
'Perimeter'	0,755	0,705455	0,53754	0,445	0,890476
'Eccentricity'	0,487619	0,565455	0,095238	0,07	0,907143
'MajorAxisLength'	0,751548	0,714545	0,542302	0,445	0,907143
'MinorAxisLength'	0,766786	0,742727	0,610238	0,555	0,87381
'ConvexArea'	0,73869	0,723636	0,547857	0,445	0,921429
'EquivDiameter'	0,76881	0,714545	0,538333	0,445	0,907143
'Solidity'	0,512857	0,585455	0	0	0,983333
'Extent'	0,399643	0,575455	0	0	0,966667
'Compactness'	0,526429	0,585455	0,033333	0,025	0,969048
'Mean'	0,535833	0,600909	0,290476	0,23	0,852381

'Std'	0,796071	0,810909	0,721825	0,62	0,938095
'Skewness'	0,726786	0,685455	0,564286	0,515	0,807143
'Kurtosis'	0,759881	0,640909	0,657489	0,865	0,488095
'Median'	0,502738	0,591818	0,26381	0,205	0,852381
'Minimum'	0,590595	0,556364	0,058333	0,045	0,904762
'P10th'	0,640179	0,640909	0,341905	0,25	0,902381
'P90th'	0,792976	0,703636	0,595397	0,555	0,804762
'Maximum'	0,722202	0,700909	0,64026	0,675	0,714286
'IQR'	0,757262	0,783636	0,680079	0,605	0,904762
'Range'	0,7425	0,668182	0,572727	0,55	0,747619
'MeanAbsoluteDeviation'	0,778929	0,820909	0,738492	0,645	0,938095
'MedianAbsoluteDeviation'	0,75244	0,792727	0,70119	0,615	0,921429
'CV'	0,701786	0,719091	0,511905	0,41	0,921429
'QCD'	0,720595	0,727273	0,533889	0,43	0,921429
'Energy'	0,640833	0,686364	0,467381	0,37	0,904762
'Entropy'	0,350476	0,576364	0	0	0,966667
'ASM^a'	0,765595	0,765455	0,674048	0,63	0,857143
'ASM^r'	0,77631	0,757273	0,716288	0,79	0,733333
'CONT^a'	0,537619	0,527273	0,090794	0,075	0,842857
'CONT^r'	0,504167	0,594545	0	0	1
'COR^a'	**0,862976**	0,765455	0,627381	0,59	0,883333
'COR^r'	0,702857	0,717273	0,512143	0,4	0,933333
'SOQ^a'	0,790833	0,707273	0,652958	0,675	0,72381
'SOQ^r'	0,465952	0,489091	0,53241	0,715	0,338095
'IDM^a'	0,573333	0,578182	0,148571	0,095	0,907143
'IDM^r'	0,58369	0,536364	0,130476	0,11	0,82619
'SAV^a'	0,69119	0,602727	0,383333	0,325	0,785714
'SAV^r'	0,572857	0,5	0,556279	0,755	0,32619
'SVAR^a'	0,786905	0,707273	0,647006	0,65	0,740476
'SVAR^r'	0,470119	0,48	0,15746	0,17	0,704762
'SENTR^a'	**0,823452**	0,822727	0,758413	0,725	0,888095
'SENTR^r'	0,532262	0,583636	0,14881	0,125	0,902381
'ENTR^a'	0,792381	0,821818	0,756667	0,725	0,888095
'ENTR^r'	0,615595	0,594545	0,475397	0,46	0,683333
'DVAR^a'	0,52131	0,51	0,169935	0,145	0,764286
'DVAR^r'	0,54119	0,575455	0	0	0,969048
'DENTR^a'	0,525833	0,577273	0,108571	0,07	0,921429
'DENTR^r'	0,680595	0,63	0,544888	0,575	0,666667
'IMC1^a'	0,568452	0,547273	0,126905	0,09	0,859524
'IMC1^r'	**0,812857**	0,774545	0,737399	0,81	0,745238
'IMC2^a'	**0,822024**	0,783636	0,731667	0,765	0,792857
'IMC2^r'	**0,827381**	0,792727	0,763658	0,855	0,745238
'MCCF^a'	0,610833	0,574545	0,24381	0,205	0,82381
'MCCF^r'	0,490952	0,594545	0	0	1
'JMX^a'	0,661429	0,632727	0,382381	0,28	0,871429
'JMX^r'	0,686667	0,620909	0,570862	0,65	0,607143

'JAV^a'	0,69119	0,602727	0,383333	0,325	0,785714
'JAV^r'	0,572857	0,5	0,556279	0,755	0,32619
'DAV^a'	0,522619	0,567273	0,04	0,025	0,938095
'DAV^r'	0,562381	0,574545	0,097143	0,07	0,921429
'IDF^a'	0,583214	0,588182	0,175238	0,12	0,907143
'IDF^r'	0,534643	0,555455	0,057143	0,045	0,904762
'NIDF^a'	0,545952	0,586364	0,178333	0,12	0,907143
'NIDF^r'	0,583333	0,565455	0,191905	0,16	0,842857
'ACOR^a'	0,727738	0,602727	0,394048	0,35	0,771429
'ACOR^r'	0,588214	0,594545	0,05	0,05	0,971429
'CLS^a'	0,669762	0,651818	0,265714	0,225	0,935714
'CLS^r'	0,568214	0,566364	0,304683	0,295	0,761905
'CLP^a'	0,776071	0,705455	0,627381	0,62	0,754762
'CLP^r'	0,79131	0,663636	0,387619	0,305	0,902381
'SRE^a'	**0,833214**	0,69	0,579394	0,565	0,780952
'SRE^r'	**0,810357**	0,785455	0,740159	0,75	0,816667
'LRE^a'	0,4975	0,622727	0,211667	0,14	0,957143
'LRE^r'	0,368214	0,594545	0,091667	0,065	0,957143
'GLNU^a'	0,708214	0,694545	0,509365	0,415	0,890476
'GLNU^r'	0,676429	0,668182	0,409048	0,305	0,921429
'RLNU^a'	**0,812024**	0,753636	0,619841	0,515	0,921429
'RLNU'	**0,813452**	0,743636	0,604762	0,49	0,919048
'RP^a'	0,571786	0,568182	0,157778	0,115	0,87619
'RP^r'	0,499405	0,585455	0,16381	0,115	0,904762
'LGRE^a'	**0,867976**	0,801818	0,748687	0,775	0,82381
'LGRE^r'	0,715595	0,634545	0,576775	0,605	0,657143
'HGRE^a'	0,738571	0,631818	0,476291	0,465	0,740476
'HGRE^r'	0,466667	0,508182	0,528443	0,71	0,369048
'SRLGE^a'	0,530119	0,567273	0,025	0,025	0,940476
'SRLGE^r'	0,438214	0,441818	0,490393	0,745	0,230952
'SRHGE^a'	**0,82381**	0,715455	0,576905	0,52	0,852381
'SRHGE^r'	**0,825238**	0,708182	0,543254	0,49	0,857143
'LRLGE^a'	0,55131	0,614545	0,165	0,12	0,957143
'LRLGE^r'	0,405476	0,576364	0,025	0,025	0,957143
'LRHGE^a'	0,476548	0,613636	0,248254	0,185	0,904762
'LRHGE^r'	0,563333	0,585455	0,137143	0,09	0,921429
'NGLNU^a'	0,76119	0,794545	0,705794	0,655	0,890476
'NGLNU^r'	0,495952	0,575455	0	0	0,966667
'NRLNU^a'	0,800952	0,672727	0,51987	0,525	0,780952
'NRLNU^r'	0,775476	0,710909	0,587937	0,56	0,816667
'GLRV^a'	**0,844048**	0,691818	0,613919	0,63	0,730952
'GLRV^r'	0,582143	0,564545	0,028571	0,02	0,933333
'RLV^a'	0,504286	0,632727	0,238333	0,165	0,957143
'RLV^r'	0,409405	0,594545	0,091667	0,065	0,957143
'RE^a'	0,40369	0,584545	0,113333	0,07	0,935714
'RE^r'	0,670119	0,630909	0,581061	0,655	0,611905

'W MV^cH'	0,597619	0,54	0,489946	0,625	0,485714
'W MED^cH'	0,744167	0,709091	0,580794	0,545	0,828571
'W MAX^cH'	0,807024	0,685455	0,545476	0,51	0,807143
'W MIN^cH'	**0,826071**	0,730909	0,6421	0,6	0,819048
'W RNG^cH'	**0,821429**	0,713636	0,604762	0,55	0,821429
'W STD^cH'	0,593214	0,583636	0,091667	0,1	0,921429
'W MDAD^cH'	0,779762	0,719091	0,611905	0,57	0,82619
'W MNAD^cH'	0,54631	0,557273	0,073016	0,075	0,895238
'W MV^cV'	0,498095	0,576364	0,093571	0,07	0,916667
'W MED^cV'	0,69631	0,716364	0,529286	0,42	0,919048
'W MAX^cV'	0,757381	0,620909	0,355873	0,3	0,847619
'W MIN^cV'	0,772143	0,677273	0,582121	0,6	0,721429
'W RNG^cV'	0,78631	0,675455	0,558045	0,53	0,778571
'W STD^cV'	0,50869	0,594545	0	0	1
'W MDAD^cV'	**0,869286**	0,832727	0,780794	0,75	0,888095
'W MNAD^cV'	0,453095	0,558182	0,04	0,025	0,92381
'W MV^cD'	0,449881	0,442727	0,509967	0,74	0,240476
'W MED^cD'	0,497619	0,585455	0,054545	0,075	0,942857
'W MAX^cD'	**0,84381**	0,694545	0,557222	0,51	0,828571
'W MIN^cD'	0,799048	0,725455	0,624286	0,58	0,821429
'W RNG^cD'	**0,853214**	0,734545	0,645476	0,605	0,82619
'W STD^cD'	0,618929	0,584545	0,553508	0,65	0,535714
'W MDAD^cD'	0,677619	0,595455	0,354286	0,29	0,809524
'W MNAD^cD'	0,514286	0,548182	0,08	0,1	0,869048

Medium Risk – High Risk 10-fold CV

Feature	Average AUC	Accuracy	F1-Score	Sensitivity	Specificity
'Area'	**0,88**	0,84	0,899242	0,955	0,45
'Perimeter'	**0,9125**	0,843333	0,899242	0,935	0,55
'Eccentricity'	0,54	0,77	0,868283	1	0
'MajorAxisLength'	**0,905**	0,82	0,882179	0,905	0,55
'MinorAxisLength'	**0,93**	0,84	0,901465	0,955	0,45
'ConvexArea'	**0,905**	0,84	0,899242	0,955	0,45
'EquivDiameter'	**0,88**	0,84	0,899242	0,955	0,45
'Solidity'	0,4875	0,736667	0,84404	0,955	0
'Extent'	0,525	0,736667	0,838283	0,95	0
'Compactness'	0,69	0,736667	0,84404	0,955	0
'Mean'	0,435	0,77	0,868283	1	0
'Std'	0,6375	0,77	0,868283	1	0
'Skewness'	**0,8475**	0,796667	0,875354	0,94	0,35
'Kurtosis'	**0,8575**	0,863333	0,912374	0,95	0,55
'Median'	0,51125	0,77	0,868283	1	0
'Minimum'	0,49375	0,77	0,868283	1	0
'P10th'	0,67375	0,77	0,868283	1	0
'P90th'	0,62	0,77	0,868283	1	0

'Maximum'	**0,9375**	0,913333	0,94329	0,955	0,8
'IQR'	0,71	0,77	0,868283	1	0
'Range'	**0,9625**	0,893333	0,92583	0,925	0,8
'MeanAbsoluteDeviation'	0,6875	0,77	0,868283	1	0
'MedianAbsoluteDeviation'	0,67	0,77	0,868283	1	0
'CV'	0,7625	0,77	0,868283	1	0
'QCD'	0,73	0,77	0,868283	1	0
'Energy'	0,735	0,753333	0,852929	0,955	0,1
'Entropy'	0,445	0,753333	0,857374	0,98	0
'ASM^a'	0,76	0,793333	0,870152	0,93	0,35
'ASM^r'	0,5125	0,733333	0,826739	0,9	0,2
'CONT^a'	**0,8875**	0,846667	0,891941	0,86	0,75
'CONT^r'	**0,835**	0,85	0,882222	0,84	0,8
'COR^a'	**0,925**	0,833333	0,882179	0,865	0,75
'COR^r'	**0,8625**	0,743333	0,763889	0,69	0,95
'SOQ^a'	**0,915**	0,883333	0,915512	0,91	0,8
'SOQ^r'	0,7775	0,66	0,724603	0,61	0,85
'IDM^a'	0,6625	0,753333	0,854949	0,975	0
'IDM^r'	0,3875	0,753333	0,854949	0,975	0
'SAV^a'	**0,8275**	0,826667	0,897576	0,96	0,4
'SAV^r'	**0,9625**	0,86	0,901984	0,885	0,85
'SVAR^a'	**0,895**	0,883333	0,915512	0,91	0,8
'SVAR^r'	**0,9025**	0,88	0,909004	0,88	0,8
'SENTR^a'	0,805	0,796667	0,872374	0,93	0,35
'SENTR^r'	0,7875	0,803333	0,883687	0,975	0,3
'ENTR^a'	0,785	0,796667	0,872374	0,93	0,35
'ENTR^r'	0,455	0,77	0,868283	1	0
'DVAR^a'	**0,92**	0,88	0,911544	0,86	0,9
'DVAR^r'	**0,895**	0,866667	0,899278	0,88	0,75
'DENTR^a'	0,6625	0,77	0,868283	1	0
'DENTR^r'	0,5375	0,77	0,868283	1	0
'IMC1^a'	0,4325	0,753333	0,854949	0,975	0
'IMC1^r'	0,65	0,786667	0,860628	0,925	0,3
'IMC2^a'	0,805	0,753333	0,833405	0,875	0,35
'IMC2^r'	0,785	0,753333	0,83785	0,9	0,3
'MCCF^a'	0,6975	0,77	0,868283	1	0
'MCCF^r'	0,515	0,77	0,868283	1	0
'JMX^a'	0,68	0,81	0,881263	0,95	0,35
'JMX^r'	0,775	0,803333	0,87829	0,93	0,35
'JAV^a'	**0,8275**	0,826667	0,897576	0,96	0,4
'JAV^r'	**0,9625**	0,86	0,901984	0,885	0,85
'DAV^a'	0,675	0,753333	0,857374	0,98	0
'DAV^r'	0,67	0,77	0,868283	1	0
'IDF^a'	0,6625	0,753333	0,854949	0,975	0
'IDF^r'	0,4375	0,753333	0,854949	0,975	0
'NIDF^a'	0,65	0,77	0,868283	1	0

'NIDF^r'	0,625	0,77	0,868283	1	0
'ACOR^a'	**0,865**	0,756667	0,841782	0,865	0,4
'ACOR^r'	0,6325	0,736667	0,84404	0,96	0
'CLS^a'	**0,85**	0,8	0,872893	0,9	0,5
'CLS^r'	**0,825**	0,773333	0,839322	0,82	0,6
'CLP^a'	**0,975**	0,846667	0,887338	0,86	0,8
'CLP^r'	**0,9075**	0,88	0,910159	0,885	0,8
'SRE^a'	0,5425	0,716667	0,830152	0,93	0
'SRE^r'	0,5675	0,733333	0,837886	0,925	0,1
'LRE^a'	0,6225	0,73	0,836537	0,95	0
'LRE^r'	**0,8625**	0,77	0,868283	1	0
'GLNU^a'	0,79	0,86	0,912576	0,975	0,5
'GLNU^r'	0,795	0,876667	0,921465	0,975	0,55
'RLNU^a'	0,6875	0,84	0,901465	0,975	0,4
'RLNU'	0,7125	0,856667	0,912576	0,975	0,5
'RP^a'	0,65	0,753333	0,854949	0,975	0
'RP^r'	0,35	0,77	0,868283	1	0
'LGRE^a'	0,53	0,77	0,868283	1	0
'LGRE^r'	0,6975	0,77	0,868283	1	0
'HGRE^a'	0,8	0,773333	0,856068	0,895	0,4
'HGRE^r'	0,7175	0,77	0,868283	1	0
'SRLGE^a'	0,5875	0,77	0,868283	1	0
'SRLGE^r'	0,69	0,77	0,868283	1	0
'SRHGE^a'	0,655	0,733333	0,843485	0,955	0
'SRHGE^r'	0,6825	0,753333	0,854949	0,975	0
'LRLGE^a'	0,655	0,733333	0,841061	0,95	0
'LRLGE^r'	0,7925	0,73	0,836537	0,95	0
'LRHGE^a'	0,615	0,77	0,868283	1	0
'LRHGE^r'	0,7225	0,736667	0,838283	0,95	0
'NGLNU^a'	**0,8175**	0,713333	0,823608	0,91	0,1
'NGLNU^r'	0,4425	0,77	0,868283	1	0
'NRLNU^a'	0,595	0,716667	0,822374	0,905	0,1
'NRLNU^r'	0,4775	0,713333	0,827172	0,925	0
'GLRV^a'	**0,975**	0,863333	0,899481	0,89	0,8
'GLRV^r'	0,7875	0,806667	0,854762	0,795	0,85
'RLV^a'	0,7125	0,753333	0,854949	0,975	0
'RLV^r'	**0,8625**	0,77	0,868283	1	0
'RE^a'	0,6025	0,733333	0,833485	0,925	0,1
'RE^r'	0,665	0,803333	0,875866	0,93	0,35
'W MV^cH'	0,7425	0,713333	0,807619	0,79	0,6
'W MED^cH'	0,59	0,77	0,861465	0,955	0,15
'W MAX^cH'	0,38	0,77	0,868283	1	0
'W MIN^cH'	0,695	0,856667	0,913997	0,975	0,35
'W RNG^cH'	0,5625	0,803333	0,881061	0,975	0,15
'W STD^cH'	**0,8425**	0,873333	0,923485	0,975	0,45
'W MDAD^cH'	0,6175	0,716667	0,820628	0,905	0,05

'W MNAD^cH'	0,7025	0,733333	0,836061	0,925	0,05
'W MV^cV'	0,775	0,696667	0,801667	0,825	0,3
'W MED^cV'	0,3125	0,733333	0,841061	0,95	0
'W MAX^cV'	0,5925	0,753333	0,857374	0,98	0
'W MIN^cV'	**0,8475**	0,873333	0,923088	0,975	0,5
'W RNG^cV'	0,7175	0,783333	0,872374	0,955	0,15
'W STD^cV'	0,7975	0,803333	0,880505	0,95	0,25
'W MDAD^cV'	0,5975	0,716667	0,820628	0,905	0,05
'W MNAD^cV'	0,6125	0,716667	0,824394	0,925	0
'W MV^cD'	0,66	0,77	0,868283	1	0
'W MED^cD'	0,375	0,703333	0,81404	0,915	0
'W MAX^cD'	0,42	0,77	0,868283	1	0
'W MIN^cD'	0,53	0,753333	0,857374	0,98	0
'W RNG^cD'	0,5025	0,77	0,868283	1	0
'W STD^cD'	**0,82**	0,95	0,967532	0,975	0,8
'W MDAD^cD'	0,73	0,786667	0,863608	0,95	0,25
'W MNAD^cD'	0,6675	0,75	0,840628	0,905	0,15

ii. Random Forest Feature Importance Results

Low Risk – High Risk Results

Feature	MDI	Permutation	SHAP
Area'	0,081722	0,005	0,030741
'Perimeter'	0,064585	0	0,028959
'Eccentricity'	0,000495	0	0,00072
'MajorAxisLength'	0,05624	0	0,023191
'MinorAxisLength'	0,085153	0,005	0,042682
'ConvexArea'	0,058698	0,005	0,034516
'EquivDiameter'	0,072994	0,005	0,039848
'Solidity'	0,00048	0	0,000292
'Extent'	0,000297	0	5,96E-05
'Compactness'	1,88E-05	0	0
'Mean'	0,000153	0	0
'Std'	0,004555	0	0,004424
'Skewness'	8,76E-06	0	0
'Kurtosis'	0,000542	0	4,58E-05
'Median'	0,000496	0	0,000264
'Minimum'	0,002293	0	0,000461
'P10th'	2,06E-05	0	0,000177
'P90th'	0,001402	0	8,99E-05
'Maximum'	0,00628	0	0,000781
'IQR'	3,15E-06	0	6,95E-05
'Range'	0,006606	0	0,000221
'MeanAbsoluteDeviation'	0,000429	0	0,000329

'MedianAbsoluteDeviation'	3,4E-06	0	0
'CV'	0,003157	0	0,000978
'QCD'	0,0001	0	0,000375
'Energy'	0,036647	0,005	0,015141
'Entropy'	0,000412	0	0,000192
'ASM^a'	0	0	0,000184
'ASM^r'	0,000428	0	4,01E-05
'CONT^a'	0,011377	0	0,004737
'CONT^r'	0,019456	0	0,019422
'COR^a'	0,000182	0	0,000243
'COR^r'	1,21E-05	0	2,22E-05
'SOQ^a'	0,000193	0	0,00028
'SOQ^r'	0,014322	0	0,004945
'IDM^a'	0,00067	0	0,00043
'IDM^r'	9,7E-06	0	2,6E-05
'SAV^a'	0,000193	0	0,000228
'SAV^r'	0,06678	0	0,033691
'SVAR^a'	0,00072	0	0,00038
'SVAR^r'	0,02164	0	0,009866
'SENTR^a'	0,000467	0	0
'SENTR^r'	0,00371	0	0,001314
'ENTR^a'	3,21E-06	0	0,00079
'ENTR^r'	0,000366	0	0,000177
'DVAR^a'	0,011914	0	0,004986
'DVAR^r'	0,01741	0	0,012323
'DENTR^a'	0,000381	0	0,000166
'DENTR^r'	0,001008	0	0,000646
'IMC1^a'	0,000258	0	0,000852
'IMC1^r'	0,000509	0	9,83E-05
'IMC2^a'	1,3E-05	0	0,000985
'IMC2^r'	0,000125	0	0,000189
'MCCF^a'	0,000876	0	0,00061
'MCCF^r'	0,000366	0	0,000284
'JMX^a'	0,000646	0	6,77E-05
'JMX^r'	0,000799	0	0,000503
'JAV^a'	1,06E-17	0	0
'JAV^r'	0,077816	0	0,032354
'DAV^a'	0,001626	0	0,001464
'DAV^r'	0,002455	0	0,001268
'IDF^a'	0,000976	0	0,000595
'IDF^r'	0,000884	0	0,000177
'NIDF^a'	0,001809	0	0,001147
'NIDF^r'	4,43E-05	0	0,000921
'ACOR^a'	0,000896	0	0
'ACOR^r'	4,86E-05	0	0,000366
'CLS^a'	0,001036	0	0,000591

'CLS^r'	0,000132	0	5,96E-05
'CLP^a'	0,000169	0	0
'CLP^r'	0,002164	0	0
'SRE^a'	0,000776	0	0,000481
'SRE^r'	0,001273	0	0,001509
'LRE^a'	0,001218	0	0,00167
'LRE^r'	0,010118	0	0,004148
'GLNU^a'	0,040062	0	0,010893
'GLNU^r'	0,028025	0	0,009516
'RLNU^a'	0,025094	0	0,006117
'RLNU'	0,01456	0	0,005239
'RP^a'	0,000716	0	0,000266
'RP^r'	2,58E-05	0	0,000579
'LGRE^a'	0,007073	0	0,002112
'LGRE^r'	0,007214	0	0,003415
'HGRE^a'	8,69E-05	0	0
'HGRE^r'	0,002051	0	0,001618
'SRLGE^a'	1,92E-05	0	0
'SRLGE^r'	0,002168	0	0,000855
'SRHGE^a'	0,000175	0	0,000588
'SRHGE^r'	0,000769	0	0,000307
'LRLGE^a'	0,003649	0	0,002763
'LRLGE^r'	0,007426	0	0,002486
'LRHGE^a'	4,67E-05	0	0,000306
'LRHGE^r'	4,81E-05	0	0,000192
'NGLNU^a'	0,000169	0	0,000644
'NGLNU^r'	0,001215	0	0,000564
'NRLNU^a'	0,001657	0	0,000183
'NRLNU^r'	0,000841	0	0,000202
'GLRV^a'	0,001303	0	7,07E-05
'GLRV^r'	0,010996	0	0,005799
'RLV^a'	0,001604	0	0,003682
'RLV^r'	0,011887	0	0,008772
'RE^a'	0,001762	0	0,000433
'RE^r'	0,000422	0	0,000313
'W MV^cH'	0,002151	0	0,000921
'W MED^cH'	0,0002	0	0,000324
'W MAX^cH'	0,000254	0	0,000663
'W MIN^cH'	0,001694	0	0,000332
'W RNG^cH'	0,000791	0	0,000537
'W STD^cH'	0,006414	0	0,003699
'W MDAD^cH'	0,001244	0	0,000294
'W MNAD^cH'	0,002247	0	0,001991
'W MV^cV'	4,69E-06	0	1,95E-05
'W MED^cV'	0,000507	0	0,000755
'W MAX^cV'	0,000731	0	0,000395

'W MIN^cV'	0,000732	0	0,00105
'W RNG^cV'	0,000253	0	0
'W STD^cV'	0,005858	0	0,003428
'W MDAD^cV'	0,000163	0	1,12E-19
'W MNAD^cV'	0,000203	0	0,000763
'W MV^cD'	9,52E-18	0	0,000802
'W MED^cD'	4,51E-18	0	0,000178
'W MAX^cD'	0,001871	0	0,000708
'W MIN^cD'	0,001667	0	0,001116
'W RNG^cD'	0,001168	0	0,001679
'W STD^cD'	0,026813	0	0,014274
'W MDAD^cD'	0,000952	0	0,000231
'W MNAD^cD'	0,010952	0	0,005499

Low Risk – Medium Risk Results

Feature	MDI	Permutation	SHAP
Area'	0,010572	0,006667	0,004971
'Perimeter'	0,004103	0	0,002165
'Eccentricity'	0,001151	0	0,001548
'MajorAxisLength'	0,006077	0	0,003114
'MinorAxisLength'	0,009027	0,004762	0,004128
'ConvexArea'	0,00377	0	0,004479
'EquivDiameter'	0,007439	0	0,003506
'Solidity'	0,000967	0	0,000613
'Extent'	0,00085	0	0,00032
'Compactness'	0,000195	0	0,000125
'Mean'	0,000434	0	0,001127
'Std'	0,035318	0,002857	0,013591
'Skewness'	0,004902	0,00381	0,006408
'Kurtosis'	0,010464	0	0,003189
'Median'	0,000683	0	0,000243
'Minimum'	0,001428	0	0,001127
'P10th'	0,002699	0	0,000601
'P90th'	0,011626	0,00381	0,008477
'Maximum'	0,010022	0	0,00291
'IQR'	0,017497	0,009524	0,011704
'Range'	0,006784	0,002857	0,002284
'MeanAbsoluteDeviation'	0,035455	0,009524	0,014248
'MedianAbsoluteDeviation'	0,014073	0,009524	0,005776
'CV'	0,003989	0	0,00106
'QCD'	0,004762	0	0,001594
'Energy'	0,005802	0	0,002504

'Entropy'	0,000334	0	0,000417
'ASM^a'	0,019452	0,000952	0,008749
'ASM^r'	0,005197	0	0,004895
'CONT^a'	0,001843	0	0,000413
'CONT^r'	0,000673	0	0,00024
'COR^a'	0,026155	0,007619	0,017092
'COR^r'	0,003479	0,006667	0,00171
'SOQ^a'	0,012333	0,002857	0,00335
'SOQ^r'	0,000647	0	0,000329
'IDM^a'	0,00168	0	0,000301
'IDM^r'	0,001695	0	0,001896
'SAV^a'	0,001629	0	0,000964
'SAV^r'	0,000512	0	0,000467
'SVAR^a'	0,011945	0,00013	0,007926
'SVAR^r'	0,000714	0	0,00027
'SENTR^a'	0,02853	0,005714	0,01667
'SENTR^r'	0,000844	0	0,000773
'ENTR^a'	0,032449	0,000952	0,012939
'ENTR^r'	0,00207	0	0,000938
'DVAR^a'	0,00053	0	0,000679
'DVAR^r'	0,000215	0	7,75E-20
'DENTR^a'	0,001149	0	0,000222
'DENTR^r'	0,005613	0,00381	0,004738
'IMC1^a'	0,001868	0	0,000998
'IMC1^r'	0,024794	-0,00654	0,01636
'IMC2^a'	0,021562	0,004762	0,014271
'IMC2^r'	0,035628	0,009524	0,019811
'MCCF^a'	0,001381	0	0,001022
'MCCF^r'	0,001252	0	0,001044
'JMX^a'	0,00075	0	0,00167
'JMX^r'	0,000228	0	0,000605
'JAV^a'	0,002415	0	0,000641
'JAV^r'	0,001171	0	0,000263
'DAV^a'	0,001111	0	0,000439
'DAV^r'	0,001254	0	0,000132
'IDF^a'	0,002014	0	0,000318
'IDF^r'	0,001095	0	0,000372
'NIDF^a'	0,000809	0	0,000393
'NIDF^r'	0,001612	0	0,001075
'ACOR^a'	0,003681	0	0,001906
'ACOR^r'	0,001489	0	0,000427
'CLS^a'	0,009293	0,009524	0,003
'CLS^r'	0,001198	0	0,000335
'CLP^a'	0,024238	0,002078	0,014208
'CLP^r'	0,00575	0	0,002184
'SRE^a'	0,041003	0,001905	0,011192

'SRE^r'	0,023749	9,02E-18	0,003648
'LRE^a'	0,000769	0	0,000426
'LRE^r'	0,000188	0	0,00037
'GLNU^a'	0,006307	0	0,002245
'GLNU^r'	0,002039	0	0,001064
'RLNU^a'	0,0223	0,006667	0,012607
'RLNU'	0,016378	0,008571	0,009084
'RP^a'	0,000929	0	0,000488
'RP^r'	0,000546	0	0,000334
'LGRE^a'	0,028157	0,003117	0,012865
'LGRE^r'	0,001775	0	0,001239
'HGRE^a'	0,00372	0	0,001341
'HGRE^r'	0,000107	0	0,000358
'SRLGE^a'	0,000703	0	0,000632
'SRLGE^r'	0,0004	0	0,00038
'SRHGE^a'	0,018656	0	0,004086
'SRHGE^r'	0,017817	0,005714	0,007251
'LRLGE^a'	0,000506	0	0,000455
'LRLGE^r'	0,001106	0	0,00031
'LRHGE^a'	0,001128	0	0,000477
'LRHGE^r'	0,00114	0	0,0003
'NGLNU^a'	0,012292	0,007619	0,006508
'NGLNU^r'	0,001219	0	0,00096
'NRLNU^a'	0,011122	4,51E-18	0,003927
'NRLNU^r'	0,025024	-0,00381	0,004432
'GLRV^a'	0,005783	0	0,002692
'GLRV^r'	0,000418	0	0,000693
'RLV^a'	0,000777	0	0,000303
'RLV^r'	0,000144	0	0,000334
'RE^a'	0,002346	0	0,000447
'RE^r'	0,005476	0	0,002536
'W MV^cH'	0,000736	0	0,000382
'W MED^cH'	0,013679	0,002857	0,002705
'W MAX^cH'	0,019868	0,006667	0,009317
'W MIN^cH'	0,017096	0,00381	0,015446
'W RNG^cH'	0,020145	0,01632	0,013576
'W STD^cH'	0,001363	0	0,000839
'W MDAD^cH'	0,008678	-0,00286	0,002945
'W MNAD^cH'	0,002234	0	0,000418
'W MV^cV'	0,0004	0	0,000811
'W MED^cV'	0,00185	0	0,000694
'W MAX^cV'	0,008645	0	0,00997
'W MIN^cV'	0,005175	0	0,007455
'W RNG^cV'	0,004335	0	0,006002
'W STD^cV'	0,001495	0	0,000526
'W MDAD^cV'	0,045858	0,005714	0,019705

'W MNAD^cV'	0,002434	0	0,000443
'W MV^cD'	0,000828	0	0,000382
'W MED^cD'	0,000893	0	0,000406
'W MAX^cD'	0,037428	-0,00078	0,015507
'W MIN^cD'	0,00367	0	0,006538
'W RNG^cD'	0,026432	0,005714	0,020456
'W STD^cD'	0,00209	0	0,001188
'W MDAD^cD'	0,003356	0,001905	0,002089
'W MNAD^cD'	0,002911	0	0,001079

Medium Risk – High Risk Results

Feature	MDI	Permutation	SHAP
'Area'	0,009849	-0,00727	0,005952
'Perimeter'	0,022936	-0,01091	0,00624
'Eccentricity'	0,000599	0	0,000243
'MajorAxisLength'	0,00727	0,004091	0,007043
'MinorAxisLength'	0,012409	0,004091	0,007906
'ConvexArea'	0,015108	0,004091	0,0046
'EquivDiameter'	0,010384	0,015	0,004452
'Solidity'	1,07E-18	0	0,000202
'Extent'	0,000162	0	0,000179
'Compactness'	0,000406	0	0,000199
'Mean'	0,000659	0	0
'Std'	3,72E-05	0	0
'Skewness'	0,004452	0	0,001099
'Kurtosis'	0,01058	-0,01091	0,004964
'Median'	4,04E-05	0	0
'Minimum'	0,001074	0	0,000201
'P10th'	0,001268	0	0,000986
'P90th'	0,001923	0	7,21E-20
'Maximum'	0,042507	0,016818	0,019028
'IQR'	0,001256	0	6,82E-20
'Range'	0,038167	0,015	0,011305
'MeanAbsoluteDeviation'	0,000179	0	0,000243
'MedianAbsoluteDeviation'	0,00099	0	0,000845
'CV'	0,001921	0	0,000889
'QCD'	0,004725	0	0,000638
'Energy'	0,002913	0	0,001588
'Entropy'	0,000325	0	0,000329
'ASM^a'	0,003307	0	0,000583
'ASM^r'	0,00077	0	0,001291
'CONT^a'	0,0348	0,004091	0,01135
'CONT^r'	0,033647	-0,00727	0,014794
'COR^a'	0,009185	-0,00545	0,001807
'COR^r'	0,009642	0,004394	0,002485

'SOQ^a'	0,026049	0,015	0,008042
'SOQ^r'	0,008399	0	0,000537
'IDM^a'	0,000563	0	0,000705
'IDM^r'	0,000371	0	0,000796
'SAV^a'	0,008131	0	0,005315
'SAV^r'	0,041554	0,000606	0,023176
'SVAR^a'	0,034498	0,015	0,010417
'SVAR^r'	0,048044	-0,01091	0,020295
'SENTR^a'	0,000982	0	0,001041
'SENTR^r'	0,005595	0	0,000438
'ENTR^a'	0,002618	0	0,001314
'ENTR^r'	0,001131	0	0,00018
'DVAR^a'	0,04642	0,004091	0,018991
'DVAR^r'	0,058353	-0,00727	0,017986
'DENTR^a'	0,000348	0	0,000447
'DENTR^r'	0,001853	0	0,001107
'IMC1^a'	0,001372	0	0,000825
'IMC1^r'	0,00331	0	0,00124
'IMC2^a'	0,001947	0	0,000859
'IMC2^r'	0,00218	0	0,003196
'MCCF^a'	0,002048	0	0,000583
'MCCF^r'	0,000345	0	0,000816
'JMX^a'	0,002166	0	0,000458
'JMX^r'	0,000856	0	0,00077
'JAV^a'	0,004834	0	0,001747
'JAV^r'	0,066326	0,009697	0,030158
'DAV^a'	0,000282	0	0,000137
'DAV^r'	0,000413	0	0,000168
'IDF^a'	0,00051	0	0,000473
'IDF^r'	0,000554	0	0,000218
'NIDF^a'	0,002385	0	0,000177
'NIDF^r'	0,00014	0	0,000393
'ACOR^a'	0,018016	0	0,010422
'ACOR^r'	0,006841	0	0,002487
'CLS^a'	0,002189	0	0,001837
'CLS^r'	0,010468	0,016667	0,007119
'CLP^a'	0,045	0,015	0,021635
'CLP^r'	0,019864	0,015	0,023068
'SRE^a'	0,000685	0	0,000237
'SRE^r'	0,000168	0	0,000238
'LRE^a'	0,000804	0	0,000474
'LRE^r'	0,001239	0	0,000335
'GLNU^a'	0,007899	0	0,002245
'GLNU^r'	0,012351	0,002273	0,007755
'RLNU^a'	0,004392	0	0,001198
'RLNU'	0,000469	0	0,002472

'RP^a'	0,000339	0	0,000256
'RP^r'	0,000633	0	0,000335
'LGRE^a'	0,001072	0	0,001032
'LGRE^r'	0,000745	0	0,000833
'HGRE^a'	0,005264	0	0,002171
'HGRE^r'	0,001055	0	0,001117
'SRLGE^a'	0,000633	0	0,000419
'SRLGE^r'	0,000149	0	1,17E-19
'SRHGE^a'	0,000925	0	0,000203
'SRHGE^r'	0,001591	0	0,000767
'LRLGE^a'	2,66E-05	0	0,000558
'LRLGE^r'	0,006669	0	0,0022
'LRHGE^a'	0,001514	0	0,00024
'LRHGE^r'	0,000727	0	0,000448
'NGLNU^a'	0,003433	0	0,00308
'NGLNU^r'	0,000345	0	0,001354
'NRLNU^a'	0,002031	0	0,00209
'NRLNU^r'	0,00068	0	0,000409
'GLRV^a'	0,045492	0,016818	0,0168
'GLRV^r'	0,012612	0,011667	0,003311
'RLV^a'	0,001792	0	0,001038
'RLV^r'	0,007999	0	0,004031
'RE^a'	0,002092	0	0,000731
'RE^r'	0,000961	0,006667	0,00085
'W MV^cH'	0,000146	0	0
'W MED^cH'	0,00039	0	0,000183
'W MAX^cH'	0,000809	0	0,000302
'W MIN^cH'	0,003338	0	0,005976
'W RNG^cH'	0,002652	0	0
'W STD^cH'	0,009915	0,016667	0,00778
'W MDAD^cH'	0,000497	0	0,000329
'W MNAD^cH'	0,002841	0	0,000178
'W MV^cV'	0,001096	0	0,000442
'W MED^cV'	0,000517	0	0,000145
'W MAX^cV'	0,00224	0	0,003888
'W MIN^cV'	0,015596	0,016667	0,015432
'W RNG^cV'	0,013132	0,016667	0,004026
'W STD^cV'	0,006553	0	0,002622
'W MDAD^cV'	0,001562	0	0,001053
'W MNAD^cV'	0,000457	0	1,72E-19
'W MV^cD'	0,000466	0	0,000674
'W MED^cD'	8,58E-19	0	0,000148
'W MAX^cD'	0,00073	0	0,000135
'W MIN^cD'	0,000765	0	0,001808
'W RNG^cD'	0,000146	0	0,000382
'W STD^cD'	0,038803	0,016667	0,017691

'W MDAD^cD'	0,002111	0	0
'W MNAD^cD'	0,008009	0	0,003499